

**FOURIER TRANSFORM INFRARED ISOTOPIC STUDIES ON NOVEL METAL-  
CARBON CLUSTERS TRAPPED IN Ar MATRIX ENVIRONMENTS**

by

**SARAH ANNE BATES**

Bachelor of Science, 2003  
Texas Christian University  
Fort Worth, TX

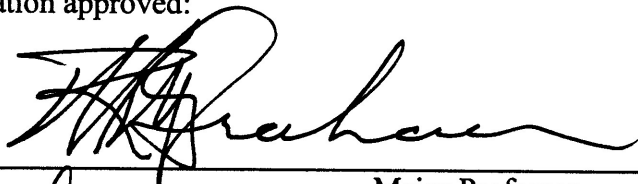
Submitted to the Graduate Faculty of the  
College of Science and Engineering  
Texas Christian University  
in partial fulfillment of the requirements  
for the degree of

**Doctor of Philosophy**

**May 2008**

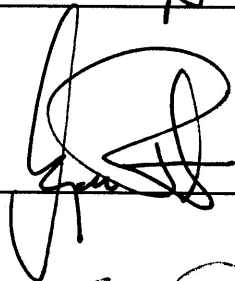
**FOURIER TRANSFORM INFRARED ISOTOPIC STUDIES ON NOVEL METAL-CARBON CLUSTERS TRAPPED IN Ar MATRIX ENVIRONMENTS**

Dissertation approved:



---

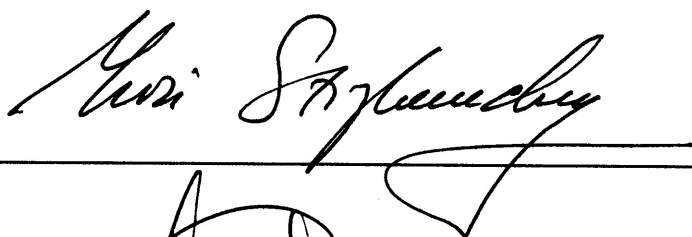
Major Professor



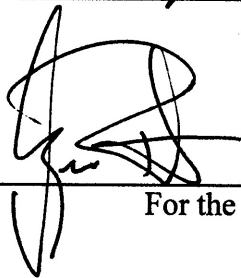
---



---



---



---

For the College of Science and Engineering

Copyright by  
Sarah Anne Bates  
2008

I would like to dedicate this dissertation to my parents who encouraged my inquisitive nature as a child and who provided unwavering support and love throughout this process.

## ACKNOWLEDGEMENTS

To my advisor, Dr. W. R. M. Graham, most sincere gratitude is expressed for his thoughtful guidance and for his continual support. Thanks also to Dr. C. M. L. Rittby for his *ab initio* calculations and for the insightful discussions.

Thanks to M. Murdock, D. Yale, and G. Katchinska for their unending patience and help in building and upgrading the vacuum system.

Thanks also to my father, William Bates, for his advice whenever chemistry questions arose.

Support of this research by the Welch Foundation, the W. M. Keck Foundation, and the TCU Research and Creative Activities Fund (TCURCAF), and support of the candidate by a Barnett Scholarship, and the Texas Space Grant Consortium (TSGC) Graduate Fellowship is also gratefully acknowledged.

## TABLE OF CONTENTS

	Page
<b>ACKNOWLEDGEMENTS .....</b>	<b>iii</b>
<b>LIST OF FIGURES .....</b>	<b>viii</b>
<b>LIST OF TABLES .....</b>	<b>xiii</b>
<b>CHAPTER I INTRODUCTION .....</b>	<b>1</b>
1.1 ASTROPHYSICAL MOTIVATION.....	1
1.2 METALLOCARBOHEDRENES.....	3
1.3 PREVIOUS WORK.....	6
1.3.1 <i>Experimental Results</i> .....	6
1.3.2 <i>Theoretical Results</i> .....	7
1.4 THE DISSERTATION RESEARCH .....	7
<b>CHAPTER II EXPERIMENTAL PROCEDURES AND TECHNIQUES .....</b>	<b>10</b>
2.1 EQUIPMENT CONSTRUCTION .....	10
2.2 EXPERIMENTAL CONDITIONS .....	13
2.3 ROD PREPARATION.....	15
2.4 ISOTOPIC SHIFTS.....	16
<b>CHAPTER III FOURIER TRANSFORM INFRARED ISOTOPIC STUDY OF LINEAR CrC<sub>3</sub>: IDENTIFICATION OF THE <math>\nu_1(\sigma)</math> MODE.....</b>	<b>19</b>
3.1. INTRODUCTION.....	19
3.2. THEORETICAL CALCULATIONS.....	22
3.3. EXPERIMENTAL PROCEDURES .....	24

3.4.	RESULTS AND DISCUSSION .....	24
3.5.	CONCLUSIONS .....	30
<b>CHAPTER IV FOURIER TRANSFORM INFRARED OBSERVATION OF THE <math>\nu_1(\sigma)</math></b>		
<b>MODE OF LINEAR <math>\text{CoC}_3</math> TRAPPED IN SOLID Ar .....</b>		<b>31</b>
4.1	INTRODUCTION.....	31
4.2	THEORETICAL CALCULATIONS.....	32
4.3	EXPERIMENTAL PROCEDURES .....	33
4.4	RESULTS AND DISCUSSION.....	36
4.5	CONCLUSIONS .....	45
<b>CHAPTER V FTIR OBSERVATION AND DFT STUDY OF THE <math>\text{AlC}_3</math> AND <math>\text{AlC}_3\text{Al}</math></b>		
<b>LINEAR CHAINS TRAPPED IN SOLID Ar .....</b>		<b>47</b>
5.1	INTRODUCTION.....	47
5.2	THEORETICAL PREDICTIONS.....	51
5.3	EXPERIMENTAL PROCEDURES .....	51
5.4	RESULTS AND DISCUSSION.....	55
5.4.1	<i>Identification of <math>\text{AlC}_3\text{Al}</math></i> .....	57
5.4.2	<i>Identification of <math>\text{AlC}_3</math></i> .....	64
5.5	CONCLUSIONS .....	68
<b>CHAPTER VI THE VIBRATIONAL SPECTRUM OF <math>\text{CuC}_3</math>: AN FTIR ISOTOPIC</b>		
<b>AND DFT INVESTIGATION .....</b>		<b>69</b>
6.1	INTRODUCTION.....	69
6.2	EXPERIMENTAL PROCEDURES .....	70
6.3	EXPERIMENTAL RESULTS AND DISCUSSION .....	71

6.4	THEORY AND ANALYSIS .....	76
6.5	CONCLUSIONS .....	81
<b>CHAPTER VII OTHER METAL–CARBON SPECIES: CrC<sub>4</sub>, AlC<sub>4</sub>Al, and V<sub>n</sub>C<sub>m</sub>.....</b>		<b>82</b>
7.1	FANLIKE (C <sub>2v</sub> ) CrC <sub>4</sub> .....	82
	7.1.1 Introduction .....	82
	7.1.2 Theoretical Calculations .....	83
	7.1.3 Results and Discussion .....	83
	7.1.4 Conclusions .....	89
7.2	LINEAR AlC <sub>4</sub> Al .....	89
	7.2.1 Theoretical Calculations .....	92
	7.2.2 Results and Discussion .....	92
	7.2.3 Conclusions .....	97
7.3	UNIDENTIFIED V <sub>n</sub> C <sub>m</sub> CANDIDATES .....	100
	7.3.1 The 2000-2050 cm <sup>-1</sup> Region.....	104
	7.3.2 The 1450-1500 cm <sup>-1</sup> Region.....	106
	7.3.3 The 900-950 cm <sup>-1</sup> Region.....	108
<b>CHAPTER VIII CONCLUSIONS AND FUTURE WORK.....</b>		<b>110</b>
8.1	CONCLUSIONS .....	110
	8.1.1 Linear CrC <sub>3</sub> .....	110
	8.1.2 Linear CoC <sub>3</sub> .....	111
	8.1.3 Linear AlC <sub>3</sub> and AlC <sub>3</sub> Al.....	112
	8.1.4 Linear CuC <sub>3</sub> .....	113
	8.1.5 Fanlike (C <sub>2v</sub> ) CrC <sub>4</sub> .....	114



8.1.6	<i>Linear AlC<sub>4</sub>Al</i> .....	114
8.1.7	<i>V<sub>n</sub>C<sub>m</sub> Candidates</i> .....	115
8.2	FUTURE WORK.....	115
8.2.1	<i>Continuing Work on CrC<sub>4</sub>, AlC<sub>4</sub>Al, and V<sub>n</sub>C<sub>m</sub> Species</i> .....	116
8.2.2	<i>Metal–Carbon Clusters</i> .....	116
8.2.3	<i>Sintering Metal–Carbon Rods</i> .....	117
8.2.4	<i>Rod Fabrication with Higher <sup>13</sup>C Enrichments</i> .....	119
<b>REFERENCES.....</b>		<b>121</b>

**VITA**

**ABSTRACT**

## LIST OF FIGURES

Figure		Page
Figure 1.1	List taken from the Cologne Database for Molecular Spectroscopy and Wootten's Database, NRAO (Ref. 5). Last updated July 2007. The red arrows indicate molecules containing two or more C atoms in a chain or ring. ....	2
Figure 1.2	A list of molecules found as of 2006 in the late-type star IRC+10216 (Ref. 9) Note the abundance of $C_n$ clusters. In columns 2-4, all the molecules have at least two C atoms, with the exception of HCN. Also note the abundance of Si-bearing species (column 5) and metal-bearing species (column 6), many of which also contain one or more C atoms. ....	4
Figure 1.3	Proposed $M_8C_{12}$ structure, with $MC_2$ building block highlighted. Metal and carbon atoms are represented with red and blue, respectively. Metcar picture from Ref. 16. ....	5
Figure 2.1	Schematic of the experimental apparatus. ....	11
Figure 2.2	Schematic of the laser ablation chamber. ....	12
Figure 2.3	Illustration of single $^{13}C$ isotopic substitutions in (a) centrosymmetric linear molecules, e.g. $C_3$ and $MC_3M$ , and (b) in non-centrosymmetric linear molecules, e.g. $MC_3$ . ....	17
Figure 3.1	(a) The $^3B_1$ fanlike ( $C_{2v}$ ) and $^5\Pi$ linear isomers of $CrC_3$ . DFT B3LYP/6-311+G(3df) predictions for their geometric parameters are given in Angstroms ( $\text{\AA}$ ). The predicted principal nuclear displacements of the atoms for the $\nu_1(\sigma)$ mode of $^5\Pi$ linear $CrC_3$ are shown in (b). ....	20
Figure 3.2	FTIR spectra produced by (a) dual ablation of Cr and $^{12}C$ rods and (b) a pure $^{12}C$ rod, for comparison. ....	25

Figure 3.3	Comparison of the FTIR spectra of the $\nu_1(\sigma)$ mode of linear $\text{CrC}_3$ and its $^{13}\text{C}$ isotopic shifts produced by the simultaneous evaporation of a Cr rod and carbon rods with (a) 30% and (b) 15% $^{13}\text{C}$ enrichments, with (c) a simulation derived from DFT calculations at the B3LYP/6-311+G(3df) level having 10% $^{13}\text{C}$ enrichment. The letters correspond to the single $^{13}\text{C}$ substituted and single $^{12}\text{C}$ substituted isotopomers listed in Table 3.2.....	27
Figure 4.1	DFT B3LYP/6-311+G(3df) predictions of bond lengths (Å) of the $^2B_1$ fanlike and $^2\Delta$ linear isomers. The predicted principal nuclear displacements of the $\nu_1(\sigma)$ mode of the $^2\Delta$ linear isomer of $\text{CoC}_3$ are shown in (b). .....	34
Figure 4.2	FTIR spectra recorded after (a) dual ablation of cobalt and pure $^{12}\text{C}$ rods and (b) ablation of a pure $^{12}\text{C}$ rod, for comparison. Note the $1918.2\text{ cm}^{-1}$ band in (a) that does not appear in (b).....	37
Figure 4.3	FTIR spectra of the $\nu_1(\sigma)$ mode of linear $\text{CoC}_3$ in an experiment with (a) 30% nominal $^{13}\text{C}$ enrichment, and (b) 20% nominal $^{13}\text{C}$ enrichment. The higher $^{13}\text{C}$ enrichment in (a) eliminates most of the absorptions attributed to $\text{C}_6^-$ and $\text{C}_7$ , leaving only a weak $\text{C}_7$ absorption at $1894.3\text{ cm}^{-1}$ , and thus shows the fully- and doubly-substituted $^{13}\text{C}$ isotopomers more clearly.....	39
Figure 4.4	(a) An FTIR spectrum with 30% $^{13}\text{C}$ enrichment for comparison with DFT simulations of a 30% $^{13}\text{C}$ enrichment spectrum using the (b) BPW91 and the (c) B3LYP functionals with a 6-311+G(3df) basis set. The DFT simulations are scaled to the main $1918.2\text{ cm}^{-1}$ band.....	43
Figure 5.1	DFT B3LYP/6-311+G(3df) predictions of bond lengths (Å) of the (a) $^2\Pi$ linear, (b) $^2A_1$ kite ( $\text{C}_{2v}$ ), and (c) $^2B_2$ fanlike ( $\text{C}_{2v}$ ) isomers of $\text{AlC}_3$ . The predicted	

	principal nuclear displacements of the $\nu_2(\sigma)$ mode of ( ${}^2\Pi$ ) linear $\text{AlC}_3$ are shown in (d).....	49
Figure 5.2	(a) DFT B3LYP/6-311+G(3 <i>df</i> ) predictions of bond lengths (Å) for the ${}^3\Sigma_g^+$ linear isomer of $\text{AlC}_3\text{Al}$ . The predicted principal nuclear displacements of the (b) $\nu_3(\sigma_u)$ and (c) $\nu_4(\sigma_u)$ modes of ( ${}^3\Sigma_g^+$ ) $\text{AlC}_3\text{Al}$ . .....	54
Figure 5.3	FTIR spectra recorded after (a) dual ablation of Al and ${}^{12}\text{C}$ rods and (b) ablation of a ${}^{12}\text{C}$ rod only, for comparison. Note the 1624.0, 1210.9, and 528.3 $\text{cm}^{-1}$ bands in the Al-C spectrum that are not in the ${}^{12}\text{C}$ spectrum. ....	56
Figure 5.4	FTIR spectra of the $\nu_3(\sigma_u)$ mode of linear $\text{AlC}_3\text{Al}$ in experiments with (a) 30% and (b) 20% nominal ${}^{13}\text{C}$ enrichments. (c) DFT simulation of an experiment with a 20% enrichment. ....	58
Figure 5.5	The $\nu_4(\sigma_u)$ mode of $\text{AlC}_3\text{Al}$ in (a) an FTIR spectrum with a nominal 30% ${}^{13}\text{C}$ enrichment compared with (b) a DFT simulation with 30% ${}^{13}\text{C}$ enrichment. ....	59
Figure 5.6	The $\nu_2(\sigma)$ mode of linear $\text{AlC}_3$ in (a) an FTIR spectrum with a nominal 30% ${}^{13}\text{C}$ enrichment compared with DFT simulations of spectra with (b) 10% and (c) 30% ${}^{13}\text{C}$ enrichments.....	65
Figure 6.1	FTIR spectra recorded after (a) dual ablation of Cu and ${}^{12}\text{C}$ rods and (b) ablation of a pure ${}^{12}\text{C}$ rod, for comparison. Note the 1830.0 $\text{cm}^{-1}$ band in (a) that is absent from (b). ....	72
Figure 6.2	FTIR spectra from experiments with (a) 30% and (b) 20% nominal ${}^{13}\text{C}$ enrichments for comparison with (c) a DFT simulation of the $\nu_1(\sigma)$ mode of ( ${}^2\Pi$ ) linear $\text{CuC}_3$ having 30% ${}^{13}\text{C}$ enrichment. ....	74

Figure 6.3	DFT B3LYP/6-311+G(3df) bond length (Å) and angle (°) predictions for the (a) ${}^2\Pi$ linear and (b) ${}^2A'$ <i>trans</i> -bent isomers of $\text{CuC}_3$ . The predicted principal nuclear displacements of the $\nu_1(\sigma)$ mode of ( ${}^2\Pi$ ) linear $\text{CuC}_3$ are shown in (c). .....78
Figure 7.1	Structures of (a) fanlike and (b) linear isomers of $\text{CrC}_4$ and (c) linear $\text{CrC}_4\text{Cr}$ , which were investigated as possible candidates for the $1554.3\text{ cm}^{-1}$ band. ....84
Figure 7.2	FTIR spectra obtained from ablation of (a) a sintered $\text{Cr}/{}^{12}\text{C}$ rod for comparison with (b) ablation of a ${}^{12}\text{C}$ rod only. Note the $\nu_1(\sigma)=1789.5\text{ cm}^{-1}$ mode of linear $\text{CrC}_3$ and the $1554.3\text{ cm}^{-1}$ band in (a) that does not appear in (b). .....86
Figure 7.3	(a) FTIR spectrum obtained from the ablation of a sintered 15% Cr/85% C rod with a 15% nominal ${}^{13}\text{C}$ enrichment for comparison with a (b) DFT simulation of the spectrum of the $\nu_1(a_1)$ mode of ( ${}^3B_1$ ) fanlike $\text{CrC}_4$ with a 10% ${}^{13}\text{C}$ enrichment, scaled to $1554.3\text{ cm}^{-1}$ . .....88
Figure 7.4	(a) DFT B3LYP/6-311+G(3df) predictions of bond lengths (Å) for ( ${}^3B_1$ ) fanlike $\text{CrC}_4$ . The $\alpha$ and $\beta$ denote pairs of equivalent C atoms. The predicted principal nuclear displacements of its $\nu_1(a_1)$ mode are shown in (b). .....91
Figure 7.5	FTIR spectra obtained after (a) dual ablation of Al and ${}^{12}\text{C}$ rods and (b) ablation of a ${}^{12}\text{C}$ rod only, for comparison. Note the $1987.3\text{ cm}^{-1}$ band in the Al–C spectrum that is not in the pure ${}^{12}\text{C}$ spectrum. Note also the identifications of $\text{AlC}_2\text{Al}$ , $\text{AlC}_3$ , and $\text{AlC}_3\text{Al}$ in the dual ablation spectrum. ....94
Figure 7.6	FTIR spectra obtained after dual ablation of an Al and a C rod with 15% nominal ${}^{13}\text{C}$ enrichment annealed at (a) 32 K and (b) 29 K compared with a (c) DFT simulation of the spectrum of the $\nu_4(\sigma_u)$ mode of linear $\text{AlC}_4\text{Al}$ with a 10% ${}^{13}\text{C}$ enrichment, scaled to $1987.3\text{ cm}^{-1}$ . .....95

Figure 7.7	(a) DFT B3LYP/6-311+G(3df) predictions for the bond lengths of linear ( $^1\Sigma_g^+$ ) $\text{AlC}_4\text{Al}$ are given in Angstroms ( $\text{\AA}$ ). The predicted principal nuclear displacements of the atoms for its $\nu_4(\sigma_u)$ mode are shown in (b).....	99
Figure 7.8	FTIR spectra of the 2000-2050 $\text{cm}^{-1}$ region recorded after laser ablation of a single rod pressed from 20% V and 80% $^{12}\text{C}$ powders annealed at (a) 24 K, (b) 20 K, and (c) prior to annealing at 10 K for comparison with (d) an FTIR spectrum obtained from ablation of a $^{12}\text{C}$ rod. ....	105
Figure 7.9	FTIR spectra of the 1450-1500 $\text{cm}^{-1}$ region recorded after dual laser ablation of a V rod and a $^{12}\text{C}$ rod (a) annealed at 33 K and (b) prior to annealing at 10 K for comparison with (c) a spectrum obtained from ablation of a $^{12}\text{C}$ rod.....	107
Figure 7.10	FTIR spectra of the 900-950 $\text{cm}^{-1}$ region recorded after laser ablation of a single rod pressed from 20% V and 80% $^{12}\text{C}$ powders annealed at (a) 24 K, (b) 20 K, and (c) prior to annealing at 10 K for comparison with (d) an FTIR spectrum obtained from ablation of a $^{12}\text{C}$ rod. ....	109
Figure 8.1	Spectrum obtained from $^{12}\text{C}$ ablation using a higher laser power, $\sim 1.0$ W, and tighter laser beam focus, $\sim 2.0$ mm, which produces intense absorptions for a number of larger $\text{C}_n$ molecules. ....	118
Figure 8.2	Proposed schematic for the (a) top and (b) front views of the split die. Note the bolts on the front are used to squeeze the carbide bushing together. Because of the small gap between the carbide bushing and the die casing, the bushing will easily slide out from the casing when the bolts are unscrewed. (c) An illustration of how the carbide bushing would be opened to remove a C rod fabricated with high $^{13}\text{C}$ enrichment without putting excessive stress on the rod. ....	120

## LIST OF TABLES

Table	Page
Table 3.1: DFT B3LYP/6-311+G(3df) predicted vibrational frequencies (cm <sup>-1</sup> ) and band intensities (km/mol) for the linear ( <sup>5</sup> Π) and fanlike ( <sup>3</sup> B <sub>1</sub> ) isomers of CrC <sub>3</sub> . .....	23
Table 3.2: Comparison of observed vibrational frequencies (cm <sup>-1</sup> ) of the ν <sub>1</sub> (σ) mode for <sup>13</sup> C-substituted isotopomers of linear CrC <sub>3</sub> with the predictions of B3LYP/6-311+G(3df) calculations. ....	29
Table 4.1: DFT predicted frequencies (cm <sup>-1</sup> ) and band intensities (km/mol) for the vibrational fundamentals of the ( <sup>2</sup> Δ) linear and ( <sup>2</sup> B <sub>1</sub> ) fanlike isomers of CoC <sub>3</sub> using the B3LYP and the BPW91 functionals with a 6-311+G(3df) basis set.....	35
Table 4.2: Comparison of the observed vibrational fundamental and all of the <sup>13</sup> C-substituted isotopomer frequencies (cm <sup>-1</sup> ) of the ν <sub>1</sub> (σ) mode of linear CoC <sub>3</sub> with the predictions of DFT B3LYP/ and BPW91/6-311G+(3df) calculations.....	44
Table 5.1: DFT B3LYP/6-311+G(3df) predicted vibrational frequencies (cm <sup>-1</sup> ) and intensities (km/mol) for linear ( <sup>3</sup> Σ <sub>g</sub> <sup>+</sup> ) AlC <sub>3</sub> Al. ....	52
Table 5.2: DFT B3LYP/6-311+G(3df) predicted vibrational frequencies (cm <sup>-1</sup> ) and intensities (km/mol) for the linear ( <sup>2</sup> Π), kite ( <sup>2</sup> A <sub>1</sub> ), and fanlike ( <sup>2</sup> B <sub>2</sub> ) isomers of AlC <sub>3</sub> .....	53
Table 5.3: Comparison of the observed isotopomer frequencies (cm <sup>-1</sup> ) of the ν <sub>3</sub> (σ <sub>u</sub> ) and ν <sub>4</sub> (σ <sub>u</sub> ) modes of linear ( <sup>3</sup> Σ <sub>g</sub> <sup>+</sup> ) AlC <sub>3</sub> Al and of the ν <sub>5</sub> (b <sub>2</sub> ) mode of fanlike ( <sup>2</sup> B <sub>1</sub> ) AlC <sub>3</sub> with the predictions of B3LYP/6-311+G(3df) calculations.....	63
Table 5.4: Comparison of observed vibrational frequencies (cm <sup>-1</sup> ) of the ν <sub>2</sub> (σ) mode for the singly- and fully-substituted <sup>13</sup> C isotopomers of linear ( <sup>2</sup> Π) AlC <sub>3</sub> with the predictions of B3LYP/6-311+G(3df) calculations.....	67

Table 6.1: DFT B3LYP/6-311+G(3df) predicted frequencies (cm <sup>-1</sup> ) and band intensities (km/mol) for the vibrational fundamentals of the ( <sup>2</sup> Π) linear and ( <sup>2</sup> A') <i>trans</i> -bent isomers of CuC <sub>3</sub> .	77
Table 6.2: Comparison of the observed vibrational fundamental and all of the <sup>13</sup> C- substituted isotopomer frequencies (cm <sup>-1</sup> ) of the ν <sub>1</sub> (σ) and the ν <sub>1</sub> (a') modes of the ( <sup>2</sup> Π) linear and ( <sup>2</sup> A') <i>trans</i> -bent isomers of CuC <sub>3</sub> with the predictions of B3LYP/6-311G+(3df) calculations.	79
Table 7.1: DFT B3LYP/6-311+G(3df) predicted vibrational frequencies (cm <sup>-1</sup> ) and band intensities (km/mol) for the <sup>5</sup> B <sub>2</sub> and <sup>3</sup> B <sub>1</sub> states of fanlike CrC <sub>4</sub> and for ( <sup>5</sup> Π) linear CrC <sub>4</sub> .	85
Table 7.2: Comparison of observed vibrational fundamental and single <sup>13</sup> C isotopomer frequencies (cm <sup>-1</sup> ) of the ν <sub>1</sub> (a <sub>1</sub> ) mode of ( <sup>3</sup> B <sub>1</sub> ) fanlike CrC <sub>4</sub> with the predictions of B3LYP/6-311+G(3df) calculations.	90
Table 7.3: DFT B3LYP/6-311+G(3df) predicted vibrational frequencies (cm <sup>-1</sup> ) and band intensities (km/mol) for ( <sup>1</sup> Σ <sub>g</sub> <sup>+</sup> ) linear AlC <sub>4</sub> Al and ( <sup>2</sup> Σ) linear AlC <sub>4</sub> .	93
Table 7.4: Comparison of observed vibrational fundamental and single <sup>13</sup> C shift frequencies (cm <sup>-1</sup> ) of the ν <sub>4</sub> (σ <sub>u</sub> ) mode of ( <sup>1</sup> Σ <sub>g</sub> <sup>+</sup> ) linear AlC <sub>4</sub> Al with the predictions of B3LYP/6-311+G(3df) calculations.	98
Table 7.5: B3LYP/6-311+G(d) calculations of vibrational frequencies (cm <sup>-1</sup> ) for linear VC <sub>n</sub> (n=1-8) clusters (from Ref. 126).	101
Table 7.6: B3LYP/6-311+G(d) calculations of vibrational frequencies (cm <sup>-1</sup> ) for fanlike VC <sub>n</sub> (n=2-8) clusters (from Ref. 126).	102
Table 7.7: B3LYP/6-311+G(d) calculations of vibrational frequencies (cm <sup>-1</sup> ) for cyclic VC <sub>n</sub> (n=6-8) clusters (from Ref. 126).	103



# CHAPTER I

## INTRODUCTION

Studies on metal–carbon clusters are of interest because of their applications to diverse areas of physics including the detection of astrophysical species,<sup>1</sup> understanding the bonding and creation of metallocarbohedrenes,<sup>2,3</sup> and as catalysts in nanomaterial formation.<sup>4</sup> Aside from diatomic clusters, MC, few studies have been done on triatomic or larger metal–carbon species.

### 1.1 Astrophysical Motivation

To date, more than 140 molecules have been found in either the interstellar medium (ISM) or in circumstellar shells (Fig. 1.1).<sup>5</sup> Carbon and carbon compounds are abundant in the circumstellar shells of stars that are advanced in evolution because of fusion in stellar cores, *i.e.* the “triple alpha” process, so it is not surprising that many of the observed circumstellar and interstellar molecules shown in Fig. 1.1 are composed of long carbon chain “backbones”, noted with red arrows, with other elements like nitrogen or hydrogen bonded to the ends, *e.g.* HC<sub>11</sub>N,<sup>6</sup> C<sub>5</sub>N,<sup>7</sup> and C<sub>6</sub>H.<sup>8,9</sup> Pure carbon chains, such as C<sub>5</sub>, have also been observed in the stellar envelope of IRC +10216.<sup>8,9</sup>

Besides observing H or N atoms bonded to C<sub>*n*</sub> species, mono-metal–carbon clusters have also been found in circumstellar shells and in the ISM. Metals such as vanadium (V), nickel (Ni), chromium (Cr), magnesium (Mg) and aluminum (Al), are cosmically abundant; hence, they are readily available to bond with interstellar or circumstellar carbon species to form M<sub>*n*</sub>C<sub>*m*</sub> molecules.<sup>10</sup> For example, silicon (Si), while not a metal, is a cosmically abundant semi-metal or metalloid and SiC<sub>*n*</sub> (*n*=1-4), SiN, and SiCN have all been detected in the circumstellar shell of IRC+10216, together with other metal-bearing species, such as MgNC, MgCN, NaCN, NaCl,

## Molecules Discovered in Space

<u>2 atoms</u>	<u>3 atoms</u>	<u>4 atoms</u>	<u>5 atoms</u>	<u>6 atoms</u>	<u>7 atoms</u>	<u>8 atoms</u>	<u>9 atoms</u>
H <sub>2</sub>	→ C <sub>3</sub>	→ c-C <sub>3</sub> H	→ C <sub>5</sub>	→ C <sub>6</sub> H	→ C <sub>6</sub> H/C <sub>6</sub> H <sup>-</sup>	→ CH <sub>3</sub> C <sub>3</sub> N	→ CH <sub>3</sub> C <sub>4</sub> H
AlF	→ C <sub>2</sub> H	→ /-C <sub>3</sub> H	→ C <sub>4</sub> H/C <sub>4</sub> H <sup>-</sup>	→ /-H <sub>2</sub> C <sub>4</sub>	CH <sub>2</sub> CHCN	HCOOCH <sub>3</sub>	CH <sub>3</sub> CH <sub>2</sub> CN
AlCl	→ C <sub>2</sub> O	→ C <sub>3</sub> N	→ C <sub>4</sub> Si	C <sub>2</sub> H <sub>4</sub>	→ CH <sub>3</sub> C <sub>2</sub> H	CH <sub>3</sub> COOH	(CH <sub>3</sub> ) <sub>2</sub> O
→ C <sub>2</sub>	→ C <sub>2</sub> S	→ C <sub>3</sub> O	→ /-C <sub>3</sub> H <sub>2</sub>	CH <sub>3</sub> CN	→ HC <sub>5</sub> N	→ C <sub>7</sub> H	CH <sub>3</sub> CH <sub>2</sub> OH
CH, CH <sup>+</sup>	CH <sub>2</sub>	→ C <sub>3</sub> S	→ c-C <sub>3</sub> H <sub>2</sub>	CH <sub>3</sub> NC	CH <sub>3</sub> CHO	→ H <sub>2</sub> C <sub>6</sub>	→ HC <sub>7</sub> N
CN	HCN	→ C <sub>2</sub> H <sub>2</sub>	→ H <sub>2</sub> CCN	CH <sub>3</sub> OH	CH <sub>3</sub> NH <sub>2</sub>	CH <sub>2</sub> OHCHO	→ C <sub>8</sub> H/C <sub>8</sub> H <sup>-</sup>
CO, CO <sup>+</sup>	HCO, HCO <sup>+</sup>	NH <sub>3</sub>	CH <sub>4</sub>	CH <sub>3</sub> SH	→ c-C <sub>2</sub> H <sub>4</sub> O	→ /-HC <sub>6</sub> H ?	CH <sub>3</sub> C(O)NH <sub>2</sub>
CP	HCS <sup>+</sup>	→ HCCN	→ HC <sub>3</sub> N	→ HC <sub>3</sub> NH <sup>+</sup>	→ H <sub>2</sub> CCHOH	CH <sub>2</sub> CHCHO	
SiC	HOC <sup>+</sup>	HCNH <sup>+</sup>	→ HC <sub>2</sub> NC	→ HC <sub>2</sub> CHO		→ CH <sub>2</sub> CCHCN	
HCl	H <sub>2</sub> O	HNCO	HCOOH	NH <sub>2</sub> CHO			
KCl	H <sub>2</sub> S	HNCS	H <sub>2</sub> CNH	→ C <sub>5</sub> N			
NH	HNC	HOCO <sup>+</sup>	→ H <sub>2</sub> C <sub>2</sub> O	→ /-HC <sub>4</sub> H ?			
NO	HNO	H <sub>2</sub> CO	H <sub>2</sub> NCN	→ /-HC <sub>4</sub> N			
NS	MgCN	H <sub>2</sub> CN	→ HNC <sub>3</sub>	→ c-H <sub>2</sub> C <sub>3</sub> O			
NaCl	MgNC	H <sub>2</sub> CS	SiH <sub>4</sub>	→ H <sub>2</sub> C <sub>2</sub> CNH ?			
OH	N <sub>2</sub> H <sup>+</sup>	H <sub>3</sub> O <sup>+</sup>	H <sub>2</sub> COH <sup>+</sup>	→ C <sub>5</sub> O			
PN	N <sub>2</sub> O	→ c-SiC <sub>3</sub>					
SO, SO <sup>+</sup>	NaCN	CH <sub>3</sub>					
SiN	OCS	→ C <sub>4</sub>					
SiO	SO <sub>2</sub>	CH <sub>2</sub> D <sup>+</sup>					
SiS	→ c-SiC <sub>2</sub>			<u>10 atoms</u>	<u>11 atoms</u>	<u>12 atoms</u>	<u>13 atoms</u>
CS	CO <sub>2</sub>			→ CH <sub>3</sub> C <sub>5</sub> N	→ HC <sub>9</sub> N	→ C <sub>6</sub> H <sub>6</sub> ?	→ HC <sub>11</sub> N
HF	NH <sub>2</sub>			(CH <sub>3</sub> ) <sub>2</sub> CO	→ CH <sub>3</sub> C <sub>6</sub> H	→ C <sub>2</sub> H <sub>5</sub> OCH <sub>3</sub> ?	
SH	H <sub>3</sub> <sup>+</sup>			(CH <sub>2</sub> OH) <sub>2</sub>			
HD	H <sub>2</sub> D <sup>+</sup>			CH <sub>3</sub> CH <sub>2</sub> CHO			
FeO ?	HD <sub>2</sub> <sup>+</sup>						
O <sub>2</sub>	SiCN						
CF <sup>+</sup>	AiNC						
SiH ?	SiNC						
	HCP						

Figure 1.1 List taken from the Cologne Database for Molecular Spectroscopy and Wootten's Database, NRAO (Ref. 5). Last updated July 2007. The red arrows indicate molecules containing two or more C atoms in a chain or ring.

and AlF (see Fig. 1.2).<sup>9,11</sup> Note that many of these molecules include at least one C atom and either metals that are known to be cosmically abundant (*e.g.* Na, Mg, Al) or the semi-metal Si.

It should be noted that although rotational spectra, observed at radio frequencies, has commonly been used to detect interstellar and circumstellar molecular species, C<sub>3</sub> (Ref. 12) and C<sub>5</sub> (Ref. 8) have been detected in IRC+10216 at infrared frequencies. Any molecule composed of a chain of like atoms has no permanent dipole moment, which is necessary for the observation of a rotational spectrum, and thus cannot be detected using radio observations. Consequently, molecules like C<sub>3</sub> and C<sub>5</sub> are concealed from radio astronomers. Very few telescopes have been sent into space that can observe in the infrared (IR) region of the spectrum, but the Spitzer Space Telescope, which can detect infrared vibrational spectra directly, was launched in August 2003.<sup>13</sup> Thus its observations will complement existing data by enabling the detection of molecules without permanent dipole moments like C<sub>3</sub> and C<sub>5</sub>. Since astronomers now have the observational tools, it is vital for infrared molecular spectra to be characterized in a laboratory setting to enable the identification of molecular species Spitzer (and its descendents) may detect.

## 1.2 Metallo-carbohedrenes

Besides their applications to astrophysics, observations of small M<sub>n</sub>C<sub>m</sub> species may aid in understanding the bonding and growth mechanisms of metallo-carbohedrenes, or “metcars”, which are cage-like structures that are composed of metal and carbon atoms.<sup>14,15</sup> Experimental studies<sup>2,3</sup> on the growth mechanisms of Ti<sub>n</sub>C<sub>m</sub> and V<sub>n</sub>C<sub>m</sub> metcars have reported that these larger clusters appear to form from MC<sub>2</sub> “building blocks”, which can be seen in the currently accepted structure<sup>16,17</sup> for the M<sub>8</sub>C<sub>12</sub> metcar (Fig. 1.3).

## Molecules in IRC +10216

CO	CCH	H <sub>2</sub> C <sub>4</sub>	CCS	SiO	NaCl
CS	C <sub>3</sub> H	H <sub>2</sub> C <sub>6</sub>	C <sub>3</sub> S	SiS	NaCN
CN	C <sub>4</sub> H	HCN	C <sub>3</sub> O	SiN	KCl
CP	C <sub>5</sub> H	HC <sub>2</sub> N	C <sub>3</sub> N	SiCN	KCN
HNC	C <sub>6</sub> H	HC <sub>3</sub> N	C <sub>5</sub> N	SiC	MgNC
CH <sub>4</sub>	C <sub>7</sub> H	HC <sub>4</sub> N	c-C <sub>3</sub> H <sub>2</sub>	SiC <sub>2</sub>	MgCN
CH <sub>3</sub> CN	C <sub>8</sub> H	HC <sub>5</sub> N	C <sub>2</sub>	SiC <sub>3</sub>	AlNC
NH <sub>3</sub>	HCCH	HC <sub>7</sub> N	C <sub>3</sub>	SiC <sub>4</sub>	AlF
H <sub>2</sub> S	H <sub>2</sub> CCH <sub>2</sub>	HC <sub>9</sub> N	C <sub>5</sub>	SiH <sub>4</sub>	AlCl
PN					

Figure 1.2 A list of molecules found as of 2006 in the late-type star IRC+10216 (Ref. 9) Note the abundance of C<sub>n</sub> clusters. In columns 2-4, all the molecules have at least two C atoms, with the exception of HCN. Also note the abundance of Si-bearing species (column 5) and metal-bearing species (column 6), many of which also contain one or more C atoms.

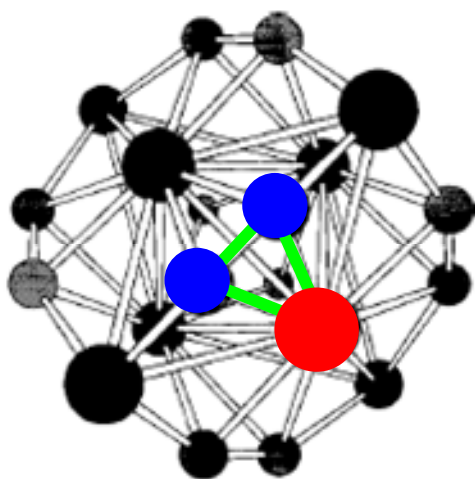


Figure 1.3 Proposed  $M_8C_{12}$  structure, with  $MC_2$  building block highlighted. Metal and carbon atoms are represented with red and blue, respectively. Metcar picture from Ref. 16.

## 1.3 Previous Work

### 1.3.1 Experimental Results

Despite the significance of  $M_nC_m$  species in astrophysics and cosmic evolution, so few of these species have been identified in extraterrestrial environments because they have not yet been observed in a laboratory. A March 2003 list of  $M_nC_m$  ( $n, m > 1$ ) vibrational fundamental identifications,<sup>18</sup> most of which had been identified using photoelectron spectroscopy (PES), was limited to  $TiC_n$  ( $n = 2-5$ ),<sup>19</sup> cyclic  $MC_3$  ( $M=Sc, V-Ni$ ),<sup>20</sup>  $Co_2C_n$  ( $n = 2,3$ ),  $V_2C_n$  ( $n = 2-4$ ),<sup>3</sup>  $NbC_n$  ( $n = 2-7$ ),<sup>21</sup> and  $MC_2$ , ( $M = Sc, V-Co$ ).<sup>22</sup> Clearly, additional vibrational fundamental measurements are needed.

Wang and Li<sup>20,22</sup> have used PES to characterize the electronic structures of first row transition metal–carbon clusters,  $MC_n$ , but only for  $n = 2$  and 3. PES results, however, can only give vibrational frequencies within  $\pm 50 \text{ cm}^{-1}$ , which is insufficient accuracy for spectroscopic identification in astrophysical sources. Unlike PES, Fourier transform infrared (FTIR) spectroscopy combined with matrix isolation in Ar, as used in the TCU Molecular Physics Lab, can give vibrational frequencies that are usually within 1% of the gas phase vibrational frequencies,<sup>23</sup> which can be sufficient for astrophysical detection. For example, the astrophysical detection<sup>1</sup> of  $C_4$  has been made on the basis of FTIR measurements<sup>24</sup> performed in the TCU Molecular Physics Lab. Furthermore, PE spectra cannot always definitively determine molecular structures, *e.g.*  $NiC_3$  and  $CoC_3$ . Although these species have been observed,<sup>20</sup> the PE spectra were too congested to resolve any vibrational features so molecular geometry determinations were impossible. To unambiguously identify vibrational fundamentals and determine structures of novel molecules, much more extensive infrared measurements are needed.

### 1.3.2 Theoretical Results

Another reason for the importance of experimental measurements is the symbiotic relationship between experimental measurements and theoretical predictions. Theoretical models cannot always definitively determine the ground state structure of a molecule when two or more isomers are predicted to be close in energy. For example, close-lying fan and linear isomers have been predicted for  $\text{CrC}_3$ ,<sup>25</sup> and three close-lying isomers: kite ( $C_{2v}$ ), fanlike ( $C_{2v}$ ) and linear have been predicted for  $\text{AlC}_3$ .<sup>26</sup> In both of these cases, the energy differences between the various isomers have been predicted to be within a few kcal/mol, which is insufficient for structure determination on the basis of current theoretical calculations alone.

Despite problems in determining ground state structures when two or more isomers are predicted to be close in energy, theoretical predictions have been essential in band identifications when two or more molecules have symmetries that can produce similar  $^{13}\text{C}$  isotopic shift patterns, such as fanlike  $\text{MC}_3$  and linear  $\text{MC}_3\text{M}$  species, which both have two equivalent C atoms and one unique C atom (see Chapter II, Section 2.4). A case in which theoretical calculations have been used to discriminate between two structures is presented in Chapter V, which details the observation of two  $\text{Al}_n\text{C}_m$  species.

## 1.4 The Dissertation Research

Because of the complementary nature of theoretical predictions and experimental measurements, studies in the TCU Molecular Physics Lab use both theoretical methods and experimental techniques to unambiguously identify vibrational fundamentals and determine molecular structures. Previous investigations have focused on silicon-carbon ( $\text{Si}_n\text{C}_m$ ),<sup>27-30</sup> germanium-carbon ( $\text{Ge}_n\text{C}_m$ ),<sup>31,32</sup> and mixed germanium-carbon-silicon ( $\text{Ge}_n\text{C}_m\text{Si}_l$ )<sup>33</sup> species, successfully employing FTIR spectroscopy, matrix isolation, and  $^{13}\text{C}$  isotopic substitution

techniques in conjunction with DFT calculations of vibrational fundamentals and isotopic shifts. It should be noted that all theoretical calculations presented in this dissertation were done by the author, except in a few marked cases, in which they were done by Rittby.

Many of the same techniques that have been effectively used in the production of novel Group IV clusters have also been applied in the present investigation on metal–carbon clusters (see Chapter II); however, the current project has necessitated the design and construction of a new experimental apparatus and a new approach to the rod fabrication process. The design modifications and benefits of the new apparatus are discussed in Chapter II. The disadvantages of the existing sintering process for the preparation of  $^{13}\text{C}$  enriched rods that has been developed in the TCU Molecular Physics Lab<sup>34</sup> along with a new technique employing unsintered “soft rods”, which has been developed as part of this dissertation research, is explained in Chapter II. The advantages of this new technique, in identifying novel chromium–, cobalt–, aluminum–, and copper–carbon clusters, respectively, are presented in Chapters III–VI.

Although previous PES reports on transition metal–carbon clusters exist,<sup>18</sup> the FTIR matrix measurements presented in this dissertation are the first reported for transition metal–carbon species in general, and for chromium–, cobalt–, and copper–carbon species in particular. The first identification of a vibrational fundamental of  $\text{CrC}_3$  and the determination of its molecular geometry is presented in Chapter III. In Chapter IV, an investigation of  $\text{CoC}_3$  is discussed in which the structure has also been established and one of its vibrational modes has been identified for the first time. The theoretical investigation presented for  $\text{CoC}_3$  is also the first for this species. Only one prior FTIR matrix study on  $\text{Al}_n\text{C}_m$  ( $n, m = 1, 2$ ) clusters has been published<sup>35</sup> and until the present research, there had been no observation of  $\text{Al}_n\text{C}_m$  species for  $m > 2$ . Two novel  $\text{Al}_n\text{C}_m$  molecules,  $\text{AlC}_3$  and  $\text{AlC}_3\text{Al}$ , have been detected and the results are presented in Chapter V. The geometries of both molecules have been clearly resolved, as well as



the assignment of one mode of  $AlC_3$  and two, of  $AlC_3Al$ . It should be noted that this is the first investigation, either theoretical or experimental, on the  $AlC_3Al$  molecule. The first experimental investigation on any  $Cu_nC_m$  species is presented in Chapter VI, in which vibrational spectrum of  $CuC_3$  has been detected, resulting in the identification of one of its vibrational fundamentals, and its structure has also been established. Moreover, the theoretical investigation presented for  $CuC_3$  is the first for this species. Additionally, tentative assignments of vibrational spectra for  $CrC_4$  and  $AlC_4Al$ , along with preliminary results of studies on  $V_nC_m$  species, are discussed in Chapter VII. Finally, Chapter VIII summarizes the conclusions of the present research and proposes directions for future investigations on metal–carbon clusters.

## CHAPTER II

### EXPERIMENTAL PROCEDURES AND TECHNIQUES

#### 2.1 Equipment Construction

A new experimental apparatus for the preparation of matrix samples was constructed and tested before experiments on metal–carbon species were performed. The apparatus is comprised of two parts (see Fig. 2.1): (1) the Ar delivery system, which controls the Ar flow into the sample chamber during laser ablation; and (2) the sample chamber system, containing the closed-cycle refrigeration system (ARS, Displex) and the laser ablation chamber (Fig. 2.2). While some components for these systems could be purchased, many were custom-built in the TCU Machine Shop.

Pieces of the apparatus were redesigned to provide smoother interior surfaces, fewer connections, reduce the volume that needed to be evacuated, and speed evacuation, resulting in shorter turnaround times between experiments. In addition, light-weight aluminum frames were built to support the Ar delivery and sample chamber systems, making the system more mobile and easier to level during optical alignment than were previous models.

The experimental apparatus was tested by performing an experiment in which the products from graphite evaporation were trapped in Ar at  $\sim 10$  K. This verified that (1) the vacuum pressure could reach the  $\leq 10^{-7}$  Torr required during experiments, (2) impurities, *e.g.* H<sub>2</sub>O, in the system were minimized, (3) the closed-cycle refrigeration system was cooling the gold mirror in the laser ablation chamber to  $\sim 10$  K, and (4) the systems were correctly leveled and the optics were properly aligned to maximize the incident light that passed through the system and reached the detector.

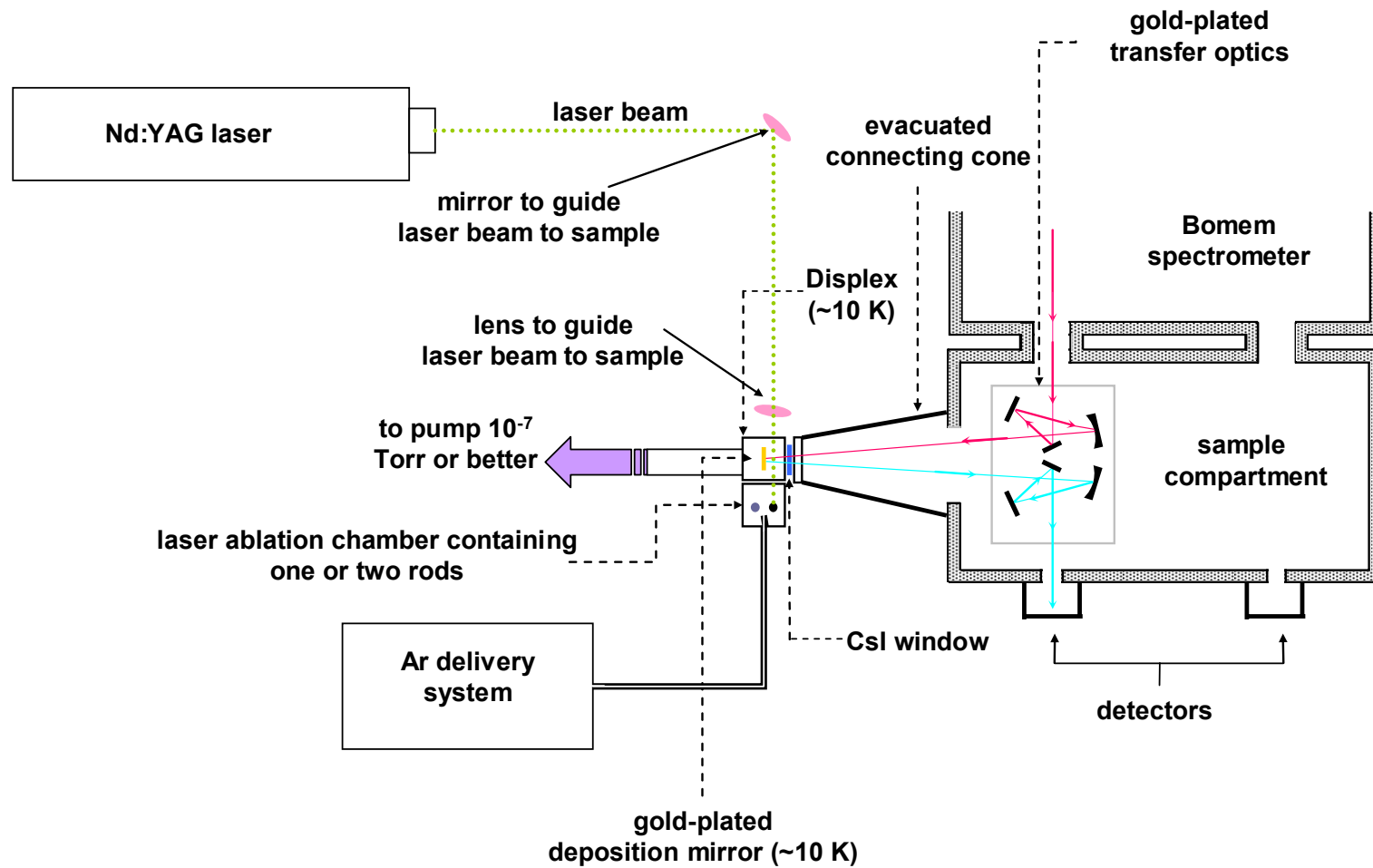


Figure 2.1 Schematic of the experimental apparatus.

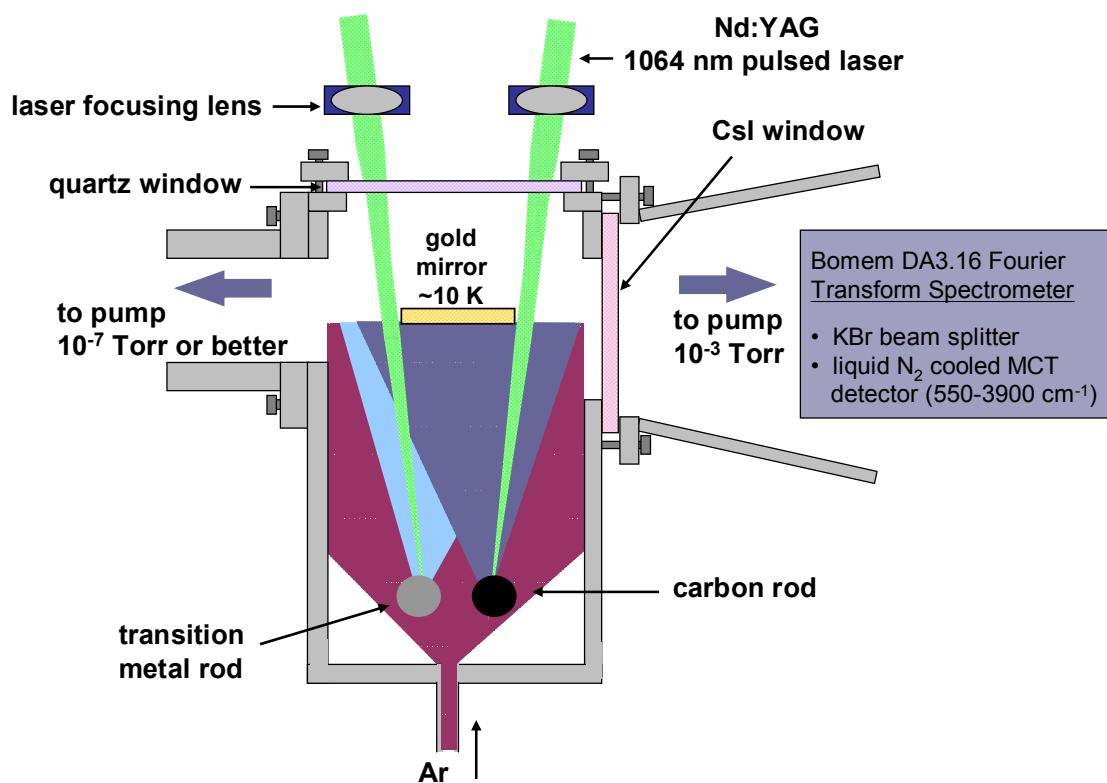


Figure 2.2 Schematic of the laser ablation chamber.

## 2.2 Experimental Conditions

Metal–carbon clusters were produced by the simultaneous ablation of carbon and metal rods, which were continually rotated and translated in order to provide clean surfaces for ablation using two 1064 nm Nd:YAG pulsed lasers (Spectra Physics). The vacuum system pressure was maintained at  $\leq 10^{-7}$  Torr during experiments prior to deposition to minimize the amounts of impurities, *e.g.* H<sub>2</sub>O, in the system. The evaporated products were condensed in solid Ar (99.995%, Matheson Tri-Gas) on a gold mirror held at  $\sim 10$  K by a closed cycle refrigeration system (ARS, Displex) [see Figs. 2.1 and 2.2].

Experimental conditions such as the laser power, the laser focus, and the Ar flow rate, explained below, were adjusted to favor the production of small  $C_n$  chains, predominantly  $C_3$ ,<sup>36</sup> which facilitated the formation of  $M_nC_3$  species.

- The laser power that was used on the metal and carbon rods is a very important experimental condition that could be adjusted separately for each rod, which provided several benefits. (1) Using a low laser power<sup>37</sup>  $\leq 1.0$  W on the C rod produces smaller carbon chains, *e.g.*  $C_3$ . (2) The C rods were fabricated in the lab and were not as durable during laser ablation as commercially produced rods, so using lower laser powers slowed their degradation. Moreover, as <sup>13</sup>C enrichment in the C rods is increased, the durability of the rods decreases and it is necessary to decrease the laser power accordingly. (3) In addition to using the laser power on the C rod to control the size of the  $C_n$  clusters produced, the laser power on the metal rod could be used in an analogous way. The metal rods used in experiments were commercially produced (ESPI) and were very durable, requiring a high laser power,  $\sim 2.0$ - $3.0$  W, for ablation. Using a laser power beyond  $>3.0$  W on the metal rod was detrimental to  $C_n$  cluster production, presumably because  $M_n$  clusters as opposed to single metal atoms were

being ablated, which decreased the throughput and resulted in a poor signal-to-noise ratio.

Keeping the laser power in the 2.0-3.0 W range balanced the C and metal ablation making it unlikely that more than one metal atom would attach to a  $C_n$  cluster. The exception to this, however, as will be discussed in Chapters V and VII, is Al ablation in which  $Al_2C_n$  ( $n=2-4$ ) species were produced.

- The **laser focus** refers to how tightly or loosely focused the laser beam is on the rod. When the laser beam is loosely focused ( $\sim 3.0$  mm diameter), the beam power is spread over a greater area and the laser does not bore as deeply into the rod. On the C rod, using a loosely focused as opposed to a tightly focused ( $\sim 1.0-1.5$  mm diameter) beam slowed its degradation and allowed for longer periods of ablation. Since the metal rods were more durable, a tight focus was used to concentrate the beam.
- The **Ar flow rate** is defined as how quickly the Ar is allowed to flow into the sample chamber during laser ablation of the metal and C rods. Higher Ar flow rates yield a dilute matrix containing few clusters, while lower flow rates produce higher concentrations of clusters. The Ar flow also serves to sweep the ablated products onto the gold mirror. If the Ar flow rate is too low, only a small percentage of the ablated products may be swept onto the gold mirror as was seen in a few early experiments in which an Ar flow rate of  $<0.5$  mm/min was used and few clusters were observed. The Ar flow rate used in all of the experiments was  $\sim 1.0$  mm/min.

Unless otherwise noted,  $M_nC_m$  clusters were created by simultaneous ablation of a soft (i.e. unbaked) carbon rod and a metal rod. Three soft carbon rods were prepared: (1) a pure  $^{12}C$  rod, (2) one with 20% and (3) one with 30% nominal  $^{13}C$  enrichment. Typical total lengths of deposition were  $\sim 30-90$  min. FTIR absorption spectra were recorded at a resolution of  $0.2$   $cm^{-1}$

over the range of 500–4000  $\text{cm}^{-1}$  using a Bomem DA 3.16 Fourier transform infrared (FTIR) spectrometer equipped with a KBr beamsplitter and a liquid nitrogen-cooled MCT (Hg–Cd–Te) detector. All reported frequencies were measured to  $\pm 0.1 \text{ cm}^{-1}$ . Additional details of the optical system have been reported previously.<sup>38</sup>

### 2.3 Rod Preparation

In the TCU Molecular Physics Lab, carbon rods containing various ratios of  $^{12}\text{C}$  and  $^{13}\text{C}$  have been fabricated using a two-step sintering process in which the  $^{12}\text{C}/^{13}\text{C}$  powder mixture is first pressed into a soft rod and then baked at  $\sim 2100 \text{ }^\circ\text{C}$  for 20–30 days.<sup>34</sup> Unfortunately, only 12–15 sintered rods can be fabricated per year using this process, which hinders the performing of experiments. Since very few  $M_nC_m$  species have been studied and the experimental conditions for their production are unknown, a month-long investment to fabricate a carbon or metal–carbon rod that may or may not produce  $M_nC_m$  clusters is unappealing. Experimental conditions pertaining to rod fabrication, *e.g.*  $^{13}\text{C}$  or metal enrichments, cannot be easily modified in sintered rods, so soft, *i.e.* unbaked, C rods have been used in the current research, which has facilitated the testing of various rod preparation conditions thus increasing the number of experiments that could be done.

The new technique eliminates the need for baking the carbon rod, except in cases where contaminant species such as CO or CO<sub>2</sub> are noted in FTIR spectra and can be traced back to carbon rod evaporation. The soft rods are fabricated from various ratios of  $^{12}\text{C}$  (99.9995%, Alfa Aesar) and  $^{13}\text{C}$  (99.3%, Isotec) powders, which are ground together to form a homogeneous mixture and then pressed under a pressure of  $\sim 4.5 \times 10^5 \text{ kPa}$ . Even when the powder is baked overnight, this new technique can fabricate a rod in less than one day.

Another modification to the previous rod fabrication process is the use of a new, more compact press with smaller, lighter dies. The previously used press, housed on the second floor

of the TCU Machine Shop, has a cube-shaped stainless steel die that is  $\sim 5'' \times 5'' \times 5''$ . The entire assembly weighs over 50 pounds, making it very difficult to maneuver and disassemble to remove the fragile soft rod without destroying it. The compact press that is currently being used fits on one corner of a lab table and has a cylindrical die,  $\sim 2.75''$  tall and  $\sim 3''$  in diameter, that can be held in one hand. The compact press can generate pressures that are equal or greater to the pressures of the TCU Machine Shop press, so the carbon rod strengths are comparable. The main disadvantage to the current technique is that the cylindrical die is one solid piece, limiting soft rods to  $\leq 50\%$   $^{13}\text{C}$  enrichment, but a solution to this problem is proposed in Chapter VIII.

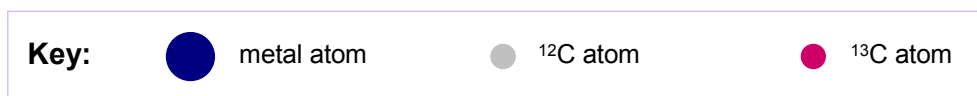
These soft rods can provide very consistent results if powder measuring and mixing is done carefully. Chapters III, IV, and VI, respectively, detail how these rods enabled identifications of one vibrational mode of each  $\text{CrC}_3$ ,  $\text{CoC}_3$ , and  $\text{CuC}_3$ ; Chapter V discusses the soft rods that were used to observe one mode of  $\text{AlC}_3$  and two, of  $\text{AlC}_3\text{Al}$ .

## 2.4 Isotopic Shifts

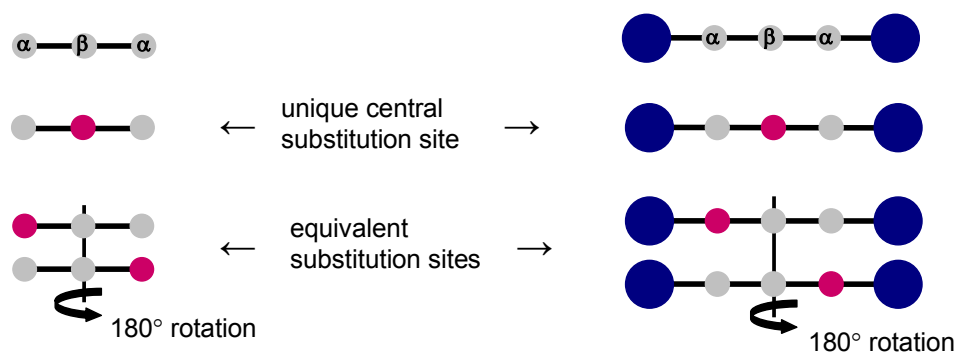
$M_n\text{C}_m$  vibrational frequency assignments are facilitated by the comparison of fundamental frequency and  $^{13}\text{C}$  shifts measurements in FTIR spectra with the results of DFT predictions. Isotopic shifts are crucial for unambiguous species identification and structure determination. Some simple molecules, detailed below, are shown in Fig. 2.3 to illustrate how  $^{13}\text{C}$  isotopic shifts are useful.

For example, using 10%  $^{13}\text{C}$  enrichment, the strongest band of  $\text{C}_3$  will correspond to the vibrational frequency of the isotopomer containing three  $^{12}\text{C}$  atoms or  $^{12}\text{C}_3$ . Because of the symmetry of linear  $\text{C}_3$ , *i.e.* a  $180^\circ$  rotation about the center of the molecule leaves the molecule unchanged [see Fig. 2.3(a)], there is a unique C atom in the center and two equivalent C atoms on either end of the molecule. Two  $^{13}\text{C}$  shifts are therefore observed, one corresponding to a  $^{13}\text{C}$  substitution on the unique C atom and one corresponding to a substitution on the two equivalent





(a) Centrosymmetric molecules (e.g.  $\text{C}_3$ ,  $\text{MC}_3\text{M}$ )



(b) Non-centrosymmetric molecules (e.g.  $\text{MC}_3$ )

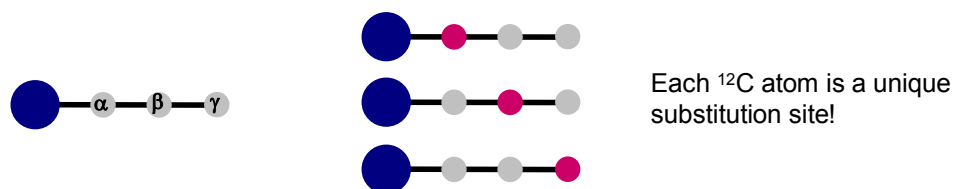


Figure 2.3 Illustration of single  $^{13}\text{C}$  isotopic substitutions in (a) centrosymmetric linear molecules, e.g.  $\text{C}_3$  and  $\text{MC}_3\text{M}$ , and (b) in non-centrosymmetric linear molecules, e.g.  $\text{MC}_3$ .

C atoms, with an intensity ratio of 1:2, assuming complete scrambling of the  $^{12}\text{C}$  and  $^{13}\text{C}$  atoms. With 10%  $^{13}\text{C}$  enrichment, the absorptions of the 12-13-12 and 13-12-12 isotopomers will therefore be ~10% and ~20%, respectively, of the intensity of the  $^{12}\text{C}_3$  band.

Adding a metal atom to one end of a  $\text{C}_n$  chain changes the symmetry of the molecule so it is no longer centrosymmetric. In this case, a rotation of  $180^\circ$  around the molecular center does not leave the molecule unchanged, thus each C atom is unique and produces a shift when substituted with  $^{13}\text{C}$  [Fig. 2.3(b)]. A linear  $\text{MC}_3$  species, therefore, would have three  $^{13}\text{C}$  shift bands of equal intensity.

In contrast, if a metal atom were attached to each end of a  $\text{C}_n$  chain,  $\text{MC}_n\text{M}$ , then the molecule becomes centrosymmetric again, similar to a linear  $\text{C}_n$  molecule [Fig. 2.3(a)]. In a linear  $\text{M-C}_\alpha\text{-C}_\beta\text{-C}_\alpha\text{-M}$  species, for example, the leftmost and rightmost C atoms,  $\text{C}_\alpha$ , are equivalent (just as for linear  $\text{C}_3$ ), producing one isotopic shift that has twice the intensity of the shift produced by  $^{13}\text{C}$  substitution on the unique central C atom,  $\text{C}_\beta$ .

**CHAPTER III**  
**FOURIER TRANSFORM INFRARED ISOTOPIC STUDY OF LINEAR CrC<sub>3</sub>:**  
**IDENTIFICATION OF THE  $\nu_1(\sigma)$  MODE**

**3.1. Introduction**

This chapter reports an FTIR study of the vibrational spectrum and structure of CrC<sub>3</sub>, the first results from investigations recently initiated by the TCU Molecular Physics Lab on small transition metal–carbon species. The spectroscopy and structures of small transition-metal carbon clusters are of considerable interest in the context of the properties of larger metallocarbohedrenes (metcars), the apparent catalytic effect of transition metals in the formation of nanotubes, and the potential for the formation of other novel transition metal-carbon nanomaterials. In the first systematic investigations of small-transition-metal carbon clusters,<sup>20,22</sup> the MC<sub>2</sub><sup>−</sup> and MC<sub>3</sub><sup>−</sup> anions (M=Sc, V–Ni) were studied using photoelectron spectroscopy (PES) and density functional theory (DFT), deriving information on their structures, electronic states, and M-C stretching vibrational frequencies. This seminal work was followed by a more detailed examination of the monochromium carbides, CrC<sub>n</sub><sup>−</sup> and CrC<sub>n</sub> (n=2-8).<sup>25</sup>

The investigation of CrC<sub>n</sub><sup>−</sup> and CrC<sub>n</sub> (n=2-8) clusters<sup>25</sup> benefited from better resolved PES spectra than in earlier work<sup>20</sup> and a much more extensive theoretical study, including calculations with the Becke exchange, Perdew-Wang correlation (BPW91)<sup>39</sup> functional and a 6-311+G\* basis set for a range of cluster sizes (n≥3). A particular focus of the work was the competition between fanlike (C<sub>2v</sub>) and linear structures [see Fig. 3.1(a)]. In the case of CrC<sub>3</sub><sup>−</sup>, DFT calculations predicted that the <sup>4</sup>B<sub>1</sub> fanlike (C<sub>2v</sub>) isomer and the linear <sup>4</sup>Σ<sup>−</sup> isomer are nearly degenerate with the fanlike form lying only 0.05 eV lower in energy. It was argued that the

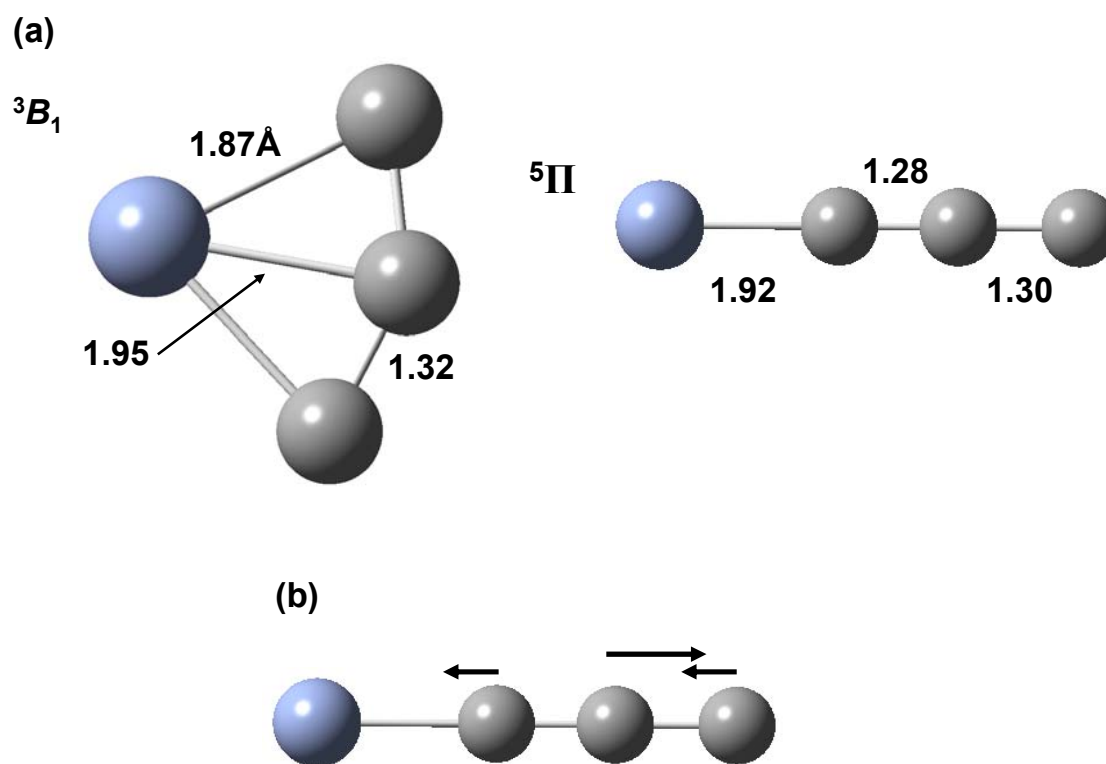


Figure 3.1 (a) The  ${}^3B_1$  fanlike ( $C_{2v}$ ) and  ${}^5\Pi$  linear isomers of  $\text{CrC}_3$ . DFT B3LYP/6-311+G(3df) predictions for their geometric parameters are given in Angstroms (Å). The predicted principal nuclear displacements of the atoms for the  $\nu_1(\sigma)$  mode of  ${}^5\Pi$  linear  $\text{CrC}_3$  are shown in (b).

calculated electron affinities of 1.69 and 1.94 eV for the fanlike and linear isomers, respectively, were in reasonable agreement with values of 1.474 and 1.936 eV measured for bands in the observed PE spectrum, and thus provided evidence of both isomers, although the authors noted that the agreement between the DFT results and the experimental spectra for the fanlike isomer was not as good as for the linear isomer. Observing that the abundance of the fanlike isomer increased for hotter source conditions, the authors concluded that the linear isomer is probably slightly more stable, contrasting with DFT predictions favoring the fanlike isomer. Observed structure in the PES bands corresponded to metal-carbon vibrational frequencies of  $700\pm 30$  and  $540\pm 20$   $\text{cm}^{-1}$  for the ground states of the fanlike and linear  $\text{CrC}_3^-$  isomers, respectively. In the case of neutral  $\text{CrC}_3$ , the DFT calculations predicted that the  ${}^3B_1$  fanlike structure ( $C_{2v}$ ) lies 0.30 eV lower than the  ${}^5\Pi$  linear structure.

Previously the TCU Molecular Physics Lab has reported FTIR and DFT studies on  $\text{Si}_n\text{C}_m$ ,<sup>27–30,40–43</sup>  $\text{Ge}_n\text{C}_m$ ,<sup>31,32</sup> and  $\text{GeC}_n\text{Si}$ <sup>33</sup> species produced by trapping the ablated products of Si and/or Ge with carbon in solid Ar. In these studies, comparison of measured and predicted isotopic shifts is crucial for species identification, assignment of vibrational fundamentals, and for structure determination. Similar techniques have been applied in the present study on chromium-carbon ( $\text{Cr}_n\text{C}_m$ ) clusters. In the case of pure  $\text{C}_n$  chains and rings, earlier studies have shown that  $\text{C}_3$  is the dominant  $\text{C}_n$  species produced by trapping the products of  ${}^{12}\text{C}$  ablation at laser power levels  $< 1.5$  W in solid Ar. As a result, subsequent annealing of the matrix predominantly generates  $\text{C}_{3n}$  species, *e.g.*  $\text{C}_6$  and  $\text{C}_9$ , which are multiples of the  $\text{C}_3$  unit.<sup>44</sup>

Considering this preference for the production of  $\text{C}_3$  clusters, and the successful earlier addition of Si and Ge to  $\text{C}_3$  clusters to form  $\text{SiC}_3\text{Si}$ ,<sup>43</sup>  $\text{GeC}_3\text{Ge}$ ,<sup>31</sup> and  $\text{GeC}_3\text{Si}$ ,<sup>33</sup> it might be expected that similar experimental conditions would enable reactions between Cr atoms and  $\text{C}_3$  chains.

The specific objective of the present work has been to look for vibrational fundamentals of  $\text{CrC}_3$  in the infrared. Although as discussed, the previous DFT and PES studies indicated a preference for the ( $C_{2v}$ ) fanlike structure for neutral  $\text{CrC}_3$ , the present study reports instead the observation of the linear species. The  $\nu_1(\sigma)$  C-C stretching mode of linear  $\text{CrC}_3$  has been detected at  $1789.5 \text{ cm}^{-1}$ , which is supported by measurements of  $^{13}\text{C}$ -substituted isotopic shifts together with DFT predictions.

### 3.2. Theoretical Calculations

DFT calculations carried out as part of earlier PES studies<sup>20,25</sup> on  $\text{CrC}_3$  have predicted a linear ( $^5\Pi$ ) isomer of  $\text{CrC}_3$  lying within 0.3 eV of the energetically favored  $C_{2v}$  ( $^3B_1$ ) structure, although the observed thermal behavior of the PES bands suggested that the linear structure might actually be the more stable of the two. In the present work, using the GAUSSIAN 03 program suite,<sup>45</sup> DFT calculations of the vibrational fundamentals and IR intensities for both the fanlike  $C_{2v}$  ( $^3B_1$ ) and linear ( $^5\Pi$ ) structures of  $\text{CrC}_3$  were done by Rittby.<sup>46</sup> The three parameter Becke exchange functional with the Lee, Yang, and Parr correlation (B3LYP)<sup>47</sup> was used in conjunction with the 6-311+G(3df) basis set.

The frequencies for both the linear and  $C_{2v}$  isomers of  $\text{CrC}_3$  are shown in Table 3.1. The results for the vibrational fundamentals of ( $C_{2v}$ )  $\text{CrC}_3$  are in good agreement with those published earlier.<sup>20</sup> Geometric parameters for the two isomers are given in Fig 3.1(a). In the case of the linear isomer, the predicted vibrational frequencies and IR intensities shown in Table 3.1 indicate the  $\nu_1(\sigma)$  mode should be the most intense fundamental. The predicted nuclear displacements of the  $\nu_1(\sigma)$  mode of linear  $\text{CrC}_3$  are shown in Fig. 3.1(b). Since the isotopic shift pattern in the FTIR spectrum observed in the present study indicates that a linear structure is responsible,  $^{13}\text{C}$  isotopic shifts have been calculated for the linear ( $^5\Pi$ )  $\text{CrC}_3$  isomer.

Table 3.1: DFT B3LYP/6-311+G(3df) predicted vibrational frequencies ( $\text{cm}^{-1}$ ) and band intensities (km/mol) for the linear ( $^5\Pi$ ) and fanlike ( $^3B_1$ ) isomers of  $\text{CrC}_3$ .

$\text{CrC}_3$ Isomer	Vibrational Mode	Frequency ( $\text{cm}^{-1}$ )	IR intensity (km/mol)
$^5\Pi$ Linear	$\nu_1(\sigma)$	1852	434
	$\nu_2(\sigma)$	1284	13
	$\nu_3(\sigma)$	385	8
	$\nu_4(\sigma)$	310/395 <sup>a</sup>	26/14
	$\nu_5(\pi)$	122/120 <sup>a</sup>	4/~0
$^3B_1$ Fanlike ( $C_{2v}$ )	$\nu_1(a_1)$	1306	8
	$\nu_2(a_1)$	816	2
	$\nu_3(a_1)$	544	63
	$\nu_4(b_1)$	514	11
	$\nu_5(b_2)$	1473	~0
	$\nu_6(b_2)$	381	49

<sup>a</sup>For the bending modes of the  $^5\Pi$  state both Renner-Teller components are reported.

### 3.3. Experimental Procedures

$\text{Cr}_n\text{C}_m$  clusters were produced by the simultaneous ablation of Cr and C rods using two Nd:YAG pulsed lasers (Spectra Physics) operating in pulsed mode at 1064 nm. The products were condensed in solid Ar (Matheson, 99.9995%) on a gold mirror held at  $\sim 10$  K by a closed cycle refrigeration system (ARS, Displex) in a vacuum of  $10^{-7}$  Torr or better during experiments.

The carbon rods were fabricated using various mixtures of  $^{12}\text{C}$  (Alfa Aesar, 99.9995%) and  $^{13}\text{C}$  (Isotec, 99.3%) powders, pressed into rods. The typical length of deposition was  $\sim 40$  min. FTIR absorption spectra were recorded at a resolution of  $0.2\text{ cm}^{-1}$  over the range  $400\text{--}4000\text{ cm}^{-1}$  using a Bomem DA 3.16 Fourier transform spectrometer equipped with a KBr beamsplitter and a liquid nitrogen-cooled MCT detector. Details of the optical system have been reported previously.<sup>38</sup>

In experiments done in the TCU Molecular Physics Lab, the successful identification of molecular species depends heavily on  $^{13}\text{C}$  isotopic shift measurements. Previously,  $^{13}\text{C}$  shifts have been used to identify a variety of  $\text{C}_n$  species bonded with Ge and Si such as  $\text{SiC}_7$ ,<sup>30</sup>  $\text{SiC}_9$ ,<sup>29</sup>  $\text{GeC}_3\text{Ge}$ ,<sup>31</sup>  $\text{GeC}_3\text{Si}$ ,<sup>33</sup>  $\text{GeC}_7$  and  $\text{GeC}_9$ .<sup>32</sup> Isotopic shifts permit ready distinction between linear structures such as  $\text{SiC}_4\text{Si}$  (Ref. 28) and cyclic structures such as planar pentagonal  $\text{Si}_3\text{C}_2$ .<sup>27</sup> In the present work, isotopic experiments employed a C rod with various  $^{13}\text{C}$  enrichments to enhance particular isotopomers.

### 3.4. Results and Discussion

In order to identify potential candidates for vibrational fundamentals of  $\text{Cr}_n\text{C}_m$  species, spectra were recorded for the simultaneous ablation of Cr and  $^{12}\text{C}$  rods. Evaporation of the Cr rod produced no absorptions in the  $400\text{--}4000\text{ cm}^{-1}$  region, but as shown in Fig. 3.2(b), the  $^{12}\text{C}$  rod gave a rich spectrum in which many of the absorptions have been previously identified.<sup>48,49</sup>



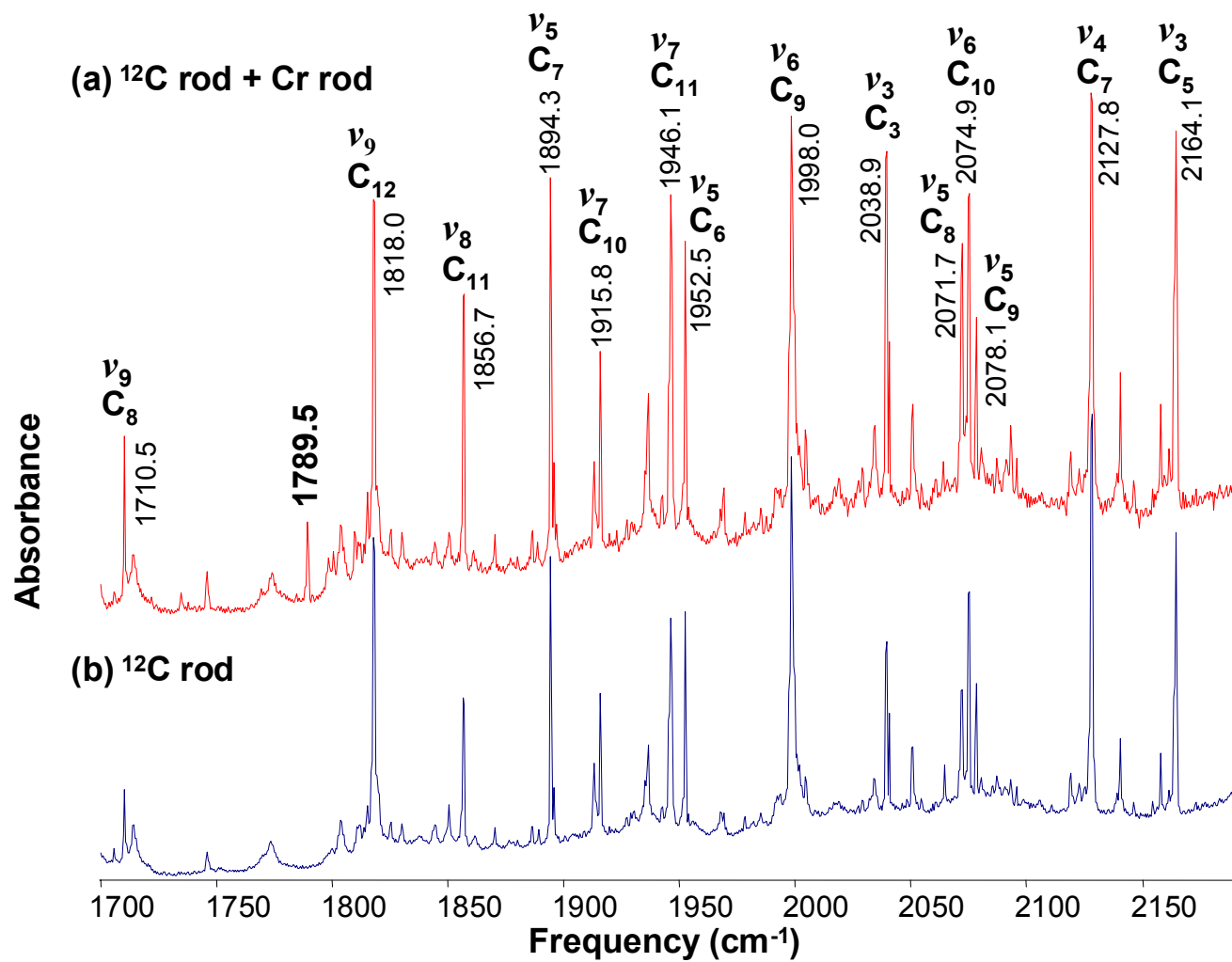


Figure 3.2 FTIR spectra produced by (a) dual ablation of Cr and <sup>12</sup>C rods and (b) a pure <sup>12</sup>C rod, for comparison.

Simultaneous ablation of Cr and  $^{12}\text{C}$  rods produced a new absorption at  $1789.5\text{ cm}^{-1}$  [Fig. 3.2(a)] that was absent from the  $^{12}\text{C}$  rod spectrum. Potential carriers for this band thus appear to be limited to either a  $\text{Cr}_n\text{C}_m$  species or a Cr-bearing contaminant such as  $\text{CrCO}$ ,  $\text{CrH}_2$ , or  $\text{CrCO}_2$ . The latter possibility is unlikely, however, as the chromium-carbon spectrum exhibits only very weak absorptions of water and of the contaminants  $\text{CO}$ , and  $\text{CO}_2$  arising from the graphite. Moreover, the vibrational frequencies of other potential Cr contaminant species are well known.  $\text{CrOCO}^{50}$  has vibrational fundamentals at  $1735.6$ ,  $721.0$ , and  $716.1\text{ cm}^{-1}$ ;  $\text{OCrCO}^{50}$  at  $2014.4$  and  $866.3\text{ cm}^{-1}$ ;  $\text{CrCO}^{51}$  at  $1975.3\text{ cm}^{-1}$ ;  $\text{HCrOH}^{52}$  at  $1639.9$ ,  $674.1$ , and  $433.8\text{ cm}^{-1}$ ; and  $\text{CrH}_2^{53}$  at  $1650.9$ , and  $1614.9\text{ cm}^{-1}$ . While the  $\text{OCrCO}$  band at  $866.3$  and the  $\text{CrOCO}$  pair at  $721.0$  and  $1735.6\text{ cm}^{-1}$  appear in the Cr/C spectrum, they are very weak when compared to the feature at  $1789.5\text{ cm}^{-1}$ . A pure  $\text{Cr}_n\text{C}_m$  molecule is therefore its most likely carrier although additional evidence suggests that it is a relatively small species.

If the molecule responsible for the  $1789.5\text{ cm}^{-1}$  band involved Cr bonded to a larger  $\text{C}_n$  ( $n \geq 6$ ) species, one might expect the absorption to become more intense during annealing as the monomer and small  $\text{C}_n$  units diffused through the matrix and combined to form larger species. Typically, annealing facilitates the reaction of small  $\text{C}_n$  clusters to form larger molecules, principally multiples of the  $\text{C}_3$  unit, such as  $\text{C}_6$ ,  $\text{C}_9$ , and  $\text{C}_{12}$ . As shown in Fig. 3.2(a) the  $\nu_3(\sigma_u) = 2038.9\text{ cm}^{-1}$  fundamental of  $\text{C}_3$  is one of the strongest features. However, while annealing increased the intensities of the bands of longer  $\text{C}_n$  chains, it did not significantly increase the intensity of the  $1789.5\text{ cm}^{-1}$  band, so a relatively small species seems to be the likely carrier.

Figure 3.3(b) shows the spectrum produced by simultaneously evaporating a Cr rod and a 15%  $^{13}\text{C}$ -enriched C rod.  $^{13}\text{C}$  isotopic shifts should appear to the low frequency side of the  $1789.5\text{ cm}^{-1}$  band, and at this enrichment, absorptions of single  $^{13}\text{C}$ -substituted isotopomers should be most prominent. Three bands appearing in this region are readily identified as  $\text{CrOCO}$

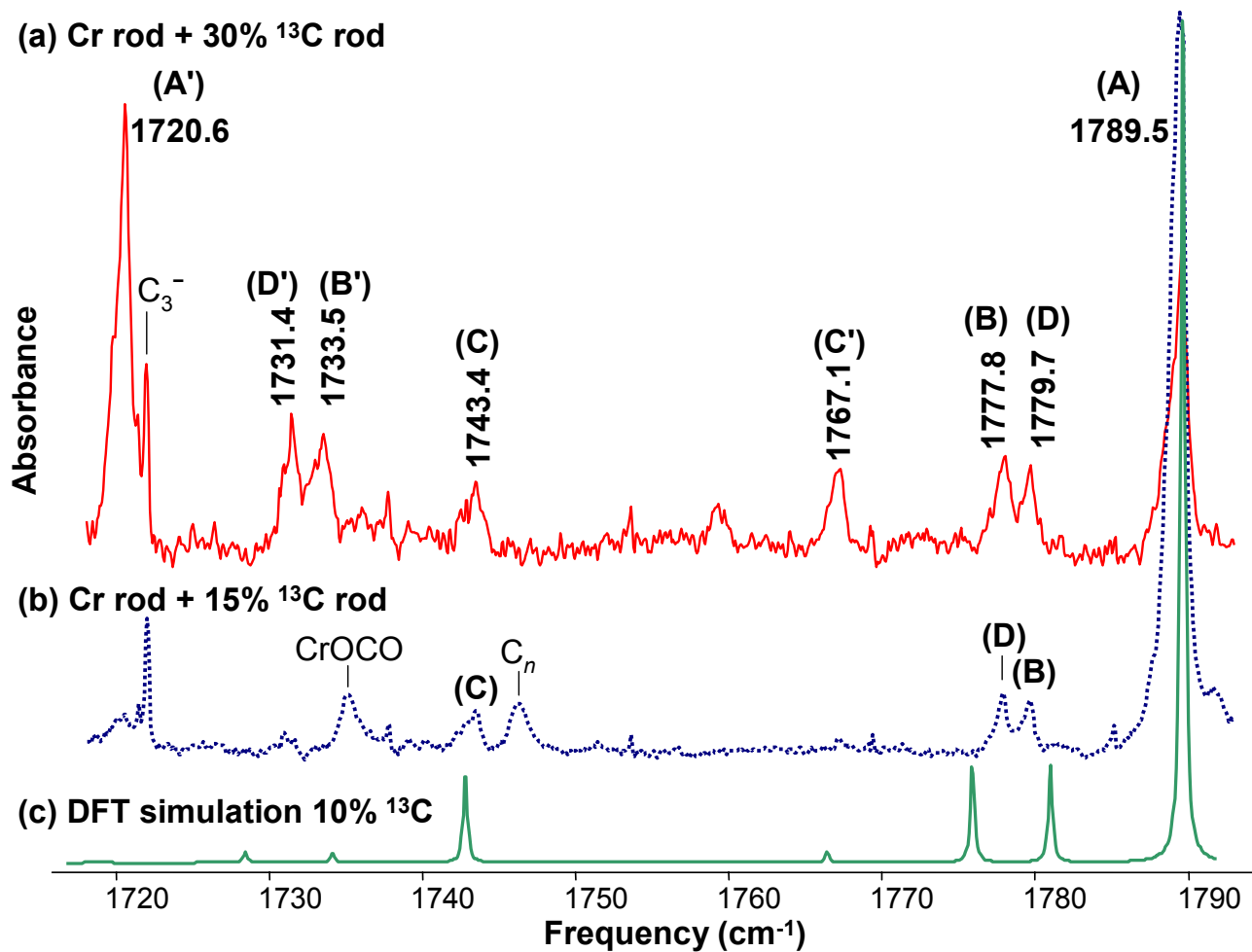


Figure 3.3 Comparison of the FTIR spectra of the  $\nu_1(\sigma)$  mode of linear  $\text{CrC}_3$  and its  $^{13}\text{C}$  isotopic shifts produced by the simultaneous evaporation of a Cr rod and carbon rods with (a) 30% and (b) 15%  $^{13}\text{C}$  enrichments, with (c) a simulation derived from DFT calculations at the B3LYP/6-311+G(3df) level having 10%  $^{13}\text{C}$  enrichment. The letters correspond to the single  $^{13}\text{C}$  substituted and single  $^{12}\text{C}$  substituted isotomers listed in Table 3.2.

at 1735.1,<sup>50</sup>  $\text{C}_3^-$  at 1721.8,<sup>54</sup> and an unidentified band at 1746.1  $\text{cm}^{-1}$ , which results from the ablation of a carbon rod. The three remaining bands at 1779.7, 1777.8, and 1743.4  $\text{cm}^{-1}$ , however, are likely isotopic shifts. Each of the absorptions is approximately 6% of the intensity of the 1789.5  $\text{cm}^{-1}$  band, and this relative intensity is maintained during annealing, with all four absorptions sharpening slightly. As discussed earlier, a small  $\text{CrC}_n$  species is probably responsible and the presence of three single  $^{13}\text{C}$ -substituted shifts of equal intensity points to linear  $\text{CrC}_3$  as the most probable candidate. This tentative conclusion is consistent the DFT calculations predicting that the strongest infrared absorption of the linear isomer will be the  $\nu_1(\sigma)$  mode at 1852  $\text{cm}^{-1}$ .

For further evidence, experiments with higher  $^{13}\text{C}$  enrichment were performed. In the case of small molecules, 50%  $^{13}\text{C}$  enrichment will show the full  $^{12}\text{C}$  species, the full  $^{13}\text{C}$  species and all of the isotopic shifts. Because the amorphous  $^{13}\text{C}$  powder used to make the rods evaporates more easily than the crystalline  $^{12}\text{C}$  material, the actual  $^{13}\text{C}$  enrichment observed in the spectrum is sometimes different from the nominal value. In Fig. 3.3(a), the spectrum obtained in an experiment with  $\sim 30\%$   $^{13}\text{C}$  enrichment in the C rod again shows the main  $\text{Cr}^{12}\text{C}_3$  band at 1789.5  $\text{cm}^{-1}$  with the three single  $^{13}\text{C}$  shifts at 1779.7, 1777.8, and 1743.4  $\text{cm}^{-1}$ . In addition, on the low frequency side, a mirror spectrum with a strong band at 1720.6  $\text{cm}^{-1}$  belonging to  $\text{Cr}^{13}\text{C}_3$  and three weaker  $^{13}\text{C}$  shift bands to its right at 1731.4, 1733.5, and 1767.1  $\text{cm}^{-1}$ , corresponding to isotopomers with a single  $^{12}\text{C}$  atom and two  $^{13}\text{C}$  atoms are also observed. The intensities of the latter three bands are  $\sim 27\%$  of the 1720.6  $\text{cm}^{-1}$  band and this ratio is maintained during annealing. The two main bands at 1720.6 and 1789.5  $\text{cm}^{-1}$  corresponding, respectively, to the  $\nu_1(\sigma)$  mode of the  $\text{Cr}^{13}\text{C}_3$  and  $\text{Cr}^{12}\text{C}_3$  isotopomers and the six bands between them comprise all of the possible isotopomers for a linear species with a chain of three inequivalent C atoms having a terminal Cr atom at one end. In Table 3.2 a detailed comparison

Table 3.2: Comparison of observed vibrational frequencies ( $\text{cm}^{-1}$ ) of the  $\nu_1(\sigma)$  mode for  $^{13}\text{C}$ -substituted isotopomers of linear  $\text{CrC}_3$  with the predictions of B3LYP/6-311+G(3df) calculations.

Isotopomer		Observed	DFT	Scaled	Difference
Cr-C-C-C		$\nu_{\text{obs}}$	$\nu$	$\nu_{\text{sc}}$	$\Delta\nu = \nu_{\text{obs}} - \nu_{\text{sc}}$
52-12-12-12	(A)	1789.5	1851.7	... <sup>a</sup>	...
52- <b>13</b> -12-12	(B)	1777.8	1837.6	1775.9	1.9
52-12- <b>13</b> -12	(C)	1743.4	1803.5	1742.9	0.5
52-12-12- <b>13</b>	(D)	1779.7	1842.6	1780.7	-1.0
52- <b>13</b> - <b>13</b> - <b>13</b>	(A')	1720.6	1778.8	... <sup>b</sup>	...
52-12- <b>13</b> -13	(B')	1733.5	1794.5	1735.8	-2.3
52- <b>13</b> -12- <b>13</b>	(C')	1767.1	1827.7	1767.9	-0.8
52- <b>13</b> - <b>13</b> -12	(D')	1731.4	1788.8	1730.3	1.1

<sup>a</sup>Results of the calculation scaled by a factor of  $1789.5/1851.7=0.96641$ .

<sup>b</sup>Results of the calculation scaled by a factor of  $1720.6/1778.8=0.96728$ .

is shown between the observed  $^{13}\text{C}$  shifts and the scaled (by the ratios  $1789.5/1851.7=0.96641$  and  $1720.6/1778.8=0.96728$  of the observed to predicted frequencies for the  $\text{Cr}^{12}\text{C}_3$  and  $\text{Cr}^{12}\text{C}_3$  isomers, respectively) DFT-B3LYP/6-311+G(3df) predictions for all of the  $^{13}\text{C}$  isotopomers. The agreement is very good and supports the identification of the  $1789.5\text{ cm}^{-1}$  absorption as the  $\nu_1(\sigma)$  mode of the linear isomer.

As discussed earlier, the interpretation of the PE spectra<sup>25</sup> for  $\text{CrC}_3^-$  indicated that both the fanlike ( $C_{2v}$ ) and linear isomers, which DFT predicts to be nearly isoenergetic, were present although the linear isomer appeared to be slightly more stable. In the present work on neutral  $\text{CrC}_3$ , the FTIR isotopic shift measurements show the presence of the linear isomer, which DFT calculations predict to be less stable (+0.30 eV) than the  $C_{2v}$  isomer. A pair of bands appearing weakly in the FTIR spectra at  $\sim 1305\text{ cm}^{-1}$  are in the vicinity of the DFT predictions (see Table 3.1) for the  $\nu_1(a_1)$  and  $\nu_5(b_2)$  modes of the  $C_{2v}$  isomer. However, no  $^{13}\text{C}$  isotopic shift evidence has been found to support the identification of these bands as modes of the fanlike isomer.

### 3.5. Conclusions

This investigation on  $\text{CrC}_3$ , which was produced by trapping the products from the dual evaporation of Cr and C rods in Ar at  $\sim 10\text{ K}$ , has resulted in the first assignment of a vibrational fundamental for the linear isomer. A prior PES study<sup>25</sup> had reported evidence of both linear and ( $C_{2v}$ ) fanlike isomers, and the first measurement of a vibrational mode for the  $C_{2v}$  structure. No evidence of the fanlike isomer was observed in the present study. The excellent agreement between  $^{13}\text{C}$  isotopic shift measurements coupled with DFT predictions has established that the ground state structure of  $\text{CrC}_3$  is linear with a  $^5\Pi$  electronic state, and its  $\nu_1(\sigma)$  carbon stretching fundamental has been identified at  $1789.5\text{ cm}^{-1}$ .

**CHAPTER IV**  
**FOURIER TRANSFORM INFRARED OBSERVATION OF THE  $\nu_1(\sigma)$  MODE OF**  
**LINEAR  $\text{CoC}_3$  TRAPPED IN SOLID Ar**

#### **4.1 Introduction**

This study of the  $\text{CoC}_3$  cluster continues the FTIR investigations of transition metal–carbon species which were initiated in the TCU Molecular Physics Lab with the  $\text{CrC}_3$  molecule discussed in Chapter III and the  $\text{TiC}_3$  molecule reported by Kinzer.<sup>55</sup> The first observations of small  $\text{Co}_n\text{C}_m$  species were made as part of two PES studies done by Wang and Li on electronic structure and bonding in the first row transition metal–carbon clusters  $\text{MC}_2^-$  ( $M = \text{Sc}, \text{V–Co}$ )<sup>22</sup> and  $\text{MC}_3^-$  ( $M = \text{Sc}, \text{V–Ni}$ ).<sup>20</sup> A vibrational spacing of  $\sim 540(60) \text{ cm}^{-1}$  for  $\text{CoC}_2$  was observed, presumably corresponding to a metal–carbon stretch,<sup>22</sup> but no vibrational features could be resolved for  $\text{CoC}_3$ .<sup>20</sup> The authors speculated that the unresolved spectra observed for  $\text{CoC}_3^-$  indicated a significant change in geometry between the anion and neutral species. Because the unresolved vibrational features made it impossible to determine the geometry, they did not include  $\text{CoC}_3$  in their DFT investigation of  $\text{MC}_3$  clusters. Calculations on all of the other  $\text{MC}_3$  clusters in their study, however, suggested that they have ( $C_{2v}$ ) fanlike ground state geometries.<sup>20</sup>

DFT/B3LYP calculations on the dicarbide  $\text{CoC}_2$  have predicted a cyclic ( $C_{2v}$ ) ground state structure with an ionic  $\text{Co}^{2+}\text{–C}_2^{2-}$  bond.<sup>56</sup> The ground state has been found to be a quartet, but its symmetry is still uncertain as the  $^4B_1$  and  $^4B_2$  states have been calculated to be nearly isoenergetic ( $\pm 0.26 \text{ kcal/mol}$ ). Recent DFT/B3LYP calculations on the  $C_{2v}$ ,  $D_{\infty h}$ , and  $C_{\infty v}$  isomers of  $\text{MC}_2$  and  $\text{MC}_2^-$  ( $M = \text{V}, \text{Cr}, \text{Fe}, \text{and Co}$ ) clusters<sup>57</sup> have confirmed that both the

neutral and the anion species have  $C_{2v}$  ground state symmetries and propose assignments for previously published PE spectral features.<sup>22</sup>

A study on  $\text{Co}_2\text{C}_n^-$  ( $n=2,3$ ) clusters<sup>3</sup> has reported PE spectra with DFT geometry predictions at the generalized gradient approximation (GGA) level, elucidating the growth mechanisms of small  $\text{Co}_n\text{C}_m$  clusters. Rather than forming a metal-carbon network composed of  $\text{MC}_2$  “building blocks” as is the case with  $\text{V}_n\text{C}_m$  and  $\text{Ti}_n\text{C}_m$  clusters,<sup>2</sup>  $\text{Co}_n\text{C}_m$  species appear to first form carbon aggregates to which Co atoms attach.

FTIR measurements in concert with DFT predictions of frequencies and  $^{13}\text{C}$  isotopic shifts have been successfully used by the TCU Molecular Physics Lab to determine the structures and identify vibrational fundamentals for a variety of  $\text{Si}_n\text{C}_m$ ,<sup>29,30</sup>  $\text{Ge}_n\text{C}_m$ ,<sup>58</sup> and  $\text{GeC}_n\text{Si}$  (Ref. 33) clusters, which have been formed by trapping the laser ablated products of Si, Ge, and C rods in solid Ar. Recently FTIR and DFT isotopic investigations were initiated on transition metal–carbon clusters using the same laser ablation and matrix isolation techniques, and have reported vibrational fundamentals and ground state structures for the  $\text{TiC}_3$  ( $C_{2v}$  fanlike)<sup>55</sup> and  $\text{CrC}_3$  (linear)<sup>46</sup> species. As presented in this chapter, the application of similar techniques to  $\text{Co}_n\text{C}_m$  clusters has resulted in the first optical detection of the  $\nu_1(\sigma)$  mode of linear  $\text{CoC}_3$ .

## 4.2 Theoretical Calculations

As previously noted, prior theoretical investigations of  $\text{Co}_n\text{C}_m$  species have been limited to  $\text{CoC}_2$ ,  $\text{CoC}_2^-$ , and  $\text{Co}_2\text{C}_n^-$  ( $n=2, 3$ ).<sup>3,56,57</sup> The DFT investigation reported in this chapter on  $\text{CoC}_3$  is thus the first for this species. The GAUSSIAN 03 program suite<sup>45</sup> with the B3LYP<sup>47</sup> and BPW91<sup>39</sup> functionals and the 6-311+G(3df) basis set were used for calculations on the two lowest energy isomers, the  $^2\Delta$  linear and  $^2B_1$  fanlike structures of  $\text{CoC}_3$ . The possibility that a non-centrosymmetric  $\text{Co}_2\text{C}_3$  species could be responsible for the spectrum in the present work has also been considered, but planar  $\text{Co}_2\text{C}_3$  structures were eliminated because prior DFT



calculations on  $\text{Co}_2\text{C}_3^-$  have shown that the lowest energy isomers have  $C_{2v}$  symmetry with two equivalent C atoms, in agreement with PE spectra<sup>3</sup> and two equivalent C atoms would not be consistent with the  $^{13}\text{C}$  isotopic shift pattern observed in the FTIR spectra and discussed in the following sections. A “Y-shaped” structure ( $C_{2v}$ ) with two equivalent Co atoms at the end of a  $\text{C}_3$  chain was investigated by Rittby,<sup>59</sup> but the  $^{13}\text{C}$  shifts are not in good agreement with the FTIR spectra. To rule out other linear  $\text{CoC}_3$  or  $\text{Co}_2\text{C}_3$  isomers, B3LYP/6-311+G(3df) calculations were also performed on CCoCC, CoCoCCC, CoCCoCC, and CoCCCoC, but none of these possibilities gave a stable minimum structure with a vibrational fundamental close in frequency to the observed FTIR spectrum.

DFT calculations were done on  $\text{CoC}_3$  using both the B3LYP and BPW91 functionals and predict that the  $^2B_1$  fanlike [see Fig. 4.1(a)] and the  $^2\Delta$  linear isomers are very close in energy. BPW91 calculations predict the  $^2B_1$  fan is the ground state by 2.7 kcal/mol, whereas B3LYP calculations predict the  $^2\Delta$  linear isomer is 3.7 kcal/mol lower than the fan. These calculations therefore do not provide any clear indication as to which state is the true ground state for  $\text{CoC}_3$ . Geometric parameters for the two states are given in Fig 4.1(a). Vibrational frequencies and infrared intensities calculated using the B3LYP and BPW91 functionals are shown in Table 4.1.

### 4.3 Experimental Procedures

$\text{CoC}_3$  was produced from a pair of C (99.9995%, Alfa Aesar) and Co (99.95%, ESPI) rods, which were continually rotated and translated in order to provide clean surfaces for ablation using two 1064 nm Nd:YAG pulsed lasers (Spectra Physics). High purity Ar (99.995%, Matheson Tri-Gas) was introduced into the sample chamber, sweeping the ablated products onto a gold mirror maintained at  $\sim 10$  K with a closed-cycle refrigeration system (ARS, Displex) under a vacuum pressure of  $\leq 10^{-7}$  Torr. Details of the experimental apparatus have been published

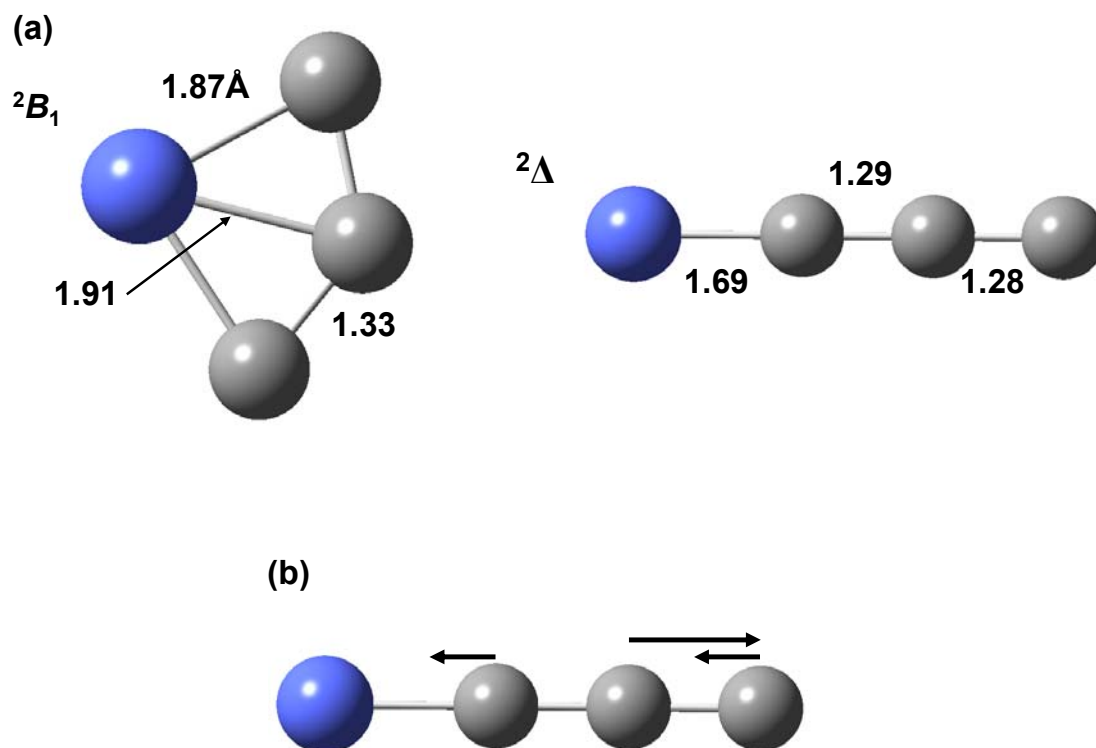


Figure 4.1 DFT B3LYP/6-311+G(3df) predictions of bond lengths (Å) of the  ${}^2B_1$  fanlike and  ${}^2\Delta$  linear isomers. The predicted principal nuclear displacements of the  $\nu_1(\sigma)$  mode of the  ${}^2\Delta$  linear isomer of  $\text{CoC}_3$  are shown in (b).

Table 4.1: DFT predicted frequencies ( $\text{cm}^{-1}$ ) and band intensities ( $\text{km/mol}$ ) for the vibrational fundamentals of the ( ${}^2\Delta$ ) linear and ( ${}^2B_1$ ) fanlike isomers of  $\text{CoC}_3$  using the B3LYP and the BPW91 functionals with a 6-311+G(3df) basis set.

CrC <sub>3</sub> Isomer	Vibrational Mode	B3LYP		BPW91	
		Frequency ( $\text{cm}^{-1}$ )	IR intensity ( $\text{km/mol}$ )	Frequency ( $\text{cm}^{-1}$ )	IR intensity ( $\text{km/mol}$ )
${}^2\Delta$	$\nu_1(\sigma)$	2014	586	1986	663
Linear	$\nu_2(\sigma)$	1358	3	1338	2
	$\nu_3(\sigma)$	497	18	514	3
	$\nu_4(\sigma)$	385	29	383	32
	$\nu_5(\pi)$	142	$\sim 0$	134	$\sim 0$
	${}^2B_1$	$\nu_1(a_1)$	1240	9	1156
Fanlike ( $C_{2v}$ )	$\nu_2(a_1)$	671	15	695	5
	$\nu_3(a_1)$	458	15	505	4
	$\nu_4(b_1)$	371	8	275	$\sim 0$
	$\nu_5(b_2)$	1563	79	1463	53
	$\nu_6(b_2)$	373	22	474	19

previously.<sup>38</sup> Experimental conditions such as the laser power, the laser focus, and the Ar flow rate were adjusted to favor the production of small carbon chains, predominantly C<sub>3</sub>. Laser powers of  $\leq 1.0$  W with a loose focus and  $\sim 2.5$  W with a tight focus were used on the C and Co rods, respectively. These conditions significantly enhanced the production of C<sub>3</sub> chains relative to other C<sub>*n*</sub> species and facilitated CoC<sub>3</sub> formation.

Carbon rods were fabricated with the <sup>13</sup>C enrichment required to produce the desired <sup>13</sup>C isotopic shifts. These rods were made from a mixture of <sup>12</sup>C (99.9995%, Alfa Aesar) and <sup>13</sup>C (99.3%, Isotec) powders, pressed under a pressure of  $\sim 4.5 \times 10^5$  kPa. Three carbon rods were prepared, a pure <sup>12</sup>C rod and rods with  $\sim 20\%$  <sup>13</sup>C and  $\sim 30\%$  <sup>13</sup>C nominal enrichment. In previous studies, the comparison of <sup>13</sup>C isotopic shift measurements with DFT predictions has enabled various geometries, such as rhomboidal Si<sub>3</sub>C,<sup>42</sup> planar pentagonal Si<sub>3</sub>C<sub>2</sub>,<sup>27</sup> and the more recently discovered “fan-shaped” TiC<sub>3</sub> (Ref. 55) to be easily distinguished from one another and from linear structures such as CrC<sub>3</sub> (Ref. 46) and GeC<sub>5</sub>Ge.<sup>58</sup>

#### 4.4 Results and Discussion

Absorptions of potential Co<sub>*n*</sub>C<sub>*m*</sub> candidates were identified by comparing the spectrum obtained from the dual ablation of Co and C rods [Fig. 4.2(a)] with the spectrum produced by the ablation of a single <sup>12</sup>C rod [Fig. 4.2(b)]. The spectrum from the <sup>12</sup>C rod shows an abundance of C<sub>*n*</sub> absorptions, most of which have been previously identified,<sup>49</sup> and many of which also appear in the Co/C spectrum. In the dual ablation experiment, low laser power ( $< 1.0$  W) ablation of the C rod favored C<sub>3</sub> production, as is readily seen by the intense  $\nu_3(\sigma_u)$  mode of C<sub>3</sub> that dwarfs most other features in the spectrum. Only trace amounts of CO impurities from the C rod appear in the spectra, and H<sub>2</sub>O absorptions are negligible. Most importantly, a strong band which appears at  $1918.2 \text{ cm}^{-1}$  in the Co/C spectrum in Fig. 4.2(a) is absent from the <sup>12</sup>C spectrum in Fig. 4.2(b),

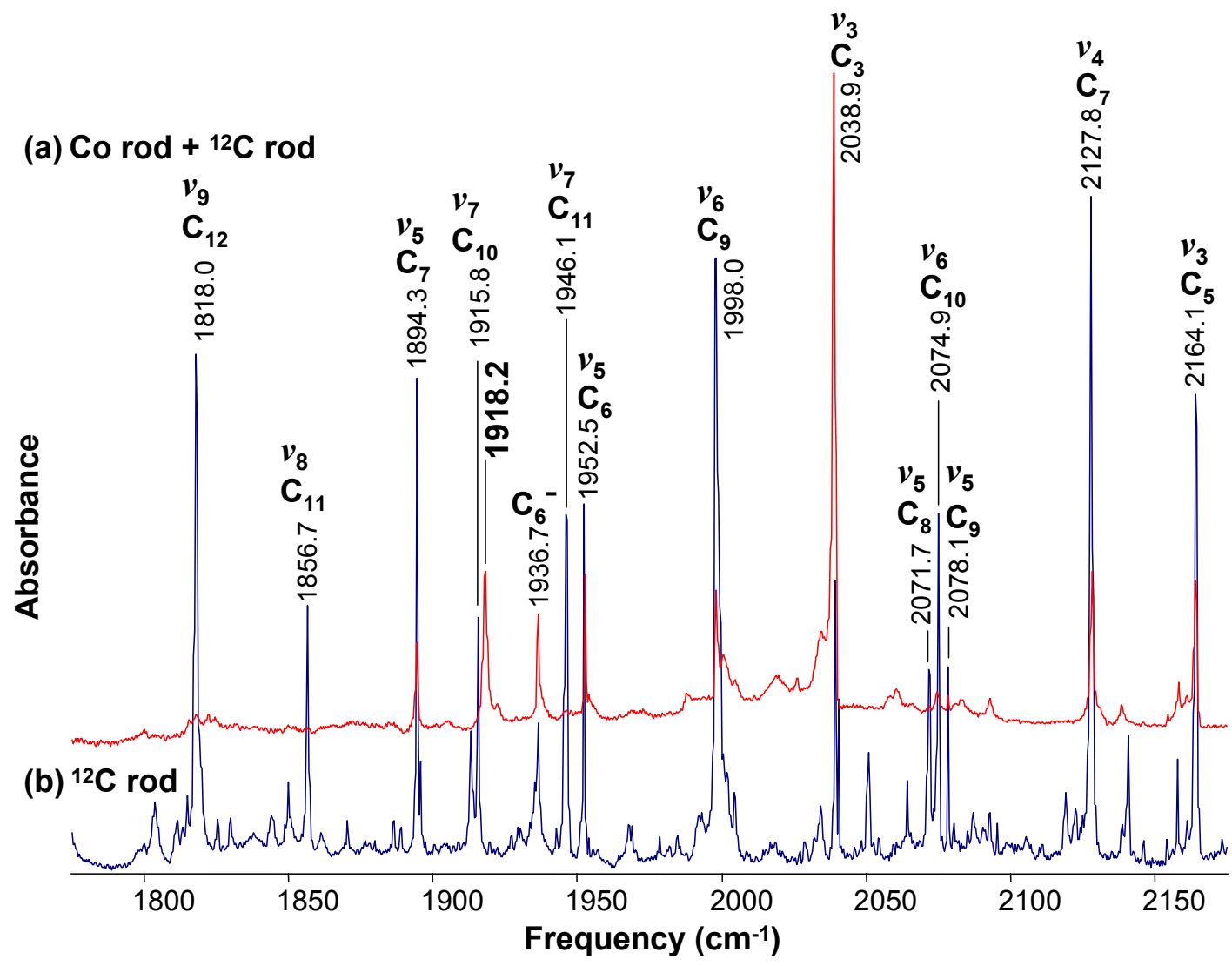


Figure 4.2 FTIR spectra recorded after (a) dual ablation of cobalt and pure <sup>12</sup>C rods and (b) ablation of a pure <sup>12</sup>C rod, for comparison. Note the 1918.2 cm<sup>-1</sup> band in (a) that does not appear in (b).

and is therefore a candidate for a  $\text{Co}_n\text{C}_m$  species.

Additional absorption features appear in the spectrum in Fig. 4.2(a) resulting from the dual ablation of Co and C rods. Absorptions of  $\text{C}_n$  anions, such as  $\text{C}_3^-$  and  $\text{C}_6^-$ ,<sup>60</sup> are more intense than in the pure  $^{12}\text{C}$  spectrum, and absorptions arising from  $\text{CO}_2$  impurities, which often appear during carbon evaporation, are also present. Baking the carbon rods usually eliminates  $\text{CO}_2$ , but this has not been the case in the present work where weak  $\text{CO}_2$  absorptions in the dual ablation spectra have been traced to the metal evaporation. However, a search using the NIST database<sup>49</sup> for the vibrational frequencies of potential contaminant species such as  $\text{Co}(\text{CO})$ ,<sup>61,62</sup>  $\text{Co}_2(\text{CO})$ ,<sup>62,63</sup>  $\text{CoH}_2$ ,  $\text{CoCH}_2$ , and  $\text{CH}_3\text{CoH}$ ,<sup>64</sup>  $\text{HCoOH}$ ,<sup>52</sup>  $\text{OCOCO}$ ,<sup>65</sup>  $\text{Co}_2\text{O}_2$ , and several  $\text{CoO}_n$  ( $n=2-4$ )<sup>66</sup> species yielded no evidence of them in the spectra.

$^{13}\text{C}$  isotopic measurements are crucial in order to unambiguously identify the vibrational fundamental and determine the geometry of the species responsible for the  $1918.2\text{ cm}^{-1}$  band. The spectra in Figs. 4.3(a) and (b) show the results of the dual evaporation of a Co rod with a carbon rod containing 30%  $^{13}\text{C}$  and 20%  $^{13}\text{C}$  isotopic enrichments, respectively. In searching for potential  $^{13}\text{C}$  shifts a number of features appearing in the vicinity of the  $1918.2\text{ cm}^{-1}$  band, which are attributable to pure  $^{12}\text{C}$  species or carbon-bearing contaminant species, can be eliminated from consideration. Weak absorptions at  $1922.5$  and  $1863.5\text{ cm}^{-1}$  belong to  $\text{C}_4\text{O}$  (Ref. 67) and  $\text{CHO}$ ,<sup>68</sup> respectively. An intense absorption at  $1936.7\text{ cm}^{-1}$  (not shown) is identified as the  $\nu_4(\sigma_u^+)$  fundamental of  $\text{C}_6^-$ ,<sup>60</sup> and an absorption at  $1914.5\text{ cm}^{-1}$  [Fig. 4.3(b)], and two other absorptions at  $1929.2$  and  $1928.6\text{ cm}^{-1}$  (not shown) are its single  $^{13}\text{C}$ -substituted shifts.<sup>69</sup> Finally, the  $\nu_5(\sigma_u)$  mode of  $\text{C}_7$  is at  $1894.3\text{ cm}^{-1}$  with relatively weak, singly-substituted  $^{13}\text{C}$  isotopomer bands at  $1886.4$  and  $1880.2\text{ cm}^{-1}$ .<sup>70</sup> A third isotopomer band of  $\text{C}_7$  lies within the envelope of the main,  $1894.3\text{ cm}^{-1}$  absorption and a fourth at  $1870.4\text{ cm}^{-1}$  is hidden by a prominent new band at  $1870.8\text{ cm}^{-1}$  which originates from a  $\text{Co}_n\text{C}_m$  species.

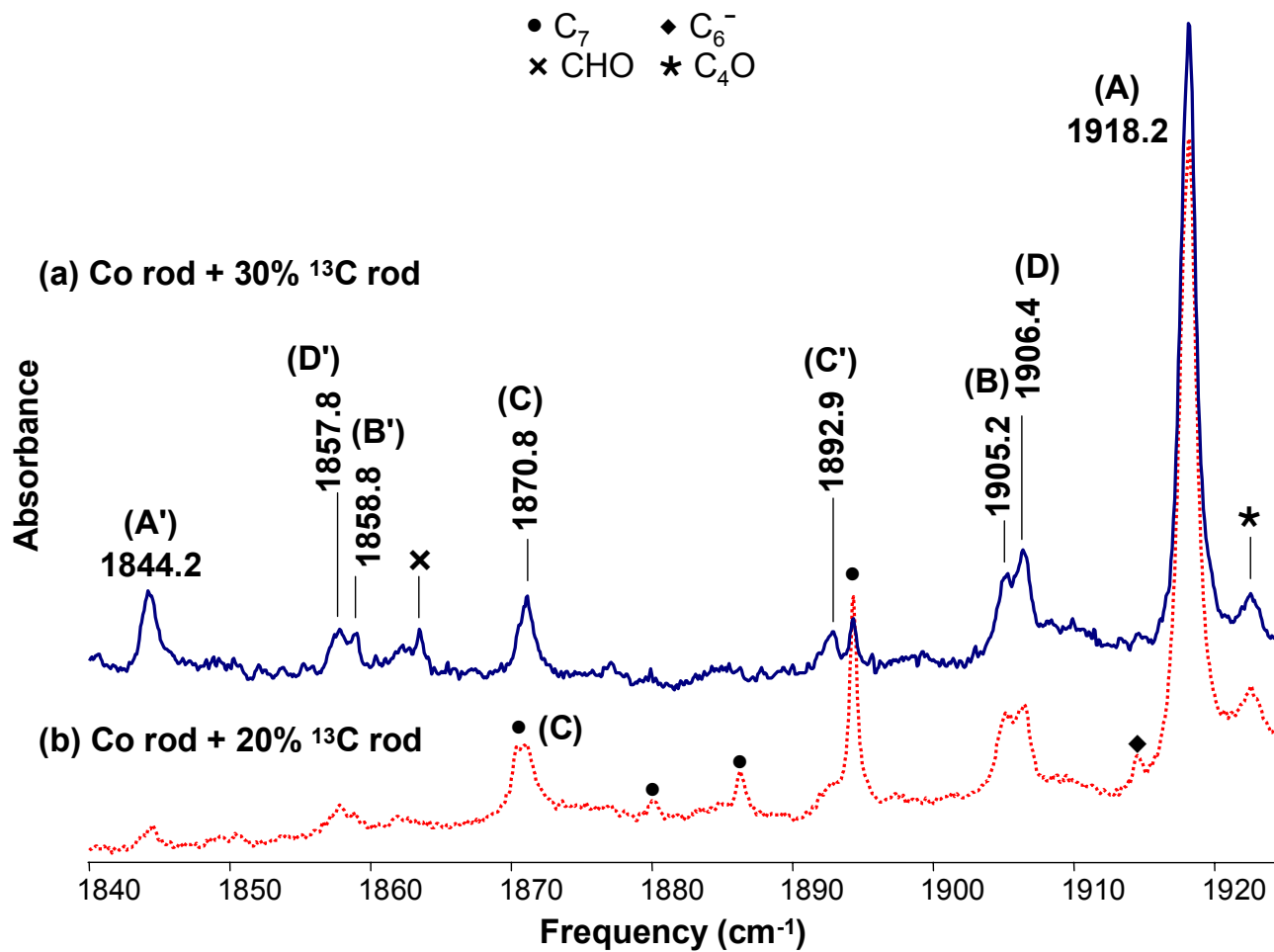


Figure 4.3 FTIR spectra of the  $\nu_1(\sigma)$  mode of linear  $CoC_3$  in an experiment with (a) 30% nominal  $^{13}C$  enrichment, and (b) 20% nominal  $^{13}C$  enrichment. The higher  $^{13}C$  enrichment in (a) eliminates most of the absorptions attributed to  $C_6^-$  and  $C_7$ , leaving only a weak  $C_7$  absorption at  $1894.3\text{ cm}^{-1}$ , and thus shows the fully- and doubly-substituted  $^{13}C$  isotopomers more clearly.

The 1870.8  $\text{cm}^{-1}$  absorption together with the remaining spectral features at 1906.4, 1905.2,  $\sim 1858$ , and 1844.2  $\text{cm}^{-1}$  are thus all possible candidates for  $^{13}\text{C}$  shifts of the 1918.2  $\text{cm}^{-1}$  band. The spectrum in Fig. 4.3(b) suggests several points immediately: (1) The relatively high vibrational frequency is indicative of a C-C stretching mode for a linear molecule, in which there is little participation by the Co atom(s). (2) There are three possible candidates at 1906.4, 1905.2, and 1870.8  $\text{cm}^{-1}$  for the single  $^{13}\text{C}$  shifts which should be prominent in the spectrum at low  $^{13}\text{C}$  enrichment. (3) The approximately equal intensity of the three bands indicates that the molecule responsible has at least three unique C atoms, which would be the case if a single Co atom were bonded to one end of a  $\text{C}_3$  chain. The third point is confirmed by the measured integrated intensities of the 1905.2 and 1906.4  $\text{cm}^{-1}$  bands. They are each  $\sim 9\%$  of the main 1918.2  $\text{cm}^{-1}$  absorption, which is consistent with the  $^{13}\text{C}$  enrichment measured for the single  $^{13}\text{C}$  shifts for  $\text{C}_3$  and other  $\text{C}_n$  species in the spectrum. The 1870.8  $\text{cm}^{-1}$  feature has a somewhat greater intensity of  $\sim 11\%$  of the 1918.2  $\text{cm}^{-1}$  band, but if the contribution from the overlapping  $\text{C}_7$  isotopomer band at 1870.4  $\text{cm}^{-1}$  is subtracted from the band envelope, the ratio with the 1918.2  $\text{cm}^{-1}$  main absorption is then  $\sim 9\%$ , which is consistent with the two other isotopic shift bands. The integrated intensity ratios ( $\sim 9\%$ ) thus indicate that the three absorptions result from three *unique*  $^{13}\text{C}$  substitutions. The  $^{13}\text{C}$  isotopic shift pattern and integrated intensity ratios rule out the possibility of a  $\text{C}_{2v}$  isomer of  $\text{Co}_2\text{C}_3$  as well as any centrosymmetric linear configuration (e.g.  $\text{CoCCCCo}$ ). Since other non-centrosymmetric linear configurations of  $\text{CoC}_3$  and  $\text{Co}_2\text{C}_3$  could be eliminated on the basis of their vibrational fundamental frequencies or IR intensities, the remaining candidate is linear  $\text{CoCCC}$ . The tentative conclusion is therefore supported that the molecule is most likely a single Co atom attached to one end of a  $\text{C}_3$  chain. Assuming that the Co atom is not participating in the vibration, and using the harmonic oscillator approximation for pure carbon clusters, the frequency for the fully  $^{13}\text{C}$ -substituted molecule should scale as



$$\nu_{^{13}\text{C}} \approx \sqrt{\frac{m_{^{12}\text{C}}}{m_{^{13}\text{C}}}} \times \nu_{^{12}\text{C}} \approx \sqrt{\frac{12.0}{13.00335}} \times \nu_{^{12}\text{C}} \quad (4.1)$$

Setting  $\nu_{^{12}\text{C}} = 1918.2$ , gives  $\nu_{^{13}\text{C}} \approx 1842.7 \text{ cm}^{-1}$ , which is close to a band observed at  $1844.2 \text{ cm}^{-1}$  in Fig. 4.3(b). Figure 4.3(a) shows the spectrum obtained when the  $^{13}\text{C}$  isotopic enrichment in the C rod was increased to 30%. Again, as in Fig. 4.3(b) the  $1918.2 \text{ cm}^{-1}$  principal band and the three single isotopic shifts at,  $1906.4$ ,  $1905.2$ , and  $1870.8 \text{ cm}^{-1}$  appear. However, in the Fig. 4.3(a) spectrum, only trace amounts of  $\text{C}_7$  appear, thus eliminating contributions from overlapping isotopic shifts from the  $1894.3 \text{ cm}^{-1}$  band of  $\text{C}_7$ . In addition to the absorption for the full  $^{13}\text{C}$ -substituted isotopomer at  $1844.2 \text{ cm}^{-1}$ , the absorptions of three more potential isotopomer bands now appear clearly: an absorption at  $1892.9 \text{ cm}^{-1}$  that previously appeared as a shoulder to the low frequency side of the  $\text{C}_7$  absorption, and the band at  $\sim 1858 \text{ cm}^{-1}$  that can now be resolved into two overlapping peaks at  $1857.8$  and  $1858.8 \text{ cm}^{-1}$ .

Further evidence in support of the tentative conclusion that the  $1918.2 \text{ cm}^{-1}$  absorption is the result of a Co atom attached to the end of a  $\text{C}_3$  chain is found in the relative intensities of the isotopomer bands appearing in Fig. 4.3(a) for a 30%  $^{13}\text{C}$  enrichment. Because the fabricated rod does not have a uniform mixture of carbon isotopes, the isotopic spectra do not exhibit the relative intensities expected for a complete randomization with 30%  $^{13}\text{C}$  enrichment. This is also the case for the  $\text{C}_3$  spectrum, and since the  $1918.2 \text{ cm}^{-1}$  absorption is a candidate for  $\text{CoC}_3$ , the intensity ratios observed for its  $^{13}\text{C}$  shifts are compared with the  $^{13}\text{C}$  isotopic intensity ratios observed for  $\text{C}_3$ . In the  $\text{C}_3$  spectrum, the integrated intensities of the single  $^{13}\text{C}$ -substituted isotopomers are each  $\sim 10\%$  of the integrated intensity of the main  $\text{C}_3$  band. Similarly, the absorptions at  $1906.4$ ,  $1905.2$ , and  $1870.8 \text{ cm}^{-1}$ , which are candidates for single  $^{13}\text{C}$  shifts of  $\text{CoC}_3$ , each have intensities that are  $\sim 9\%$  of the main  $1918.2 \text{ cm}^{-1}$  absorption. The doubly-substituted  $^{13}\text{C}$  isotopomer bands of  $\text{C}_3$  all have integrated intensities that are  $\sim 4\%$  of the main  $\text{C}_3$

band. Likewise, the ratios of the intensities of the bands at 1892.9, 1857.8, and 1858.8  $\text{cm}^{-1}$  to the main 1918.2  $\text{cm}^{-1}$  band are each  $\sim 4\%$ , making them good candidates for double  $^{13}\text{C}$  shifts. The ratio of the intensity of the 1844.2  $\text{cm}^{-1}$  band to the 1918.2  $\text{cm}^{-1}$  band is  $\sim 9\%$ , which is consistent with the observation for  $\text{C}_3$  that the intensity of the fully-substituted  $^{13}\text{C}_3$  band is 9.5% of the main  $^{12}\text{C}_3$  band. The evidence from the isotopic shift pattern therefore indicates that the 1918.2  $\text{cm}^{-1}$  band results from a Co atom attached to the end of a linear  $\text{C}_3$  chain with single  $^{13}\text{C}$ -substituted isotopomers at 1906.4, 1905.2, and 1870.8  $\text{cm}^{-1}$ , double  $^{13}\text{C}$ -substituted isotopomers at 1892.9, 1857.8, and 1858.8  $\text{cm}^{-1}$ , and the full  $^{13}\text{C}$ -substituted isotopomer at 1844.2  $\text{cm}^{-1}$ .

Considering the evidence from the  $^{13}\text{C}$  isotopic shift pattern for the 1918.2  $\text{cm}^{-1}$  band and comparing its frequency with those predicted in Table 4.1 for the  $^2\Delta$  linear isomer of  $\text{CoC}_3$ , it is clear that the most probable assignment for the 1918.2  $\text{cm}^{-1}$  band is to the  $\nu_1(\sigma)$  fundamental, which is predicted by both the B3LYP and BPW91 calculations to be the most intense mode at 2014 and 1986  $\text{cm}^{-1}$ , respectively. The predicted principal nuclear displacements for the  $\nu_1(\sigma)$  mode are given in Fig. 4.1(b) and show that this C–C stretching mode is similar to an asymmetric  $\text{C}_3$  stretch with a stationary Co atom attached to one end.

Figure 4.4 compares the FTIR spectrum with 30%  $^{13}\text{C}$  enrichment with DFT BPW91/ and B3LYP/6-311+G(3df) simulations, which are both scaled to the 1918.2  $\text{cm}^{-1}$  band. Table 4.2 compares the FTIR measured frequencies with the results of the DFT/B3LYP and /BPW91 calculations, respectively. The predicted frequencies for the  $\text{Co}^{12}\text{C}_3$  and the  $\text{Co}^{13}\text{C}_3$  isotopomers have been scaled to the observed frequencies (scale factors =  $1918.2/2013.6=0.95262$  and  $1844.2/1934.4=0.95337$ , respectively, for the B3LYP predictions and  $1918.2/1986.0=0.96586$  and  $1844.2/1907.9=0.96661$ , respectively, for the BPW91 calculations). Two scale factors have been used in order to eliminate anharmonic effects. The calculated, harmonic  $\text{Co}^{12}\text{C}_3$  and  $\text{Co}^{13}\text{C}_3$

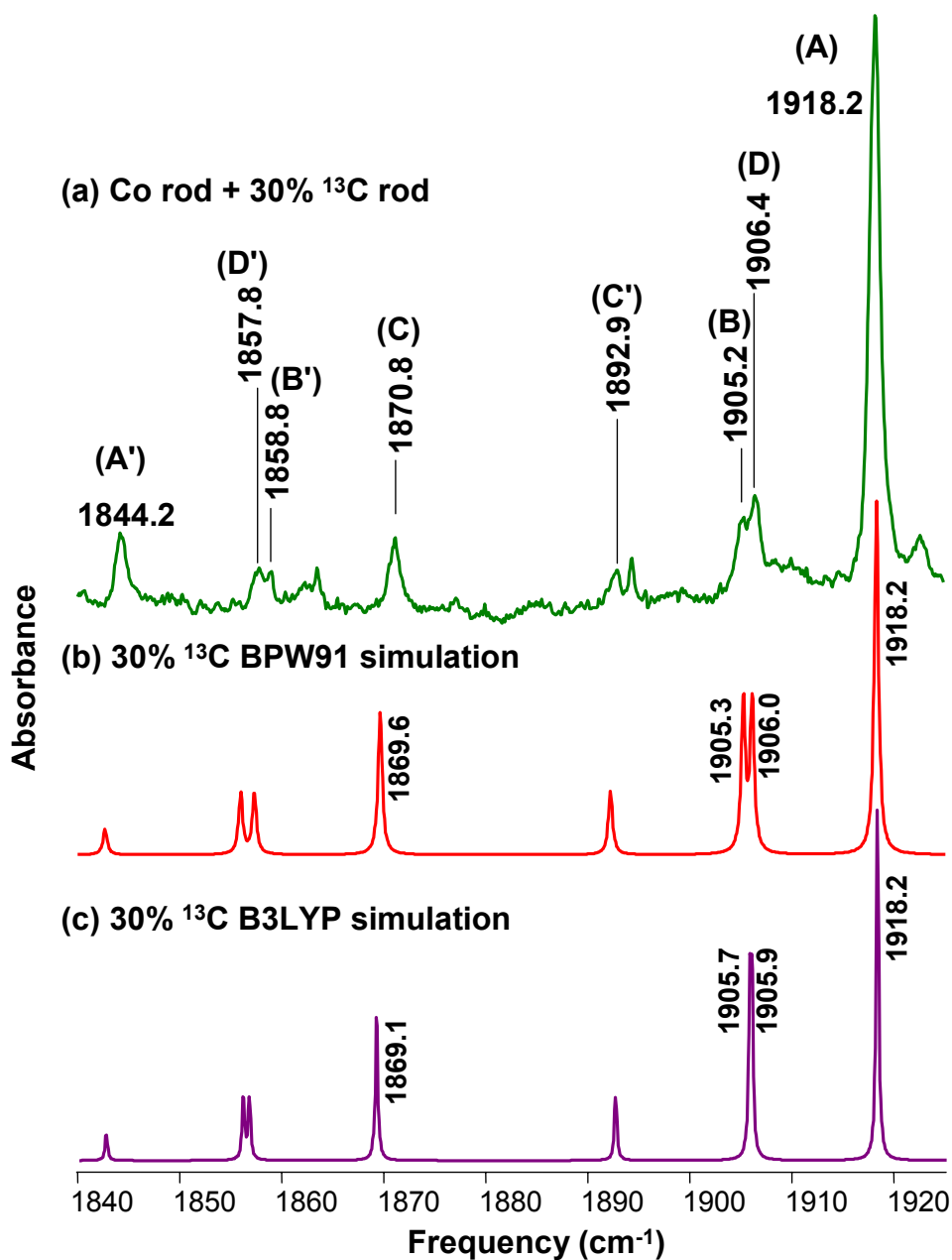


Figure 4.4 (a) An FTIR spectrum with 30%  $^{13}\text{C}$  enrichment for comparison with DFT simulations of a 30%  $^{13}\text{C}$  enrichment spectrum using the (b) BPW91 and the (c) B3LYP functionals with a 6-311+G(3df) basis set. The DFT simulations are scaled to the main 1918.2  $\text{cm}^{-1}$  band.

Table 4.2: Comparison of the observed vibrational fundamental and all of the  $^{13}\text{C}$ - substituted isotopomer frequencies ( $\text{cm}^{-1}$ ) of the  $\nu_1(\sigma)$  mode of linear  $\text{CoC}_3$  with the predictions of DFT B3LYP/ and BPW91/6-311G+(3df) calculations.

Isotopomer	Observed	B3LYP			BPW91		
		Theory	Scaled	Difference	Theory	Scaled	Difference
Co-C-C-C	$\nu$	$\nu$	$\nu$	$\Delta\nu$	$\nu$	$\nu$	$\Delta\nu$
59-12-12-12 (A)	1918.2	2013.6	... <sup>a</sup>	...	1986.0	... <sup>c</sup>	...
59- <b>13</b> -12-12 (B)	1905.2	2000.5	1905.7	-0.5	1972.6	1905.3	-0.1
59-12- <b>13</b> -12 (C)	1870.8	1962.1	1869.1	1.7	1935.7	1869.6	1.2
59-12-12- <b>13</b> (D)	1906.4	2000.7	1905.9	0.5	1973.4	1906.0	0.4
59- <b>13</b> - <b>13</b> - <b>13</b> (A')	1844.2	1934.4	... <sup>b</sup>	...	1907.9	... <sup>d</sup>	...
59-12- <b>13</b> -13 (B')	1858.8	1949.0	1858.1	0.7	1923.0	1858.8	0.0
59- <b>13</b> -12- <b>13</b> (C')	1892.9	1986.7	1894.1	-1.2	1959.1	1893.7	-0.8
59- <b>13</b> - <b>13</b> -12 (D')	1857.8	1948.5	1857.6	0.2	1921.6	1857.4	0.4

<sup>a</sup>Results of the calculation scaled by a factor of  $1918.2/2013.6=0.95262$ .

<sup>b</sup>Results of the calculation scaled by a factor of  $1844.2/1934.4=0.95337$ .

<sup>c</sup>Results of the calculation scaled by a factor of  $1918.2/1986.0=0.96586$ .

<sup>d</sup>Results of the calculation scaled by a factor of  $1844.2/1907.9=0.96661$ .

frequencies are related through Eq. (4.1), but the corresponding experimental frequencies are not (see Table 4.2), indicating that there is anharmonicity in the observed carbon stretch. In this situation, it is more appropriate to consider single  $^{13}\text{C}$  and  $^{12}\text{C}$  shifts as coming from the full  $^{12}\text{C}$  species and  $^{13}\text{C}$  species, respectively. The largest deviation occurs when a substitution is made on the middle C atom, which is expected, as it is the atom with the largest displacement in the vibration [see Fig. 4.1 (b)]. The very good agreement ( $\pm 1.7\text{ cm}^{-1}$  for the B3LYP and  $\pm 1.2\text{ cm}^{-1}$  for the BPW91 functionals) between the scaled predictions and the observed frequencies confirms the assignment of the  $1918.2\text{ cm}^{-1}$  band to the  $\nu_1(\sigma)$  mode of linear  $\text{CoC}_3$  in its  ${}^2\Delta$  state.

As shown in Table 4.1, DFT calculations predict the  $\nu_5(b_2)$  vibrational fundamental of the  ${}^2B_1$  fanlike isomer of  $\text{CoC}_3$  should lie in the  $1400\text{-}1600\text{ cm}^{-1}$  region and could have sufficient intensity to be observed. In other studies done in the TCU Molecular Physics Lab, the analogous vibration for fanlike  $\text{TiC}_3$  (Ref. 55) and  $\text{ScC}_3$  (Ref. 71) have been observed, however, a careful search of the region revealed no absorption that could be assigned to fanlike  $\text{CoC}_3$ .

#### 4.5 Conclusions

The first detection of the vibrational spectrum of  $\text{CoC}_3$  has been reported accompanied by a DFT investigation of its two lowest-lying isomers. The earlier PE spectra<sup>20</sup> had broad, unresolved vibrational structure that made it impossible to determine the geometry of  $\text{CoC}_3$  and led to its exclusion from the theoretical part of the investigation. In the present work, matrix isolation of the evaporated products of the dual laser ablation of Co and C rods has produced a band at  $1918.2\text{ cm}^{-1}$  and the signature isotopic shift pattern of a non-centrosymmetric linear molecule with three C atoms. The excellent agreement between the FTIR measured  $^{13}\text{C}$  shifts and the results of DFT BPW91/ and B3LYP/6-311+G(3df) calculations confirms the assignment of the  $1918.2\text{ cm}^{-1}$  absorption to the  $\nu_1(\sigma)$  vibrational fundamental of linear  $\text{CoC}_3$ .

These results indicate that the  $^2\Delta$  state of the linear isomer is the universal ground state (as predicted by DFT/B3LYP calculations), rather than the  $^2B_1$  state of the fanlike isomer (as predicted by DFT/BPW91 calculations), lying only  $\sim 4$  kcal/mol lower in energy. The linear structure found for  $\text{CoC}_3$  in the present investigation contrasts with the recent report of the observation of ( $^1A_1$ ) fanlike  $\text{TiC}_3$  which is, however, well separated energetically from competing linear and kite-shaped structures.<sup>55</sup> The current findings, however, are similar to those presented in Chapter III for the  $^5\Pi$  linear  $\text{CrC}_3$  species for which close-lying fanlike and linear structures are also predicted.<sup>46</sup> This study on  $\text{CoC}_3$  both the first theoretical investigation on this molecule and the first optical detection of the linear isomer and measurement of a vibrational fundamental.

## CHAPTER V

### FTIR OBSERVATION AND DFT STUDY OF THE $\text{AlC}_3$ AND $\text{AlC}_3\text{Al}$ LINEAR CHAINS TRAPPED IN SOLID Ar

#### 5.1 Introduction

Studies on aluminum–carbon ( $\text{Al}_n\text{C}_m$ ) clusters have been carried out as part of a project on the characterization of novel metal–carbon species. The study of the infrared spectra and structures of small  $\text{Al}_n\text{C}_m$  species is motivated in part by the astrophysical detection of small Al-bearing molecules<sup>9</sup> and by the desire to understand the formation and bonding of metal carbides. Previous studies have shown  $\text{Al}_n\text{C}_m$  species may have novel chemical structures and bonding.<sup>72</sup>

The AlC molecule has been extensively studied both by theorists<sup>35,73,74</sup> and experimentalists.<sup>35,74,75</sup> Its ground state is predicted to be  $^4\Sigma^-$  and its vibrational fundamental<sup>35</sup> has been measured at  $629.8\text{ cm}^{-1}$ . The only studies on the excited states of AlC and on the ground and excited states of  $\text{AlC}^-$  are theoretical investigations,<sup>76</sup> which have predicted a  $^2\Pi$  first excited state for AlC and  $^3\Pi$  ground and  $^3\Sigma^-$  first excited states for  $\text{AlC}^-$ . The  $\text{Al}_2\text{C}$  molecule has been observed<sup>35</sup> in its  $^2A_1$  ground state and its  $\nu_3(b_2)=802.0\text{ cm}^{-1}$  mode has been identified.

Aluminum dicarbides,  $\text{AlC}_2$ ,<sup>74,77–79</sup>  $\text{Al}_2\text{C}_2$ ,<sup>35,72</sup> and  $\text{Al}_3\text{C}_2$ ,<sup>80</sup> have also been investigated.  $\text{AlC}_2$  is predicted to have an ionic  $\text{Al}^+\text{C}_2^-$  electronic structure<sup>77</sup> with T-shaped ( $C_{2v}$ ) geometry and a  $^2A_1$  ground state,<sup>77–79</sup>  $\sim 11\text{--}16\text{ kcal/mol}$  lower in energy than the  $^2\Sigma^+$  linear AlCC isomer, which is supported by PE<sup>79</sup> and ESR<sup>74</sup> spectra. For the anion,  $\text{AlC}_2^-$ , DFT predicts that the  $^1\Sigma^+$  isomer is the ground state by  $1.4\text{ kcal/mol}$ , which is supported by PES measurements,<sup>79</sup> but CCSD(T) calculations indicate the  $C_{2v}$  isomer is  $\sim 2.1\text{ kcal/mol}$  lower in energy.

The first detection of  $\text{Al}_2\text{C}_2$  reported that the molecule is linear based on the agreement between the  $^{13}\text{C}$  isotopic shifts observed for the  $\nu_3(\sigma_u) = 605.1 \text{ cm}^{-1}$  mode and predictions at the complete active space self-consistent field level of theory.<sup>35</sup> A subsequent PES and theoretical investigation<sup>72</sup> of  $\text{Al}_2\text{C}_2$  and  $\text{Al}_2\text{C}_2^-$  using DFT, second-order Møller-Plesset (MP2), and CCSD(T) calculations has revealed the presence of two isomers of the anion in PE spectra, a slightly *trans*-bent  $C_{2h}$  structure (quasilinear) with  ${}^2B_g$  symmetry and a rhombic  $D_{2h}$  ( ${}^2B_{3g}$ ) structure with a transannular C–C bond 7.2 kcal/mol higher in energy. For neutral  $\text{Al}_2\text{C}_2$ , only one minimum has been found corresponding to a quasilinear structure. FTIR measurements performed as part of the present work, support a linear ( ${}^1\Sigma_g^+$ ) structure for  $\text{AlC}_2\text{Al}$  and the assignment of the  $\nu_3(\sigma_u)$  mode at  $605.1 \text{ cm}^{-1}$ , as concluded earlier.<sup>35</sup>

In a combined theoretical and PES study<sup>80</sup> of the  $\text{Al}_3\text{C}_2$  anion, the predicted fanlike ( $C_{2v}$ ) structure with a  ${}^1A_1$  electronic ground state has been confirmed by PE spectra. The neutral species has also been predicted to be fanlike, slightly distorted out of the plane, lowering its symmetry to  $C_2$ , with a  ${}^2B$  ground state.

Combined PES and DFT studies have been reported on the hyperaluminum–carbon molecules  $\text{Al}_3\text{C}$ ,<sup>81</sup>  $\text{Al}_4\text{C}$ ,<sup>82</sup> and  $\text{Al}_5\text{C}$ .<sup>83</sup> A theoretical investigation on  $\text{Al}_7\text{C}$ <sup>84</sup> and a PES characterization of  $\text{Al}_{12}\text{C}^-$  (Ref. 85) have been motivated by the discovery of the unusually stable and abundant  $\text{Al}_{13}^-$  cluster.<sup>86</sup>

Until the present work, there have been many theoretical investigations,<sup>26,77,87–90</sup> but no experimental observation of  $\text{AlC}_3$ . The initial study<sup>77</sup> included the fanlike ( $C_{2v}$ ) and the linear  $\text{AlCCC}$  and  $\text{CAICC}$  structures, and concluded, based on both DFT and MP2 calculations, that the  ${}^4B_1$  state of the fanlike isomer is well separated energetically from the other structures and is the ground state. Subsequently, extensive calculations have been reported<sup>26</sup> on three low-lying isomers of  $\text{AlC}_3$  [see Figs. 5.1(a)-(c)]: linear  $\text{AlCCC}$ , the ( $C_{2v}$ ) fan, and a ( $C_{2v}$ ) rhomboidal four-



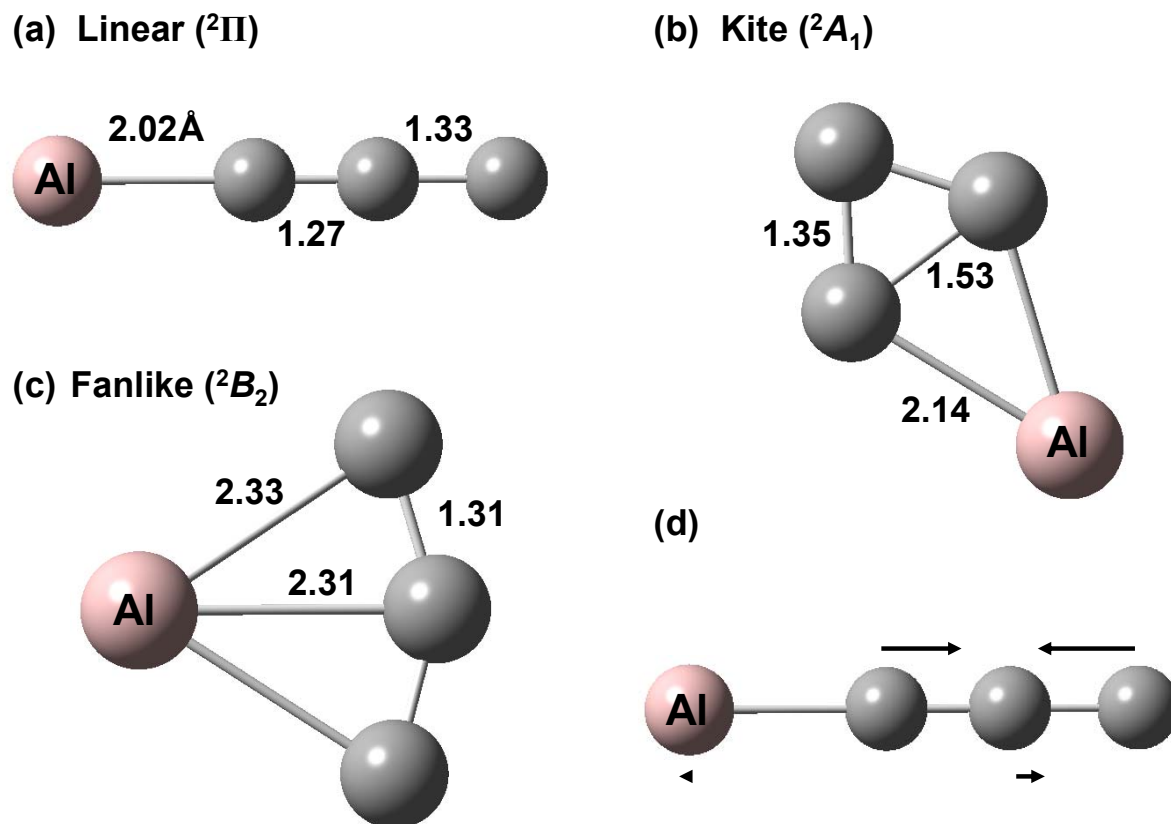


Figure 5.1 DFT B3LYP/6-311+G(3df) predictions of bond lengths ( $\text{\AA}$ ) of the (a)  ${}^2\Pi$  linear, (b)  ${}^2A_1$  kite ( $C_{2v}$ ), and (c)  ${}^2B_2$  fanlike ( $C_{2v}$ ) isomers of  $\text{AlC}_3$ . The predicted principal nuclear displacements of the  $\nu_2(\sigma)$  mode of ( ${}^2\Pi$ ) linear  $\text{AlC}_3$  are shown in (d).

membered ring structure, hereafter referred to as a “kite”. Various theoretical methods including DFT, MP2, and CCSD(T), were employed to investigate both doublet and quartet spin states for each structure. Regardless of the method of calculation used, the doublet states of each structure were predicted to be 24-52 kcal/mol lower in energy than the quartet states. Moreover, the doublet kite and linear structures were predicted to be nearly isoenergetic with the doublet fan, always lying ~6-8 kcal/mol higher in energy. The authors concluded that the three isomers are close enough in energy that any or all of them could be observed, but asserted that the linear ( ${}^2\Pi$ ) isomer is the most probable ground state. In their subsequent study of the  $\text{AlC}_3^+$  cation,<sup>90</sup> the authors found that the  ${}^1\Sigma$  linear isomer is ~6-10 kcal/mol lower in energy than the  ${}^1A_1$  ( $C_{2v}$ ) kite isomer, but concluded that either or both of the isomers could be experimentally detected.

Over the next few years, theoretical studies on the stabilities of  $\text{AlC}_n$ ,  $\text{AlC}_n^-$ , and  $\text{AlC}_n^+$  ( $n=1-7$ )<sup>87,89</sup> and ( $n=1-10$ )<sup>88</sup> clusters found that chains with odd- $n$  are more stable than those with even- $n$  in the neutral and cation species, but that the reverse is true in anion species.<sup>87,88</sup> Linear chains were predicted to be more stable than the cyclic or fanlike structures,<sup>89</sup> with the exceptions of  $\text{AlC}_2$ ,  $\text{AlC}_2^+$ , and  $\text{AlC}_6^+$ . These results support the earlier conclusion<sup>26</sup> that linear  $\text{AlC}_3$  is probably more stable than the fanlike isomer and is thus the ground state structure.

Previous FTIR and DFT investigations of  $\text{M}_n\text{C}_3$  clusters in the TCU Molecular Physics Laboratory have resulted in the characterization of the vibrational spectra and structures of linear  $\text{CrC}_3$ ,<sup>46</sup>  $\text{CoC}_3$ ,<sup>91</sup>  $\text{NiC}_3\text{Ni}$ ,<sup>92</sup> and fanlike ( $C_{2v}$ )  $\text{TiC}_3$ ,<sup>55</sup> all produced by trapping the laser ablated products of metal and carbon rods in solid Ar. Comparing measured fundamental frequencies and  ${}^{13}\text{C}$  isotopic shifts with DFT predictions has confirmed vibrational frequency assignments and geometry determinations. In the present work, similar techniques have been used to identify the  $\nu_3(\sigma_u)=1624.0$  and  $\nu_4(\sigma_u)=528.3\text{cm}^{-1}$  modes of ( ${}^3\Sigma_g^+$ ) linear  $\text{AlC}_3\text{Al}$  as well as the  $\nu_2(\sigma)=1210.9\text{cm}^{-1}$  fundamental of ( ${}^2\Pi$ ) linear  $\text{AlC}_3$ .

## 5.2 Theoretical Predictions

The two most comprehensive investigations<sup>26,77</sup> on  $\text{AlC}_3$  reached different conclusions. Using MP2/6-311+G\* calculations, Zheng *et al.*<sup>77</sup> predicted that the  $^4B_1$  fanlike ( $C_{2v}$ ) isomer is the ground state, well separated energetically from the linear AICCC and CAICC isomers. Barrientos *et al.*<sup>26</sup> using DFT, MP2, and CCSD(T) methods have found that the  $^2A_1$  kite and the  $^2\Pi$  linear isomers are nearly isoenergetic ( $\pm 3$  kcal/mol) but the  $^2B_2$  fanlike isomer is  $\sim 6$ -8 kcal/mol higher in energy [Figs. 5.1 (a)-(c)]. In the case of  $\text{AlC}_3\text{Al}$ , the DFT calculations in the present work are apparently the first for this molecule.

The DFT calculations on  $\text{AlC}_3$  and  $\text{AlC}_3\text{Al}$  were performed with the GAUSSIAN 03 program suite,<sup>45</sup> using the B3LYP functional<sup>47</sup> and a 6-311+G(3df) basis set. Frequencies and IR intensities were calculated for the linear isomer of  $\text{AlC}_3\text{Al}$  (see Table 5.1) and for the linear, kite, and fanlike isomers of  $\text{AlC}_3$  (see Table 5.2). Geometric parameters for  $\text{AlC}_3\text{Al}$  are given in Fig. 5.2(a) and for the three  $\text{AlC}_3$  isomers in Fig. 5.1 (a)-(c).

DFT calculations on the  $\text{AlC}_3\text{Al}$  cluster, done as part of the present work, yield a stable minimum linear structure in the  $^3\Sigma_g^+$  state. For  $\text{AlC}_3$ , the present DFT calculations agree with the predictions made by Barrientos *et al.*<sup>26</sup> The quartet states are predicted to be much higher in energy for all three isomers investigated. Although the  $^2\Pi$  linear isomer is predicted to be the lowest energy isomer, the  $^2A_1$  kite and  $^2B_2$  fanlike isomers are only 1.0 and 7.1 kcal/mol higher in energy, leaving the true ground state structure in question.

## 5.3 Experimental Procedures

$\text{AlC}_3$  and  $\text{AlC}_3\text{Al}$  were produced by the simultaneous ablation of Al (99.999%, ESPI) and C (99.9995%, Alfa Aesar) rods, which were continuously rotated and translated to provide clean surfaces for two 1064 nm pulsed Nd:YAG lasers (Spectra Physics). High purity Ar (99.995%,

Table 5.1: DFT B3LYP/6-311+G(3*df*) predicted vibrational frequencies ( $\text{cm}^{-1}$ ) and intensities ( $\text{km/mol}$ ) for linear ( ${}^3\Sigma_g^+$ )  $\text{AlC}_3\text{Al}$ .

Vibrational Mode	Frequency ( $\text{cm}^{-1}$ )	IR intensity ( $\text{km/mol}$ )
$\nu_1(\sigma_g)$	1393	0
$\nu_2(\sigma_g)$	333	0
$\nu_3(\sigma_u)$	1710	388
$\nu_4(\sigma_u)$	541	710
$\nu_5(\pi_g)$	106	0
$\nu_1(\pi_u)$	45	$\sim 0$

Table 5.2: DFT B3LYP/6-311+G(3df) predicted vibrational frequencies ( $\text{cm}^{-1}$ ) and intensities ( $\text{km/mol}$ ) for the linear ( ${}^2\Pi$ ), kite ( ${}^2A_1$ ), and fanlike ( ${}^2B_2$ ) isomers of  $\text{AlC}_3$ .

${}^2\Pi$ Linear			${}^2A_1$ Kite ( $C_{2v}$ )			${}^2B_2$ Fanlike ( $C_{2v}$ )		
Mode	Frequency <sup>a</sup> ( $\text{cm}^{-1}$ )	Intensity ( $\text{km/mol}$ )	Mode	Frequency <sup>a</sup> ( $\text{cm}^{-1}$ )	Intensity ( $\text{km/mol}$ )	Mode	Frequency <sup>a</sup> ( $\text{cm}^{-1}$ )	Intensity ( $\text{km/mol}$ )
$\nu_1(\sigma)$	1922	43	$\nu_1(a_1)$	1585	45	$\nu_1(a_1)$	1244	7
$\nu_2(\sigma)$	1245	223	$\nu_2(a_1)$	809	99	$\nu_2(a_1)$	477	42
$\nu_3(\sigma)$	414	163	$\nu_3(a_1)$	395	56	$\nu_3(a_1)$	295	71
$\nu_4(\pi)$	396/259 <sup>b</sup>	5/2	$\nu_4(b_1)$	248	1	$\nu_4(b_1)$	142	30
$\nu_5(\pi)$	76/66 <sup>b</sup>	1/7	$\nu_5(b_2)$	1231	1	$\nu_5(b_2)$	1678	127
			$\nu_6(b_2)$	267	38	$\nu_6(b_2)$	117	26

<sup>a</sup>Frequencies for all three isomers were initially published by Barrientos *et al.* in Ref. 26. Subsequent theoretical studies by the same group again reported the linear and kite frequencies (Refs. 87 and 89, respectively), but no IR intensities were given. These calculations are in good agreement with those previously published.

<sup>b</sup>Both Renner-Teller components are given.

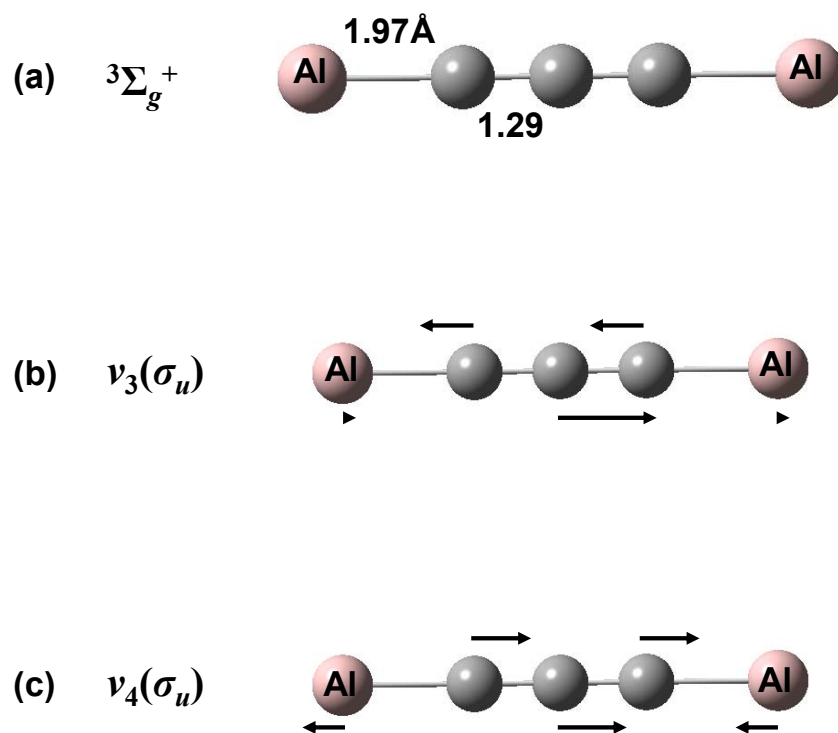


Figure 5.2 (a) DFT B3LYP/6-311+G(3*df*) predictions of bond lengths (Å) for the  ${}^3\Sigma_g^+$  linear isomer of  $\text{AlC}_3\text{Al}$ . The predicted principal nuclear displacements of the (b)  $\nu_3(\sigma_u)$  and (c)  $\nu_4(\sigma_u)$  modes of ( ${}^3\Sigma_g^+$ )  $\text{AlC}_3\text{Al}$ .

Matheson Tri-Gas), introduced through the rear of the sample chamber, swept the ablated material onto a gold mirror that was kept at  $\sim 10$  K by a closed-cycle refrigeration system (ARS, Displex). The vacuum chamber was maintained at a pressure of  $\leq 10^{-7}$  Torr. Spectra were then recorded with a resolution of  $0.2 \text{ cm}^{-1}$  over the  $400\text{-}4000 \text{ cm}^{-1}$  frequency range using a Bomem DA 3.16 FTIR spectrometer equipped with a liquid  $\text{N}_2$ -cooled MCT detector. All frequencies reported were measured to  $\pm 0.1 \text{ cm}^{-1}$ . Additional details of the experimental apparatus have been reported previously.<sup>38</sup> The production of small  $\text{C}_n$  clusters, predominantly  $\text{C}_3$ , was enhanced by adjusting experimental conditions such as laser power, laser focus, and Ar flow rate.

The identification of molecular species and their vibrational spectra is dependent on obtaining  $^{13}\text{C}$  isotopic shifts. The C rods were fabricated with various mixtures of  $^{13}\text{C}$  (99.3%, Isotec) and  $^{12}\text{C}$  (99.9995%, Alfa Aesar) powders, pressed under a pressure of  $\sim 4.5 \times 10^5$  kPa. In the experiments with Al, three carbon rods were prepared, a  $^{12}\text{C}$  rod, and two other rods with 20% and 30%  $^{13}\text{C}$  enrichments. Measurements of  $^{13}\text{C}$  shifts have previously enabled the TCU Molecular Physics Lab to determine various molecular geometries including planar pentagonal  $\text{Si}_3\text{C}_2$ ,<sup>42</sup> rhomboidal  $\text{Si}_3\text{C}$ ,<sup>40</sup> fan-shaped ( $\text{C}_{2v}$ )  $\text{TiC}_3$ ,<sup>55</sup> non-centrosymmetric linear structures such as  $\text{GeC}_3\text{Si}$ ,<sup>33</sup> and  $\text{CoC}_3$ ,<sup>91</sup> and the centrosymmetric linear  $\text{NiC}_3\text{Ni}$  molecule.<sup>92</sup>

#### 5.4 Results and Discussion

In order to identify potential candidates for  $\text{Al}_n\text{C}_m$  absorptions, the spectrum obtained from the simultaneous ablation of Al and  $^{12}\text{C}$  rods shown in Fig. 5.3(a) was compared with the spectrum in Fig. 5.3(b) obtained by ablating only a  $^{12}\text{C}$  rod. In addition to absorptions previously assigned to  $\text{C}_n$  species,<sup>49</sup> a prominent feature in the Al/C spectrum at  $605.1 \text{ cm}^{-1}$  was noted, which had earlier been identified as  $\text{Al}_2\text{C}_2$ .<sup>35</sup> Frequencies measured at  $596.8$  and  $589.0 \text{ cm}^{-1}$  for the  $^{13}\text{C}$  isotopomers,  $\text{Al}^{12}\text{C}^{13}\text{CAl}$  and  $\text{Al}^{13}\text{C}_2\text{Al}$ , respectively, are identical to earlier results.<sup>35</sup>

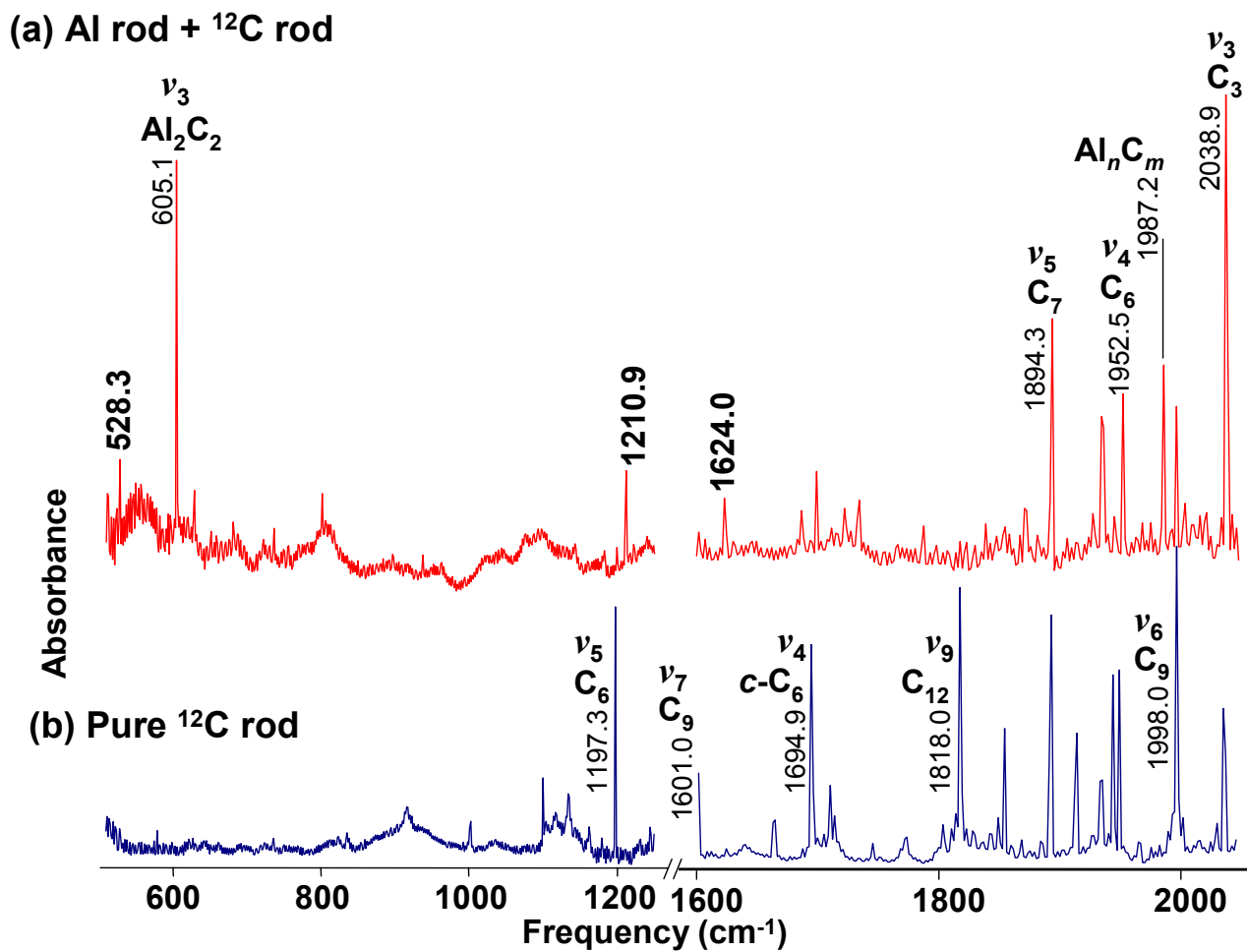


Figure 5.3 FTIR spectra recorded after (a) dual ablation of Al and  $^{12}\text{C}$  rods and (b) ablation of a  $^{12}\text{C}$  rod only, for comparison. Note the 1624.0, 1210.9, and 528.3  $\text{cm}^{-1}$  bands in the Al-C spectrum that are not in the  $^{12}\text{C}$  spectrum.



The observation of  $\text{Al}_2\text{C}_2$  indicates that  $\text{Al}_n\text{C}_m$  species have been created and that multiple Al atoms could be attached to a  $\text{C}_n$  species. Only trace amounts of CO and  $\text{H}_2\text{O}$  appear in the dual ablation spectrum, resulting in very weak absorptions of  $\text{Al}_2\text{O}$  at  $992.8$ ,<sup>93</sup>  $\text{HAlAlH}$  at  $1646.9$ ,<sup>94</sup>  $\text{AlH}_2$  at  $1769.6$ ,<sup>94,95</sup>  $\text{Al}(\text{CO})$  at  $1867.7$ ,<sup>96,97</sup> and  $\text{Al}(\text{CO})_2$  at  $1907.9 \text{ cm}^{-1}$ .<sup>96,98</sup> Otherwise, no absorptions in the spectra in Fig. 5.3(a) suggest the presence of species with combinations of O and H atoms bonded to  $\text{Al}_n$  or  $\text{Al}_n\text{C}_m$  clusters, such as  $\text{HCCAl}$ ,  $\text{HCCAlH}$ ,  $(\text{C}_2\text{H}_2)\text{Al}$ , or  $c\text{-HC=CHAl}$ ,<sup>35,99</sup>  $\text{HAlO}$  or  $\text{HAlOH}$ ,<sup>100</sup>  $\text{Al}_2(\text{CO})_2$ ,<sup>101</sup>  $\text{H}(c\text{-AlHAl})$ ,<sup>94,102</sup>  $\text{AlH}_3$ ,<sup>94,95</sup>  $\text{OAlOO}$  or  $\text{Al}_2\text{O}_3$ ,<sup>93</sup>  $(\text{AlO})_2$ ,<sup>93,103</sup>  $\text{AlO}_2$ ,<sup>104</sup> or  $c\text{-AlO}_2$ .<sup>93,103,105</sup> It is therefore likely that unidentified absorptions result from pure  $\text{Al}_n\text{C}_m$  molecules rather than impurity species.

In the dual ablation experiment, low laser powers ( $<1.0 \text{ W}$ ) were used with the C rod to favor the production of  $\text{C}_3$ . As a result, an intense absorption of the  $\nu_3(\sigma_u)$  mode of  $\text{C}_3$  dwarfs most other features in the spectrum. Under these conditions, several strong absorptions appear in the dual ablation spectrum at  $1624.0$ ,  $1210.9$ , and  $528.3 \text{ cm}^{-1}$  that are candidates for  $\text{Al}_n\text{C}_m$  species. To assign these bands and determine the geometry of the molecule or molecules responsible requires  $^{13}\text{C}$  isotopic shifts. The  $^{13}\text{C}$  shift patterns that have resulted from a dual ablation experiment using a C rod with a 30%  $^{13}\text{C}$  enrichment demonstrate that the  $1624.0$  and  $528.3 \text{ cm}^{-1}$  bands result from a different molecule than the  $1210.9 \text{ cm}^{-1}$  absorption.

#### 5.4.1 Identification of $\text{AlC}_3\text{Al}$

The behavior of two absorptions at  $1624.0$  and  $528.3 \text{ cm}^{-1}$  in the spectrum in Fig. 5.3(a) indicates that they could be two vibrational modes of the same molecule. In different experiments and after annealing, the intensity of the  $528.3 \text{ cm}^{-1}$  absorption is consistently  $\sim 1.3$  times the intensity of the  $1624.0 \text{ cm}^{-1}$  band. The isotopic shift patterns for the  $1624.0$  and  $528.3 \text{ cm}^{-1}$  bands observed for a C rod with 30%  $^{13}\text{C}$  enrichment are shown in Figs. 5.4(a) and 5.5(a), respectively. Further analysis confirms that the two bands result from the same carrier species.

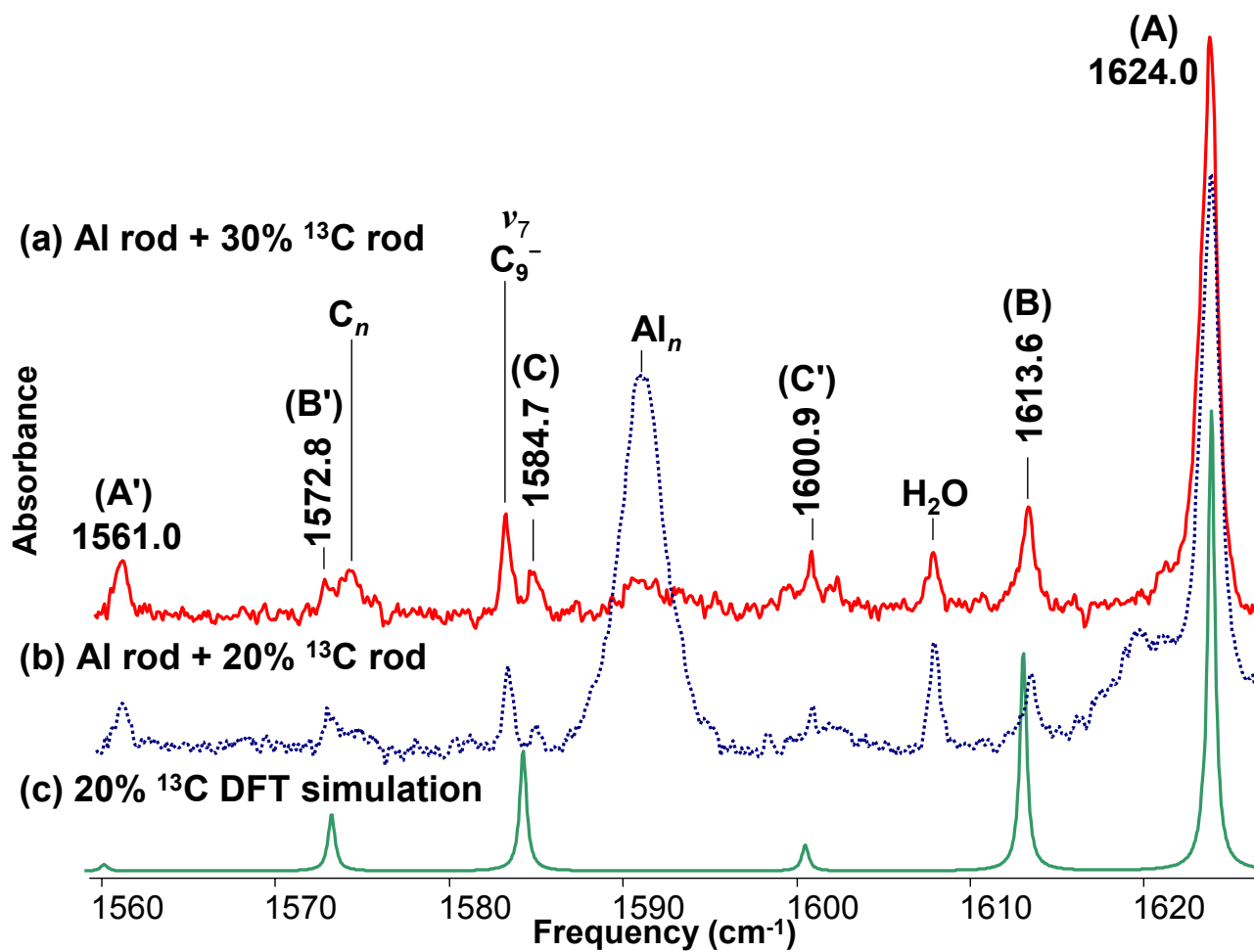


Figure 5.4 FTIR spectra of the  $\nu_3(\sigma_u)$  mode of linear  $\text{AlC}_3\text{Al}$  in experiments with (a) 30% and (b) 20% nominal  $^{13}\text{C}$  enrichments. (c) DFT simulation of an experiment with a 20% enrichment.

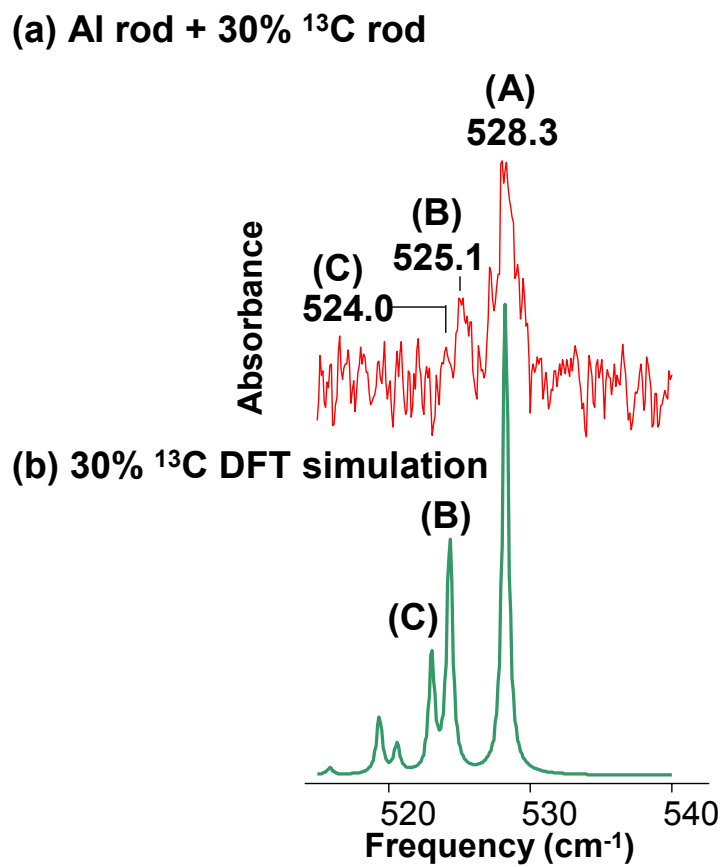


Figure 5.5 The  $\nu_4(\sigma_u)$  mode of  $\text{AlC}_3\text{Al}$  in (a) an FTIR spectrum with a nominal 30%  $^{13}\text{C}$  enrichment compared with (b) a DFT simulation with 30%  $^{13}\text{C}$  enrichment.

In the Fig. 5.4(a) spectrum, several features can be seen to the low frequency side of the 1624.0 cm<sup>-1</sup> absorption. The band at 1607.9 cm<sup>-1</sup> originates with H<sub>2</sub>O contamination, while the broad feature at ~1574 cm<sup>-1</sup> results from an unidentified pure C<sub>n</sub> species. Absorptions at 1583.3 and 1686.7 cm<sup>-1</sup> (not shown) belong respectively, to the ν<sub>7</sub>(σ<sub>u</sub>) and ν<sub>6</sub>(σ<sub>u</sub>) fundamentals of C<sub>9</sub><sup>-</sup>.<sup>60,106</sup> The remaining bands at 1613.6, 1600.9, 1584.7, 1572.8, and 1561.0 cm<sup>-1</sup> appear to be good candidates for <sup>13</sup>C shifts from the 1624.0 cm<sup>-1</sup> absorption.

Since the ν<sub>3</sub>(σ<sub>u</sub>)=2038.9 cm<sup>-1</sup> mode of C<sub>3</sub> is the dominant absorption in Fig. 5.3(a), a molecule containing the C<sub>3</sub> unit is a strong contender for the carrier of the 1624.0 cm<sup>-1</sup> absorption. The isotopic shift pattern for the 1624.0 cm<sup>-1</sup> spectrum shown in Fig. 5.4(a) supports this tentative conclusion. In this experiment, the isotopic shift band intensities for single inequivalent <sup>13</sup>C substitutions in C<sub>n</sub> species are ~8% of the intensity of the <sup>12</sup>C<sub>n</sub> isotopomer band. Thus for C<sub>3</sub>, two shifts of 8% and 16% are observed corresponding to one unique and two equivalent substitution sites. The <sup>13</sup>C shift bands at 1613.6 and 1584.7 cm<sup>-1</sup> labeled (B) and (C) in Fig. 5.4(a) are ~16% and ~8% of the intensity of the main absorption at 1624.0 cm<sup>-1</sup>, which suggests the possibility that the molecule contains at least two equivalent C atoms and one unique atom. A C<sub>3</sub> chain with a terminal Al atom is thus eliminated as a possible carrier of the 1624.0 cm<sup>-1</sup> band, but linear AlC<sub>3</sub>Al [Fig. 5.2(a)] or an AlC<sub>3</sub> species with C<sub>2v</sub> symmetry, such as the kite or fanlike isomers [see Figs. 5.1(b) and (c)], are all possible candidates.

The vibrational frequency of the fully-substituted Al<sub>n</sub><sup>13</sup>C<sub>3</sub> species responsible for the 1624.0 cm<sup>-1</sup> absorption can be estimated by assuming the Al atom(s) are not participating strongly in the vibration and using the harmonic oscillator approximation

$$\nu_{^{13}\text{C}} \approx \sqrt{\frac{m_{^{12}\text{C}}}{m_{^{13}\text{C}}}} \times \nu_{^{12}\text{C}} \approx \sqrt{\frac{12.0}{13.00335}} \times \nu_{^{12}\text{C}} \quad (1)$$

Assuming  $\nu_{12C} = 1624.0$ , gives  $\nu_{13C} \approx 1560.1 \text{ cm}^{-1}$ , which is very near the  $1561.0 \text{ cm}^{-1}$  absorption in Fig. 5.4(a), and suggests that it is the fully-substituted  $^{13}\text{C}$  isotopomer band  $\text{Al}_n^{13}\text{C}_3$ . The measured intensity, which is  $\sim 9\%$  of the main  $\text{Al}^{12}\text{C}_3$  absorption intensity, reflects the absence of complete randomization in the  $^{12}\text{C}/^{13}\text{C}$  mixture in the rod, which was fabricated with  $30\%$   $^{13}\text{C}$ . The  $^{13}\text{C}$  shifts for the  $\nu_3(\sigma_u) = 2038.9 \text{ cm}^{-1}$  mode of  $\text{C}_3$  show a similar intensity behavior. The intensity of the  $^{13}\text{C}_3$  isotopomer band is  $\sim 9\%$  of the main  $^{12}\text{C}_3$  absorption, the same as for the  $1561.0 \text{ cm}^{-1}$  band proposed for a fully  $^{13}\text{C}$ -substituted  $\text{Al}_n^{13}\text{C}_3$  species.

Aside from the isotopomer bands proposed for the single and full  $^{13}\text{C}$  substitutions, the only remaining candidates for isotopic shifts are the absorptions at  $1572.8$  and  $1600.9 \text{ cm}^{-1}$  that are labeled (B') and (C') in Fig. 5.4(a). The pattern of these two absorptions shifted from the  $1561.0 \text{ cm}^{-1}$  band proposed for  $\text{Al}_n^{13}\text{C}_3$  mirrors the shifts of the  $1613.6$  and  $1584.7 \text{ cm}^{-1}$  bands shifted from the  $1624.0 \text{ cm}^{-1}$  band proposed for an  $\text{Al}_n^{12}\text{C}_3$  fundamental. Consequently, they are good candidates for the shifts corresponding to doubly-substituted  $^{13}\text{C}$  isotopomers. However, a comparison of the intensity ratio of the  $1600.9$  to the  $1572.8 \text{ cm}^{-1}$  band in the spectrum shown in Fig. 5.4 (a) is not possible because the  $1572.8 \text{ cm}^{-1}$  band is partially overlapped by the broad feature at  $\sim 1574 \text{ cm}^{-1}$  belonging to an unidentified  $\text{C}_n$  molecule. In addition, the  $1600.9 \text{ cm}^{-1}$  band may have a contribution from the  $\nu_7(\sigma_u)$  mode of  $\text{C}_9$  at  $1601.0 \text{ cm}^{-1}$ .<sup>107</sup> An experiment using a C rod with  $20\%$   $^{13}\text{C}$  enrichment was done under conditions that allowed the band at  $1572.8 \text{ cm}^{-1}$  to be better resolved and also eliminated  $\text{C}_9$  as a product. In the resulting spectrum shown in Fig. 5.4(b), the intensity of the  $1572.8 \text{ cm}^{-1}$  absorption (B') is approximately twice that of the  $1600.9 \text{ cm}^{-1}$  absorption (C'), which would be consistent with the (B') band belonging to the isotopomer with  $^{13}\text{C}$  atoms substituted at the central and one end site and (C') belonging to the isotopomer with  $^{13}\text{C}$  substituted at both of the end sites. It should be noted that the additional

broad feature at  $\sim 1591.1 \text{ cm}^{-1}$  in Fig. 5.4(b) also appears when Al is ablated in the absence of C and thus likely belongs to an  $\text{Al}_n$  or  $\text{Al}_n$ -bearing species.

Linear  $\text{AlC}_3\text{Al}$  [Fig. 5.2(a)] or isomers of  $\text{AlC}_3$  with  $C_{2v}$  symmetry, such as the kite or fan [Figs. 5.1(b) and (c)], would thus be consistent with the observed  $^{13}\text{C}$  isotopic shift pattern for the  $1624.0 \text{ cm}^{-1}$  band. It is worth noting that the analogous  $\text{AlC}_2\text{Al}$  chain is observed via its  $605.1 \text{ cm}^{-1}$  band,<sup>35</sup> which is a prominent absorption in the spectra [see Fig. 5.3(a)]. The  $\text{AlC}_3$  kite is unlikely as the carrier since the  $\nu_1(a_1)\sim 1585 \text{ cm}^{-1}$  mode frequency prediction is significantly lower than the observed  $1624.0 \text{ cm}^{-1}$  band and its  $\nu_2(a_1)\sim 809 \text{ cm}^{-1}$  fundamental, predicted to be twice as intense as its  $\nu_1(a_1)$  mode, is not observed in the spectra. However, as can be seen from Tables 5.1 and 5.2, respectively, the  $\nu_3(\sigma_u)\sim 1710 \text{ cm}^{-1}$  mode predicted for linear  $\text{AlC}_3\text{Al}$  and the  $\nu_5(b_2)\sim 1678 \text{ cm}^{-1}$  mode of fanlike  $\text{AlC}_3$  are both possibilities for the observed  $1624.0 \text{ cm}^{-1}$  band. In order to discriminate between the two, the observed  $^{13}\text{C}$  shifts are compared with the predicted shifts for the  $\nu_3(\sigma_u)$  mode of ( $^3\Sigma_g^+$ )  $\text{AlC}_3\text{Al}$  and for the  $\nu_5(b_2)$  mode of fanlike ( $^2B_2$ )  $\text{AlC}_3$  in Table 5.3. It is readily seen that the agreement between the observed and predicted shifts for the  $\nu_3(\sigma_u)$  mode of  $\text{AlC}_3\text{Al}$  is within  $\pm 0.5 \text{ cm}^{-1}$  for all but one isotopomer. In contrast, discrepancies are  $\geq 1 \text{ cm}^{-1}$  for all but one of the shifts of the  $\nu_5(b_2)$  mode of fanlike ( $^2B_2$ )  $\text{AlC}_3$ . Similarly, there are discrepancies of  $\pm 5 \text{ cm}^{-1}$  with the already discounted  $\nu_1(a_1)$  fundamental of the  $\text{AlC}_3$  kite.

Additional support for the identification of  $1624.0 \text{ cm}^{-1}$  as the  $\nu_3(\sigma_u)$  mode of  $\text{AlC}_3\text{Al}$  is found in the analysis of the  $^{13}\text{C}$  shifts for the  $528.3 \text{ cm}^{-1}$  absorption. The observation that its intensity in the Fig. 5.3(a) spectrum is  $\sim 1.3$  times the intensity of the  $1624.0 \text{ cm}^{-1}$  feature is consistent with the prediction shown in Table 5.1 that the  $\nu_4(\sigma_u)$  fundamental of  $\text{AlC}_3\text{Al}$  should be  $\sim 1.8$  times the intensity of its  $\nu_3(\sigma_u)\sim 541.1 \text{ cm}^{-1}$  mode. Two  $^{13}\text{C}$  isotopic shifts are observed in the spectrum in Fig. 5.5(a) at  $525.1$  and  $524.0 \text{ cm}^{-1}$  labeled (B) and (C) for a C rod with 30%  $^{13}\text{C}$  enrichment. The intensity of the  $525.1 \text{ cm}^{-1}$  band is  $\sim 19\%$  of the intensity of the main  $528.3$

Table 5.3: Comparison of the observed isotopomer frequencies ( $\text{cm}^{-1}$ ) of the  $\nu_3(\sigma_u)$  and  $\nu_4(\sigma_u)$  modes of linear ( ${}^3\Sigma_g^+$ )  $\text{AlC}_3\text{Al}$  and of the  $\nu_5(b_2)$  mode of fanlike ( ${}^2B_1$ )  $\text{AlC}_3$  with the predictions of B3LYP/6-311+G(3df) calculations.

Mode	Isotopomer	Observed	DFT	Scaled	Difference	Mode	Isotopomer	Observed	DFT	Scaled	Difference		
	Al-C $_{\alpha}$ -C $_{\beta}$ -C $_{\beta}$ -Al	$\nu$	$\nu$	$\nu$	$\Delta\nu$		Al-C $_{\alpha}$ -C $_{\beta}$ -C $_{\alpha}$	$\nu$	$\nu$	$\nu$	$\Delta\nu$		
$\nu_3(\sigma_u)$	27-12-12-12-27 (A)	1624.0	1710.4	... <sup>a</sup>	...	$\nu_5(b_2)$	27-12-12-12	1624.0	1678.4	... <sup>c</sup>	...		
	27- <b>13</b> -12-12-27 (B)	1613.6	1699.0	1613.2	0.4		27- <b>13</b> -12-12	1613.6	1667.6	1613.5	0.1		
	27-12- <b>13</b> -12-27 (C)	1584.7	1668.6	1584.3	0.4		27-12- <b>13</b> -12	1584.7	1635.7	1582.7	2.0		
	27- <b>13</b> - <b>13</b> -13-27 (A')	1561.0	1643.2	1560.2	0.8		27- <b>13</b> - <b>13</b> -13	1561.0	1612.4	1560.1	0.9		
	27-12- <b>13</b> - <b>13</b> -27 (B')	1572.8	1657.0	1573.3	-0.5		27-12- <b>13</b> - <b>13</b>	1572.8	1624.6	1571.9	0.9		
	27- <b>13</b> -12- <b>13</b> -27 (C')	1600.9	1685.8	1600.6	0.3		27- <b>13</b> -12- <b>13</b>	1600.9	1655.7	1602.0	-1.1		
	$\nu_4(\sigma_u)$	27-12-12-12-27 (A)	528.3	541.1	... <sup>b</sup>		...						
		27- <b>13</b> -12-12-27 (B)	525.1	537.1	524.4		0.7						
		27-12- <b>13</b> -12-27 (C)	524.0	535.8	523.1		0.9						

<sup>a</sup>Results of the calculation are scaled by a factor of  $1624.0/1710.4=0.94949$ . <sup>b</sup>Scale factor is  $528.3/541.1=0.9763$ . <sup>c</sup>Scale factor is  $1624.0/1678.4=0.96759$ .

$\text{cm}^{-1}$  absorption, which is similar to the intensity of  $\sim 16\%$  observed for the  $1613.6 \text{ cm}^{-1}$  absorption compared to the  $1624.0 \text{ cm}^{-1}$  band, suggesting that the  $525.1 \text{ cm}^{-1}$  feature corresponds to a single  $^{13}\text{C}$  substitution on either of the two equivalent C atoms. The intensity of the other tentative band at  $524.0 \text{ cm}^{-1}$  could not be accurately measured because of the noise level.

Although its identification as a  $^{13}\text{C}$  shift is tentative, it is a recurrent feature in many spectra and the line shapes of the  $524.0$ ,  $525.1$ , and  $528.3 \text{ cm}^{-1}$  bands are similar. The observed FTIR spectrum is compared with a DFT simulation of the spectrum of the  $\nu_4(\sigma_u)$  mode of  $\text{AlC}_3\text{Al}$  assuming a  $30\%$   $^{13}\text{C}$  enrichment in Fig. 5.5. A comparison between the observed  $^{13}\text{C}$  shifts at  $525.1$  and  $524.0 \text{ cm}^{-1}$  and scaled DFT predictions (scale factor =  $528.3/541.1=0.9763$ ) appears in Table 5.3 and shows good agreement ( $\pm 0.9 \text{ cm}^{-1}$ ), which supports the assignment of the  $\nu_4(\sigma_u)$  mode of linear  $\text{AlC}_3\text{Al}$  at  $528.3 \text{ cm}^{-1}$ .

In summary, the identification of the  $\nu_3(\sigma_u)=1624.0 \text{ cm}^{-1}$  and  $\nu_4(\sigma_u)=528.3 \text{ cm}^{-1}$  modes of  $\text{AlC}_3\text{Al}$  has been confirmed on the basis of the good agreement between DFT predictions and the FTIR measurements of the  $^{13}\text{C}$  shifts ( $\pm 0.9 \text{ cm}^{-1}$ ) and their relative intensity ratio, which is predicted to be  $\nu_4:\nu_3\sim 1.8$  and is observed as  $\sim 1.3$ . The predicted principal nuclear displacements for these modes are shown in Figs. 5.2(b) and (c).

#### 5.4.2 Identification of $\text{AlC}_3$

Figure 5.6(a) shows the  $^{13}\text{C}$  shift pattern obtained for the  $1210.9 \text{ cm}^{-1}$  absorption when a C rod enriched with  $30\%$   $^{13}\text{C}$  is used. The observation of four features to the low frequency side at  $1208.2$ ,  $1192.3$ ,  $1185.4$ , and  $1164.0 \text{ cm}^{-1}$  with approximately equal intensities might suggest a molecule containing four unique C atoms. However, only a trace amount of the  $\nu_3(\sigma_u)=1543.4 \text{ cm}^{-1}$  mode<sup>108</sup> of  $\text{C}_4$  was produced in this experiment, while the  $\nu_3(\sigma_u)=2038.9 \text{ cm}^{-1}$  mode of  $\text{C}_3$  is the dominant  $\text{C}_n$  species in the FTIR spectrum shown in Fig. 5.3(a). Moreover, DFT predictions eliminate both linear ( $^2\Sigma$ )  $\text{AlC}_4$  and linear ( $^1\Sigma_g^+$ )  $\text{AlC}_4\text{Al}$ , as the band carrier. For  $\text{AlC}_4$ , the only



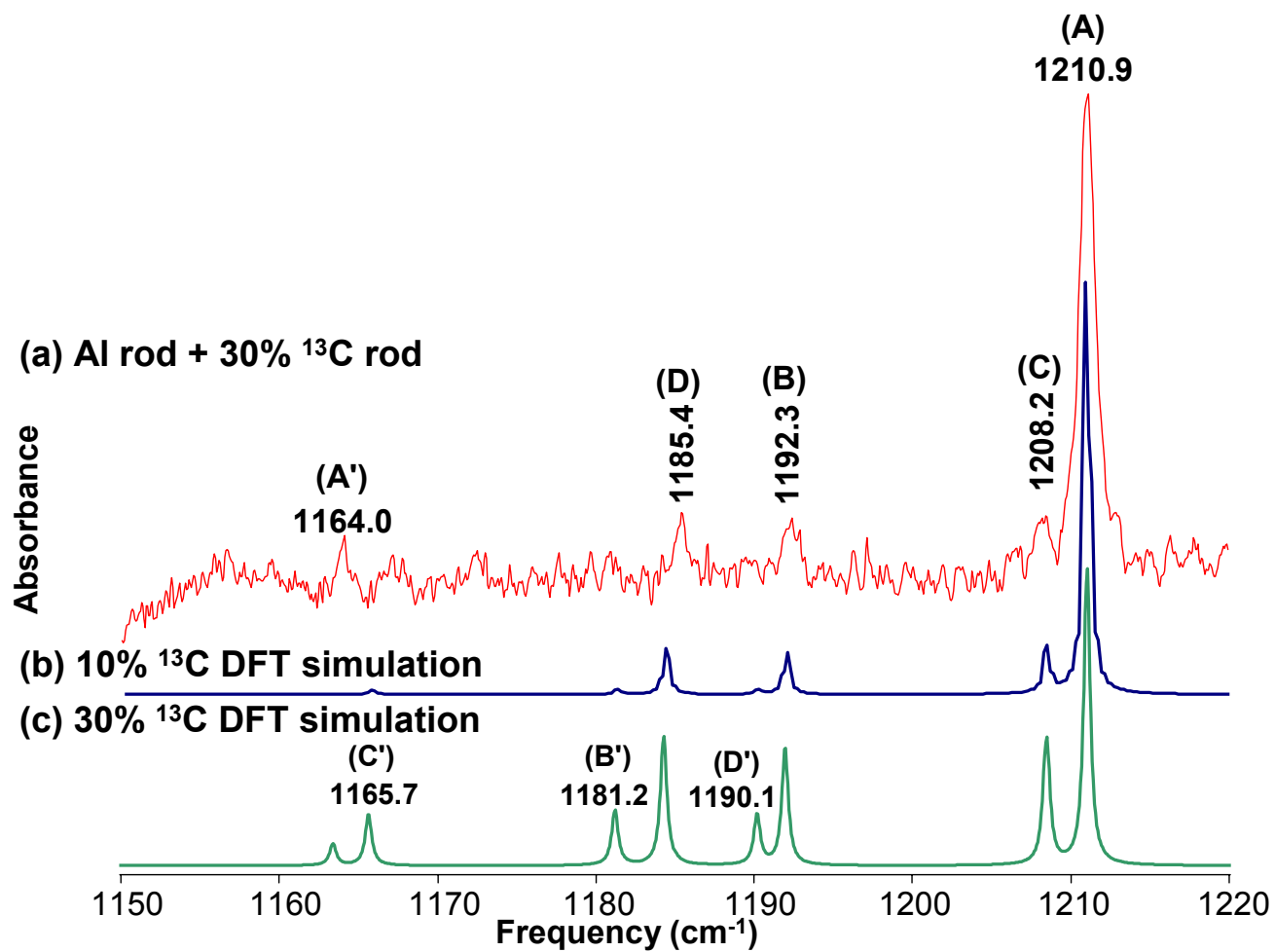


Figure 5.6 The  $\nu_2(\sigma)$  mode of linear  $\text{AlC}_3$  in (a) an FTIR spectrum with a nominal 30%  $^{13}\text{C}$  enrichment compared with DFT simulations of spectra with (b) 10% and (c) 30%  $^{13}\text{C}$  enrichments.

mode predicted near  $1210.9\text{ cm}^{-1}$ ,  $\nu_3(\sigma)\sim 1131\text{ cm}^{-1}$ , is too low and has weak intensity  $\sim 30$  km/mol. Furthermore, its most intense fundamental,  $\nu_1(\sigma)\sim 2141\text{ cm}^{-1}$ , has an intensity that is  $\sim 68$  times the intensity of the  $\nu_3$  mode, but no band is observed near this frequency.

Centrosymmetric linear  $\text{AlC}_4\text{Al}$  has only two vibrational modes predicted to have significant IR intensity,  $\nu_4(\sigma_u)\sim 2070$  and  $\nu_5(\sigma_u)\sim 492\text{ cm}^{-1}$ , but neither is close to the  $1210.9\text{ cm}^{-1}$  frequency. Additionally, because of the molecular symmetry, one would only expect to see two single  $^{13}\text{C}$  shifts, corresponding to the two pairs of equivalent C atoms, rather than the four shifts observed in the Fig. 5.6(a) spectrum.

As indicated earlier, because of nonrandom mixing of  $^{12}\text{C}$  and  $^{13}\text{C}$  atoms, both the singly and fully-substituted  $^{13}\text{C}$  isotopomer bands in the  $\text{C}_3$  spectrum have intensities that are  $\sim 8\%$  of the main  $^{12}\text{C}_3$  isotopomer band. Thus the observation of four shifts having approximately equal intensities of  $\sim 9\%$  compared to the  $1210.9\text{ cm}^{-1}$  band could be indicative of three singly-substituted and the fully-substituted  $^{13}\text{C}$  isotopomer bands of a non-centrosymmetric linear  $\text{C}_3$ -bearing species, such as linear  $\text{AlC}_3$ . Estimating the frequency of the fully  $^{13}\text{C}$  substituted isotopomer using Eq. (1), under the assumption that the Al atom(s) do not strongly participate in the vibration, gives a shift from  $\nu_{^{12}\text{C}} = 1210.9$  to  $\nu_{^{13}\text{C}} \approx 1163.2\text{ cm}^{-1}$ , which is very close to the band observed at  $1164.0\text{ cm}^{-1}$ .

As discussed earlier in the Theoretical Calculations section, the lowest lying state for linear  $\text{AlC}_3$  is predicted to be  $^2\Pi$ , and the prediction for its most intense mode,  $\nu_2(\sigma)\sim 1245\text{ cm}^{-1}$  (see Table 5.2), are close to the observed  $1210.9\text{ cm}^{-1}$  band, thereby making this mode the most probable assignment. The predicted principal nuclear displacements of the  $\nu_2(\sigma)$  mode are shown in Fig. 5.1(d). Figure 5.6 compares the FTIR spectrum using a C rod enriched with 30%  $^{13}\text{C}$  [Fig. 5.6(a)] with DFT B3LYP/6-311+G(3df) simulations of the  $\nu_2(\sigma)$  mode of linear  $\text{AlC}_3$  scaled to  $1210.9\text{ cm}^{-1}$  with 10% and 30%  $^{13}\text{C}$  enrichments [Figs. 5.6(b) and (c)]. Table 5.4, in which the

Table 5.4: Comparison of observed vibrational frequencies ( $\text{cm}^{-1}$ ) of the  $\nu_2(\sigma)$  mode for the singly- and fully-substituted  $^{13}\text{C}$  isotopomers of linear ( $^2\Pi$ )  $\text{AlC}_3$  with the predictions of B3LYP/6-311+G(3*df*) calculations.

Isotopomer		Observed	B3LYP/ 6-311+G(3 <i>df</i> )	Scaled	Difference
Al-C-C-C		$\nu$	$\nu$	$\nu$	$\Delta\nu$
27-12-12-12	(A)	1210.9	1245.0	... <sup>a</sup>	...
27- <b>13</b> -12-12	(B)	1192.3	1225.5	1191.9	0.4
27-12- <b>13</b> -12	(C)	1208.2	1242.4	1208.4	-0.2
27-12-12- <b>13</b>	(D)	1185.4	1217.7	1184.3	1.1
27- <b>13</b> - <b>13</b> - <b>13</b>	(A')	1164.0	1196.2	1163.4	0.6
27-12- <b>13</b> -13	(B')	...	1214.5	1181.2	...
27- <b>13</b> -12- <b>13</b>	(C')	...	1198.5	1165.7	...
27- <b>13</b> - <b>13</b> -12	(D')	...	1223.7	1190.1	...

<sup>a</sup>Results of the calculation are scaled by a factor of  $1210.9/1245.0=0.97261$ .

predicted frequency for the  $\text{Al}^{12}\text{C}_3$  species is scaled to the observed frequency (scale factor =  $1210.9/1245.0=0.97261$ ), shows good agreement,  $\pm 1.1\text{ cm}^{-1}$ , between the observed and DFT predicted frequencies for the singly- and fully-substituted  $^{13}\text{C}$  isotopomers. No doubly-substituted  $^{13}\text{C}$  isotopomers are observed because of the non-randomization of  $^{12}\text{C}$  and  $^{13}\text{C}$  atoms, which is also the case in the  $\text{C}_3$  spectrum.

Although the  $^2A_1$  kite and  $^2B_2$  fanlike isomers are predicted to be within a few kcal/mol of ( $^2\Pi$ ) linear  $\text{AlC}_3$ , a careful search of the spectra has revealed no evidence of either the  $\nu_2(a_1)\sim 809\text{ cm}^{-1}$  band, predicted to be the most intense mode of the kite, or the  $\nu_5(b_2)\sim 1678\text{ cm}^{-1}$  vibration, which is the strongest vibration of the fan. As discussed earlier, an absorption at  $1624.0\text{ cm}^{-1}$  has been identified as the  $\nu_3(\sigma_u)$  mode of  $\text{AlC}_3\text{Al}$ .

## 5.5 Conclusions

This is the first experimental or theoretical investigation of the  $\text{AlC}_3\text{Al}$  molecule. Linear  $\text{AlC}_3\text{Al}$  in its  $^3\Sigma_g^+$  ground state has been identified and its  $\nu_3(\sigma_u)=1624.0$  and  $\nu_4(\sigma_u)=528.3\text{ cm}^{-1}$  fundamentals, which are the only IR-active modes with significant intensity, have been assigned. The assignments are based on the excellent agreement between DFT B3LYP/6-311+G(3df) predictions and the observed  $^{13}\text{C}$  isotopic shift pattern.

Although theoretical investigations<sup>26,87-89</sup> on  $\text{AlC}_3$  have indicated that the  $^2\Pi$  linear,  $^2A_1$  kite, and  $^2B_2$  fanlike isomers are close in energy,<sup>26</sup> in the present work the  $^2\Pi$  linear isomer has been observed, and its  $\nu_2(\sigma)=1210.9\text{ cm}^{-1}$  mode has been identified based on the good agreement between DFT B3LYP/6-311+G(3df) calculations and the observed  $^{13}\text{C}$  isotopic spectrum. No evidence of either the fanlike or kite isomers has been observed. The results reported here are similar to prior investigations on ( $^5\Pi$ )  $\text{CrC}_3$  (Ref. 46) and ( $^2\Delta$ )  $\text{CoC}_3$  (Ref. 91), presented in Chapters III and IV of this work, respectively, for which close-lying fanlike and linear structures have been predicted but only the linear isomers detected.

**CHAPTER VI**  
**THE VIBRATIONAL SPECTRUM OF  $\text{CuC}_3$ : AN FTIR ISOTOPIC AND DFT**  
**INVESTIGATION**

## **6.1 Introduction**

Transition metal–carbon clusters have recently received much attention because of their applications to modern materials science. Understanding the formation, bonding, and geometries of small transition metal–carbon species may reveal the growth mechanisms and bonding of metallocarbohedrenes, or metcars.<sup>2,3</sup> Besides forming metcars, transition metals can be incorporated into fullerenes to form networked metallofullerenes, and late transition metals are also used as catalysts for carbon nanotube (CNT) formation.<sup>109</sup> CNTs filled with various materials have been found to have interesting structures, and metal nanowires encapsulated in CNTs have potential applications to data storage nanotechnology.<sup>110</sup>

Despite the strong interest in small transition metal–carbon cluster bonding and geometries, very few investigations have included the late transition metal, copper. Recently, however, as part of extensive theoretical investigations<sup>109,111</sup> of the linear, ( $C_{2v}$ ) ring, and ( $C_{2v}$ ) T-shaped isomers of  $\text{MC}_2$  and  $\text{MC}_2^+$  ( $\text{M}=\text{Sc-Zn}$ ) clusters, the results of DFT B3LYP/6-311+G(3df) calculations on  $\text{CuC}_2$  (Ref. 109) and  $\text{CuC}_2^+$  (Ref. 111) have been reported. In general, the ( $C_{2v}$ ) T-shaped geometry, where the metal atom is bonded to the  $\text{C}_2$  unit, is the preferred ground state structure.  $\text{CuC}_2$ , with a ( $C_{2v}$ ) T-shaped structure and  $^2A_1$  electronic state,<sup>109</sup> conforms to this pattern, but in contrast the  $\text{CuC}_2^+$  cation is predicted to be linear ( $^3\Pi$ ), and  $C_{2v}$  ( $^3B_1$ ) ring isomer is predicted to 2.1 kcal/mol higher in energy.<sup>111</sup> The authors note that the M-C bonds of the ring curve inward, approaching a T-shaped structure.

Apparently no experimental investigations have been done on  $\text{Cu}_n\text{C}_m$  species prior to the present one. The scarcity of information on  $\text{Cu}_n\text{C}_m$  clusters and the recent success of the TCU Molecular Physics Laboratory in producing and characterizing the infrared spectra of  $\text{M}_n\text{C}_3$  species,<sup>46,55,91,92,112</sup> has prompted the present investigation on  $\text{CuC}_3$ . In prior reports, infrared fundamentals have been assigned for  $\text{MC}_3$  (M=Ti, Co, Sc, Cr, Al) and  $\text{MC}_3\text{M}$  (M=Ni, Al) formed by trapping the ablated products of metal and carbon rods in solid Ar. In the case of  $\text{MC}_3$  species, there is a competition between the linear and fanlike structures. Structure determinations and vibrational fundamental identifications are critically dependent on FTIR measurements of  $^{13}\text{C}$  isotopic shifts coupled with the predictions of DFT calculations. A similar approach has been employed in the present work and has enabled the first identification of the  $\nu_1(\sigma)=1830.0\text{ cm}^{-1}$  mode of ( $^2\Pi$ ) linear  $\text{CuC}_3$ .

## 6.2 Experimental Procedures

$\text{CuC}_3$  was produced using two 1064 nm pulsed Nd:YAG lasers (Spectra Physics), to ablate a pair of Cu (99.999%, ESPI) and C rods, which were continuously rotated and translated to provide clean surfaces for evaporation. High purity Ar gas (99.995%, Matheson Tri-Gas) swept the products toward condensation onto a gold mirror maintained at  $\sim 10\text{ K}$  by a closed-cycle refrigeration system (ARS, Displex). Experiments were conducted in a vacuum chamber with a pressure of  $\leq 10^{-7}$  Torr prior to sample deposition. Experimental conditions, including laser power, laser focus, and Ar flow rate were initially set to maximize the production of  $\text{C}_3$  as measured by the intensity of its  $\nu_3(\sigma_u)=2038.9\text{ cm}^{-1}$  mode and then adjusted to optimize absorptions of interest in the FTIR spectra. Spectra were recorded over the frequency range of  $450\text{-}4000\text{ cm}^{-1}$  at a resolution of  $0.2\text{ cm}^{-1}$  using a Bomem DA 3.16 FTIR spectrometer equipped with a liquid  $\text{N}_2$ -cooled MCT detector. All frequencies reported were measured to  $\pm 0.1\text{ cm}^{-1}$ . Additional details of the experimental apparatus and procedures have been reported previously.<sup>38</sup>

$^{13}\text{C}$  isotopic shifts are key to assigning vibrational fundamentals and determining the geometric structure of the molecular carrier. Various molecular structures, such as centrosymmetric linear  $\text{GeC}_5\text{Ge}$ ,<sup>58</sup> non-centrosymmetric linear  $\text{CoC}_3$ ,<sup>91</sup> fanlike ( $C_{2v}$ )  $\text{TiC}_3$ ,<sup>55</sup> and cyclic ( $D_{6h}$ )  $\text{C}_6$  (Ref. 113) have been identified by comparing  $^{13}\text{C}$  isotopic shifts measured in FTIR spectra with those predicted by DFT calculations. In the present work in which Cu and C rods were simultaneously ablated, three carbon rods were prepared from  $^{13}\text{C}$  (99.3%, Isotec) and  $^{12}\text{C}$  (99.9995, Alfa Aesar) powders pressed under a pressure of  $\sim 4.5 \times 10^5$  kPa: a  $^{12}\text{C}$  rod with 1% natural  $^{13}\text{C}$  abundance, and one rod each having 20% and 30%  $^{13}\text{C}$  enrichments.

### 6.3 Experimental Results and Discussion

Potential candidates for  $\text{Cu}_n\text{C}_m$  absorptions have been identified by comparing a spectrum obtained from the dual ablation of Cu and  $^{12}\text{C}$  rods [Fig. 6.1(a)] with one obtained from the ablation of a  $^{12}\text{C}$  rod alone [Fig. 6.1(b)]. Many absorptions previously assigned to  $\text{C}_n$  species<sup>49</sup> appear in both spectra; however, an intense absorption at  $1830.0\text{ cm}^{-1}$ , observed in the dual ablation spectrum, is absent when only the  $^{12}\text{C}$  rod is ablated, making it a potential candidate for a vibration of a  $\text{Cu}_n\text{C}_m$  species.

Since only weak bands of  $\text{CO}_2$  and  $\text{H}_2\text{O}$  are observed in FTIR spectra, it is unlikely that a  $\text{Cu}_n\text{C}_m$  molecule that also contains O or H atoms is responsible for the band at  $1830.0\text{ cm}^{-1}$ . Moreover, the vibrational frequencies of species, such as  $\text{Cu}_n\text{H}_m$ ,<sup>114</sup>  $\text{CuCH}_2$ ,<sup>115</sup>  $\text{CuO}_n\text{H}_m$ ,<sup>52,116</sup>  $\text{Cu}_n\text{O}_m$ ,<sup>117</sup> and  $\text{CuC}_n\text{O}_m$  clusters,<sup>65,118</sup> are well known, and no evidence of any of these is observed in the spectra. The  $\nu(e')=1829.7\text{ cm}^{-1}$  fundamental of  $\text{Cu}(\text{CO})_3^-$  has been identified<sup>118</sup> via its  $^{13}\text{C}$  isotopic shifts, and although its frequency is very close to the  $1830.0\text{ cm}^{-1}$  absorption, its  $^{13}\text{C}$  shifts do not match those observed in the present work for the  $1830.0\text{ cm}^{-1}$  band.

The  $1830.0\text{ cm}^{-1}$  frequency is characteristic of a C–C stretch for a linear  $\text{C}_n$  molecule. Since  $^{13}\text{C}$  isotopic shifts are necessary for assigning vibrational spectra and for determining

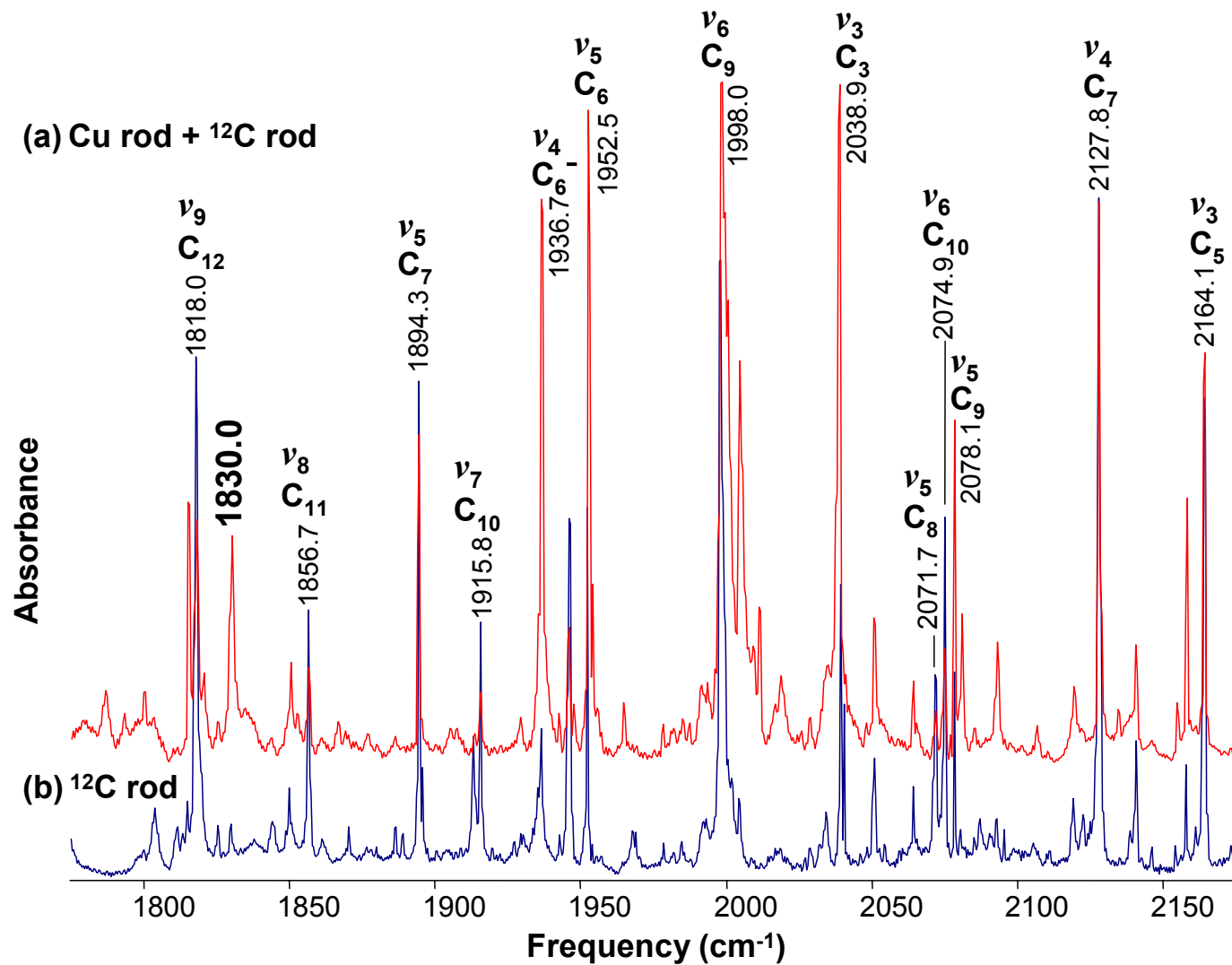


Figure 6.1 FTIR spectra recorded after (a) dual ablation of Cu and  $^{12}\text{C}$  rods and (b) ablation of a pure  $^{12}\text{C}$  rod, for comparison. Note the  $1830.0 \text{ cm}^{-1}$  band in (a) that is absent from (b).



geometric structures, an experiment with a nominal 20%  $^{13}\text{C}$  enrichment was conducted and the spectrum obtained is shown in Fig. 6.2(b). To the low frequency side of the main  $1830.0\text{ cm}^{-1}$  band, three absorptions can be seen at  $1825.5$ ,  $1807.5$ , and  $1788.2\text{ cm}^{-1}$  with approximately equal intensity. They are labeled (D), (B), and (C), respectively in Fig. 2(b). These three bands, which are seen more clearly in the spectrum shown in Fig. 6.2(a) having a 30%  $^{13}\text{C}$  enrichment, appear to be good candidates for the singly-substituted  $^{13}\text{C}$  isotopomers that should be the most prominent at low  $^{13}\text{C}$  enrichment levels. Since, as previously mentioned, the experimental conditions were chosen to optimize the yield of  $\text{C}_3$  as monitored by the intensity of its  $\nu_3(\sigma_u)=2038.9\text{ cm}^{-1}$  fundamental, a non-centrosymmetric linear molecule containing a  $\text{C}_3$  unit, such as  $\text{CuC}_3$ , is the most likely carrier of the  $1830.0\text{ cm}^{-1}$  band.

In order to observe the doubly- and fully-substituted  $^{13}\text{C}$  isotopomers, which will appear to mirror the singly-substituted  $^{13}\text{C}$  and the full  $^{12}\text{C}$  isotopomers, an experiment was done in which the  $^{13}\text{C}$  enrichment was increased to 30% [Fig. 6.2(a)]. It can be readily seen in the Fig. 6.2(a) spectrum, that the full  $^{12}\text{C}_n$  isotopomer at  $1830.0\text{ cm}^{-1}$ , labeled (A), and the proposed singly-substituted  $^{13}\text{C}$  isotopomer bands at  $1825.5$ ,  $1807.5$ , and  $1788.2\text{ cm}^{-1}$ , labeled (D), (B), and (C), respectively, are mirrored by the bands at  $1759.4$ ,  $1764.5$ ,  $1783.9$ , and  $1802.6\text{ cm}^{-1}$ , labeled (A'), (D'), (B'), and (C'), respectively. This suggests that the  $1759.4\text{ cm}^{-1}$  (A') band corresponds to the fully  $^{13}\text{C}$  substituted counterpart of the  $1830.0\text{ cm}^{-1}$  absorption (A). In the harmonic approximation an estimate of the frequency of the fully  $^{13}\text{C}$  substituted isotopomer absorption, assuming that the Cu atom is not strongly participating in the vibration, is given by

$$\nu_{^{13}\text{C}} \approx \sqrt{\frac{m_{^{12}\text{C}}}{m_{^{13}\text{C}}}} \times \nu_{^{12}\text{C}} \approx \sqrt{\frac{12.0}{13.00335}} \times \nu_{^{12}\text{C}} \quad (1)$$

If  $\nu_{^{12}\text{C}}=1830.0$ , then  $\nu_{^{13}\text{C}} \approx 1758.0\text{ cm}^{-1}$ , which is close to the observed  $1759.4\text{ cm}^{-1}$  band and supports its assignment to the fully-substituted  $\text{Cu}^{13}\text{C}_3$  isotopomer. The remaining  $1764.5$  (D'),

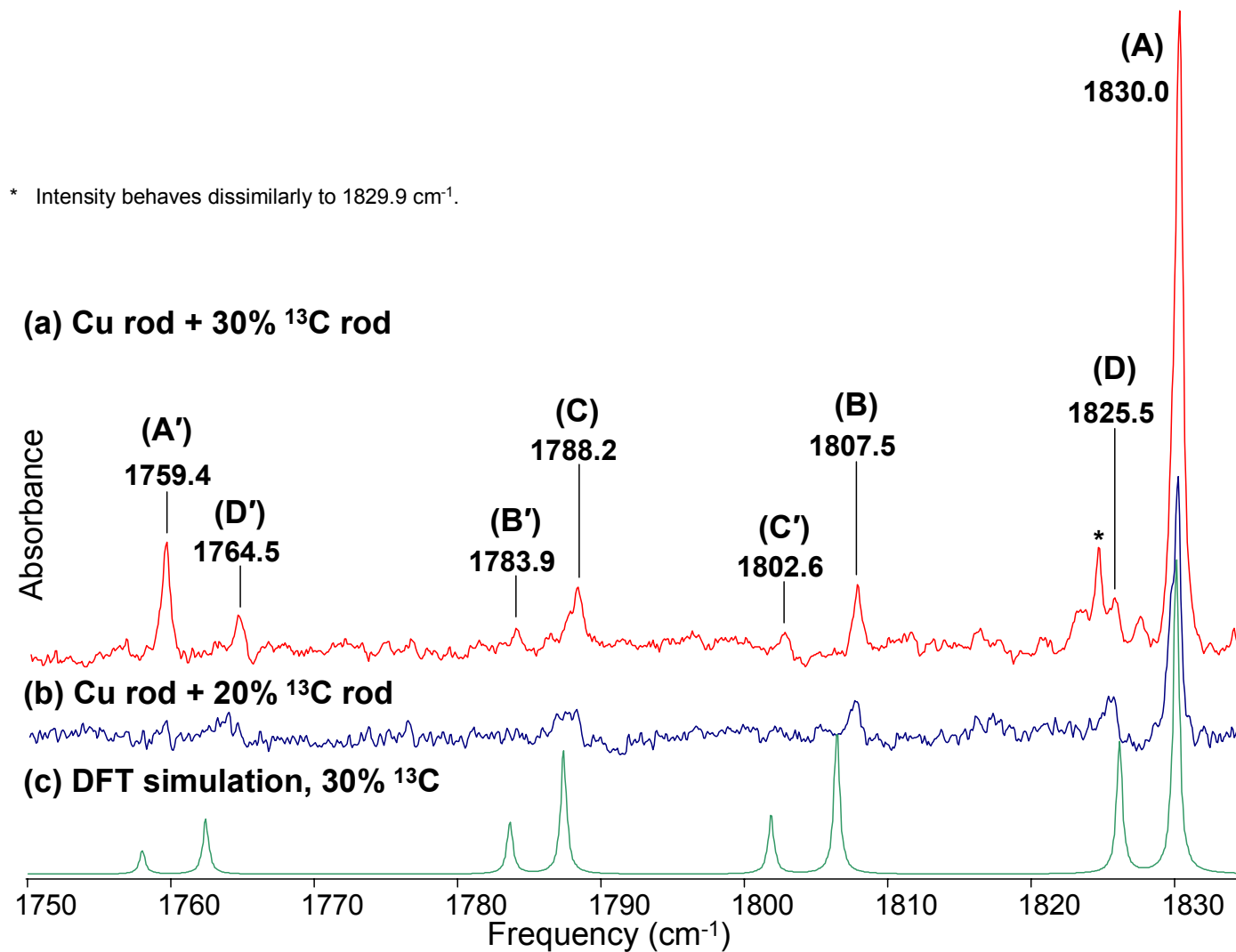


Figure 6.2 FTIR spectra from experiments with (a) 30% and (b) 20% nominal <sup>13</sup>C enrichments for comparison with (c) a DFT simulation of the  $\nu_1(\sigma)$  mode of (<sup>2</sup>Π) linear CuC<sub>3</sub> having 30% <sup>13</sup>C enrichment.

1783.9 (B'), and 1802.6 (C')  $\text{cm}^{-1}$  bands are thus likely candidates for the three double  $^{13}\text{C}$  substituted isotopomers.

The discrepancy between the nominal  $\sim 30\%$   $^{13}\text{C}$  enrichment of the rod and the  $\sim 10\%$  intensity of the single  $^{13}\text{C}$  substituted isotopomer bands at 1825.5 (D), 1802.5 (B), and 1788.2 (C)  $\text{cm}^{-1}$  relative to the 1830.0  $\text{cm}^{-1}$  absorption results from inhomogeneities in the  $^{12}\text{C}/^{13}\text{C}$  mixture in the rod. In the spectrum from which Fig. 6.2(a) is extracted, the relative intensities of the shifts for single  $^{13}\text{C}$  substitutions at inequivalent C sites are all similarly measured to be  $\sim 10\%$  of the intensity of the  $^{12}\text{C}_n$  absorptions.

Since the molecular carrier of the 1830.0  $\text{cm}^{-1}$  band is likely a  $\text{C}_3$  unit with a terminal Cu atom and the spectrum of the  $\nu_3(\sigma_u)=2038.9 \text{ cm}^{-1}$  mode of  $\text{C}_3$  also exhibits anomalies in its  $^{13}\text{C}$  isotopomer intensity ratios, it is useful to compare the singly-, doubly-, and fully-substituted isotopomer intensities observed in the 1830.0  $\text{cm}^{-1}$  spectrum with their counterparts in the  $\text{C}_3$  spectrum. The 1825.5 (D), 1807.5 (B), and 1788.2 (C)  $\text{cm}^{-1}$  bands, in Fig. 6.2(a), respectively, are each  $\sim 9\%$  of the main 1830.0  $\text{cm}^{-1}$  band, similar to the singly-substituted isotopomer ratio of  $\sim 10\%$  observed in the  $\text{C}_3$  spectrum. Bands D, B, and C are thus confirmed as singly-substituted  $^{13}\text{C}$  isotopomers. The candidates for the doubly-substituted  $^{13}\text{C}$  isotopomers at 1764.5 (D'), 1783.9 (B'), and 1802.6  $\text{cm}^{-1}$  (C'), each have  $\sim 5\%$  of the intensity of the main 1830.0  $\text{cm}^{-1}$  absorption, identical to the relative intensity of the doubly-substituted  $^{13}\text{C}$  isotopomer measured in the  $\text{C}_3$  spectrum. Finally, the candidate at 1759.4  $\text{cm}^{-1}$  (A'), for the fully-substituted  $^{13}\text{C}$  isotopomer band is  $\sim 15\%$  of the intensity of the main 1830.0  $\text{cm}^{-1}$  band, in good agreement with the  $\sim 13\%$  intensity ratio of the  $^{13}\text{C}_3:^{12}\text{C}_3$  bands in the  $\text{C}_3$  spectrum. The pattern of the isotopic shift spectrum is thus consistent with the suggested molecular carrier, linear  $\text{CuC}_3$ .

## 6.4 Theory and Analysis

As previously noted, prior theoretical investigations<sup>109,111</sup> of  $\text{Cu}_n\text{C}_m$  clusters have apparently been limited to  $\text{CuC}_2$  and  $\text{CuC}_2^+$ , making the present investigation the first for  $\text{CuC}_3$ . All calculations were done using DFT with a B3LYP functional<sup>47</sup> and a 6-311+G(3df) basis set in the Gaussian 03 program suite.<sup>45</sup>

Since the isotopic shift pattern in Figs. 6.2(a) and (b) indicates a non-centrosymmetric linear species with three unique C atoms, DFT calculations were performed for linear and near linear  $\text{CuC}_3$  geometries having multiple spin states.  $\text{CuC}_3$  isomers with  $C_{2v}$  symmetry and linear  $\text{CuC}_3\text{Cu}$  were also investigated, but these calculations are not included since these species do not produce isotopic shift patterns that are consistent with the FTIR spectra presented in Figs. 6.2(a) and (b) and thus cannot be responsible for the  $1830.0\text{ cm}^{-1}$  band.

The  ${}^2\Pi$  state of linear  $\text{CuC}_3$  is predicted to lie much lower in energy ( $>36\text{ kcal/mol}$ ), than the higher spin states, but as shown in Table 6.1, it is also predicted to have one imaginary frequency at  $\sim 168i\text{ cm}^{-1}$ , indicating that at the B3LYP/6-311+G(3df) level of theory, this structure is a transition state, rather than the ground state. With one exception, subsequent calculations relaxing the condition of linearity have also yielded one imaginary frequency of approximately the same magnitude. The exception, a ( ${}^2A'$ ) *trans*-bent isomer [see Fig. 6.3(b)], has all real frequencies (Table 6.1) and is predicted to be nearly isoenergetic with the linear isomer ( $\pm 0.7\text{ kcal/mol}$ ). Geometric parameters for the ( ${}^2\Pi$ ) linear and ( ${}^2A'$ ) *trans*-bent isomers of  $\text{CuC}_3$  are given, respectively, in Fig. 6.3.

From Table 6.1, it can be seen that either the  $\nu_1(\sigma)\sim 1895\text{ cm}^{-1}$  frequency predicted for the linear isomer or the corresponding  $\nu_1(a')\sim 1902\text{ cm}^{-1}$  mode of the *trans*-bent isomer is consistent with the observed  $1830.0\text{ cm}^{-1}$  frequency.  ${}^{13}\text{C}$  isotopic shifts have therefore been calculated for the  $\nu_1$  mode of each isomer and are compared with FTIR measurements in Table 6.2. The

Table 6.1: DFT B3LYP/6-311+G(3*df*) predicted frequencies ( $\text{cm}^{-1}$ ) and band intensities ( $\text{km/mol}$ ) for the vibrational fundamentals of the ( ${}^2\Pi$ ) linear and ( ${}^2A'$ ) *trans*-bent isomers of  $\text{CuC}_3$ .

${}^2\Pi$ Linear			${}^2A'$ <i>trans</i> -bent		
Vibrational mode	Frequency <sup>a</sup> ( $\text{cm}^{-1}$ )	Intensity ( $\text{km/mol}$ )	Vibrational mode	Frequency <sup>a</sup> ( $\text{cm}^{-1}$ )	Intensity ( $\text{km/mol}$ )
$\nu_1(\sigma)$	1895	215	$\nu_1(a')$	1902	132
$\nu_2(\sigma)$	1277	60	$\nu_2(a')$	1274	9
$\nu_3(\sigma)$	410	9	$\nu_3(a')$	453	20
$\nu_4(\pi)$	362/317 <sup>a</sup>	22/~0	$\nu_4(a')$	365	25
$\nu_5(\pi)$	130/168 <sup>a</sup>	~0/~0	$\nu_5(a')$	117	16
			$\nu_6(a'')$	226	9

<sup>a</sup>Both Renner-Teller components are reported.

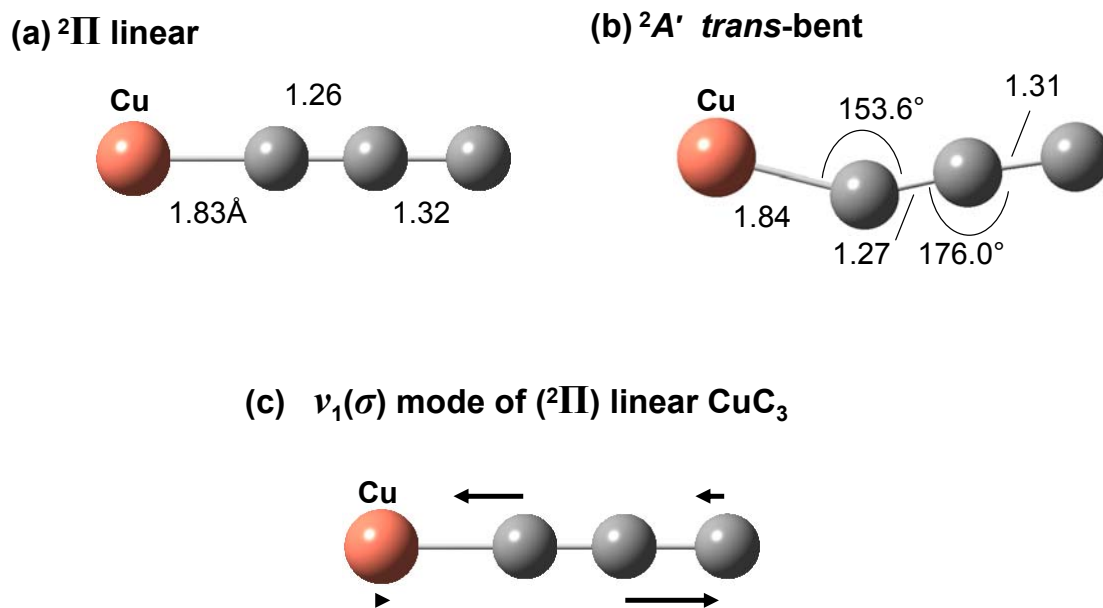


Figure 6.3 DFT B3LYP/6-311+G(3*df*) bond length (Å) and angle (°) predictions for the (a)  ${}^2\Pi$  linear and (b)  ${}^2A'$  *trans*-bent isomers of  $\text{CuC}_3$ . The predicted principal nuclear displacements of the  $\nu_1(\sigma)$  mode of ( ${}^2\Pi$ ) linear  $\text{CuC}_3$  are shown in (c).

Table 6.2: Comparison of the observed vibrational fundamental and all of the  $^{13}\text{C}$ - substituted isotopomer frequencies ( $\text{cm}^{-1}$ ) of the  $\nu_1(\sigma)$  and the  $\nu_1(a')$  modes of the ( $^2\Pi$ ) linear and ( $^2A'$ ) *trans*-bent isomers of  $\text{CuC}_3$  with the predictions of B3LYP/6-311G+(3df) calculations.

Isotopomer	Observed	$(^2\Pi)$ Linear			$(^2A')$ <i>Trans</i> -bent		
		$\nu_1(\sigma)$ mode			$\nu_1(a')$ mode		
		Theory	Scaled	Difference	Theory	Scaled	Difference
Cu-C-C-C	$\nu$	$\nu$	$\nu$	$\Delta\nu$	$\nu$	$\nu$	$\Delta\nu$
64-12-12-12 (A)	1830.0	1894.4	... <sup>a</sup>	...	1901.7	... <sup>c</sup>	...
64- <b>13</b> -12-12 (B)	1807.5	1870.2	1806.6	0.9	1881.1	1810.2	-2.7
64-12- <b>13</b> -12 (C)	1788.2	1850.5	1787.6	0.6	1855.3	1785.3	2.9
64-12-12- <b>13</b> (D)	1825.5	1890.6	1826.3	-0.8	1895.7	1824.2	1.3
64- <b>13</b> - <b>13</b> - <b>13</b> (A')	1759.4	1820.2	... <sup>b</sup>	...	1826.9	... <sup>d</sup>	...
64-12- <b>13</b> - <b>13</b> (B')	1783.9	1846.7	1785.0	-1.1	1849.4	1781.1	2.8
64- <b>13</b> -12- <b>13</b> (C')	1802.6	1865.5	1803.2	-0.6	1874.4	1805.1	-2.5
64- <b>13</b> - <b>13</b> -12 (D')	1764.5	1824.7	1763.8	0.7	1833.6	1765.9	-1.4

<sup>a</sup>Results of the calculation scaled by a factor of  $1830.0/1894.4=0.96601$ .

<sup>b</sup>Scale factor =  $1759.4/1820.2=0.96662$ .

<sup>c</sup>Results of the calculation scaled by a factor of  $1830.0/1901.7=0.96230$ .

<sup>d</sup>Scale factor =  $1759.4/1826.9=0.96305$ .

frequencies predicted for single  $^{13}\text{C}$ -substituted isotopomers have been scaled by the ratio between the calculated and observed  $\text{Cu}^{12}\text{C}_3$  frequencies (scale factors =  $1830.0/1894.7=0.96601$  and  $1830.0/1901.7=0.96230$  for the linear and *trans*-bent isomers, respectively). The double  $^{13}\text{C}$ -substituted isotopomer frequencies have been similarly scaled by the ratio between the calculated and observed  $\text{Cu}^{13}\text{C}_3$  frequencies (scale factors =  $1759.4/1820.2=0.96662$  and  $1759.4/1826.9=0.96305$  for the linear and *trans*-bent isomers, respectively). The two scale factors have been used in order to eliminate the effects of anharmonicity. The calculated harmonic frequencies for  $\text{Cu}^{12}\text{C}_3$  and  $\text{Cu}^{13}\text{C}_3$  are related through Eq. (1), however the corresponding experimental frequencies are not. It is therefore appropriate to consider the single  $^{13}\text{C}$  and the double  $^{13}\text{C}$  (or single  $^{12}\text{C}$ ) shifts as originating from the full  $^{12}\text{C}$  and full  $^{13}\text{C}$  species, respectively.

As Table 6.2 shows, for the  $\nu_1(a')$  mode of *trans*-bent  $\text{CuC}_3$ , the discrepancies between the observed and predicted  $^{13}\text{C}$  shifts are  $\geq 2.5 \text{ cm}^{-1}$  in all cases except two, where the differences are still  $\sim 1.5 \text{ cm}^{-1}$ , suggesting that although the linear isomer is predicted to have one imaginary frequency, it may actually be the ground state. It should be noted that there are examples in which popularly used *ab initio* calculations have predicted at least one imaginary frequency even when a molecule is known to have a specific ground state geometry, *e.g.* planar ( $D_{6h}$ ) benzene.<sup>119</sup> For the  $\nu_1(\sigma)$  mode of ( $^2\Pi$ ) linear  $\text{CuC}_3$ , the discrepancies between the observed and predicted shifts are  $\sim 1 \text{ cm}^{-1}$  or less for all cases (see Table 6.2). Interestingly, the smallest discrepancy listed in Table 6.2 for the *trans*-bent isomer ( $1.3 \text{ cm}^{-1}$ ) is still greater than the largest difference reported for the linear structure ( $1.1 \text{ cm}^{-1}$ ). The excellent agreement ( $\pm 1.1 \text{ cm}^{-1}$ ) between the observed and predicted  $^{13}\text{C}$  shifts indicates that although calculations point toward a bent or floppy geometry like the  $\text{NiC}_3\text{Ni}$  molecule,<sup>92</sup>  $\text{CuC}_3$  behaves as if it were linear, and so the  $\nu_1(\sigma)$  mode of ( $^2\Pi$ ) linear  $\text{CuC}_3$  can be assigned to  $1830.0 \text{ cm}^{-1}$ . Figure 6.2 compares a DFT B3LYP/6-



311+G(3df) simulation of the  $\nu_1(\sigma)$  mode of linear  $\text{CuC}_3$  that has been scaled to  $1830.0\text{ cm}^{-1}$  with FTIR spectra having 30% and 20%  $^{13}\text{C}$  enrichments. The predicted principle nuclear displacements of the  $\nu_1(\sigma)$  mode of ( $^2\Pi$ ) linear  $\text{CuC}_3$  are shown in Fig. 6.3(c).

## 6.5 Conclusions

There are no prior theoretical investigations on  $\text{CuC}_3$  or experimental investigations on any  $\text{Cu}_n\text{C}_m$  cluster; therefore, this work is the first experimental and theoretical study of  $\text{CuC}_3$ , resulting not only in the first assignment of a vibrational fundamental for  $\text{CuC}_3$ , but also for any  $\text{Cu}_n\text{C}_m$  cluster. The  $\text{CuC}_3$  molecule was created by the dual laser ablation of Cu and C rods and trapping the evaporated products in solid Ar at  $\sim 10\text{ K}$ , which produced the band at  $1830.0\text{ cm}^{-1}$  and the signature  $^{13}\text{C}$  isotopic shift pattern of a non-centrosymmetric linear molecule with three inequivalent carbon atoms.

DFT calculations have predicted that a ( $^2A'$ ) *trans*-bent geometry is the universal ground state,  $\sim 0.7\text{ kcal/mol}$  lower in energy than the  $^2\Pi$  linear isomer; however, the predicted  $^{13}\text{C}$  isotopic shift pattern is not in agreement with the observed spectra. The predicted  $^{13}\text{C}$  shifts for the ( $^2\Pi$ ) linear isomer of  $\text{CuC}_3$  is in very good agreement with FTIR spectra; however, this isomer is predicted to have one imaginary frequency at  $\sim 168i\text{ cm}^{-1}$ , suggesting that the linear geometry is a transition state and not the true ground state at the DFT B3LYP/6-311+G(3df) level of theory. A similar situation occurred for  $\text{NiC}_3\text{Ni}$ , as reported by Kinzer *et al.*,<sup>92</sup> where the molecular geometry has been found to be slightly floppy. It should be noted that the vibrational spectrum of  $\text{CuC}_3$  behaves as if the molecule were linear; thus the molecule can be considered as such and its  $\nu_1(\sigma)$  mode is assigned to  $1830.0\text{ cm}^{-1}$ . This is the first assignment of a vibrational fundamental for any  $\text{Cu}_n\text{C}_m$  molecule.

## CHAPTER VII

### OTHER METAL–CARBON SPECIES: CrC<sub>4</sub>, AlC<sub>4</sub>Al, and V<sub>n</sub>C<sub>m</sub>

#### 7.1 Fanlike (C<sub>2v</sub>) CrC<sub>4</sub>

##### 7.1.1 Introduction

A discussion on Cr<sub>n</sub>C<sub>m</sub> clusters was presented in Chapter III, so only a few remarks pertinent to CrC<sub>4</sub> will be made. An earlier study<sup>25</sup> on CrC<sub>n</sub> (n=2-8) clusters is the only prior investigation on either CrC<sub>4</sub> or CrC<sub>4</sub><sup>-</sup> and included both theoretical calculations and PE spectra. DFT BPW91/6-311+G\* calculations have predicted that CrC<sub>4</sub> is (C<sub>2v</sub>) fanlike with a <sup>5</sup>B<sub>2</sub> ground state, only 3.0 and 7.8 kcal/mol lower in energy, respectively, than the <sup>3</sup>B<sub>1</sub> state and the <sup>5</sup>Π linear isomer. For CrC<sub>4</sub><sup>-</sup>, the <sup>6</sup>Σ<sup>+</sup> linear isomer has been predicted to be the ground state, well-separated energetically from the <sup>6</sup>A<sub>1</sub>, <sup>4</sup>B<sub>2</sub>, and <sup>2</sup>B<sub>1</sub> fanlike isomers. Besides the <sup>6</sup>Σ<sup>+</sup> linear isomer, evidence of a nonlinear isomer has also been observed in PE spectra, which the authors have speculated to be small populations of the closest-lying <sup>6</sup>A<sub>1</sub> fanlike isomer, predicted to be ~15 kcal/mol higher in energy.

Comparisons between FTIR measurements and DFT predictions of vibrational frequencies and <sup>13</sup>C isotopic shifts have been successfully used by the TCU Molecular Physics Laboratory to determine the structures and identify vibrational fundamentals of novel molecules including (C<sub>2v</sub>) fanlike MC<sub>3</sub> (M=Ti, Sc)<sup>55,71</sup> linear MC<sub>3</sub> (M=Cr, Co, Al, Cu),<sup>46,91,112, 120</sup> linear NiC<sub>3</sub>Ni,<sup>92</sup> and linear AlC<sub>3</sub>Al species.<sup>112</sup> Results for the four linear MC<sub>3</sub> and the linear AlC<sub>3</sub>Al clusters have been presented in this dissertation.

The experimental techniques and procedures were explained in Chapters II-VI. The only difference between the experimental techniques that have been used to produce the species

presented here and the molecules discussed in earlier chapters is that sintered Cr/C rods were used, rather than simultaneously evaporating Cr and C rods. Two sintered rods were prepared, one having an atomic composition of 15% Cr/85%  $^{12}\text{C}$ , and the other having 15% Cr/85% C, where the carbon was 15%  $^{13}\text{C}$ .

### 7.1.2 Theoretical Calculations

Calculations on  $\text{CrC}_4$  have predicted that the  $^5B_2$  fanlike,  $^3B_1$  fanlike, and  $^5\Pi$  linear isomers are close in energy ( $\pm 8$  kcal/mol), thus any of the isomers could be observed.<sup>25</sup> A similar situation prevailed for  $\text{CrC}_3$  in which the  $^3B_1$  fanlike isomer has been observed in PE spectra and has been predicted to be the ground state structure, only  $\sim 7$  kcal/mol lower in energy than the  $^5\Pi$  linear isomer, which has been observed in FTIR spectra<sup>46</sup> as reported in Chapter III.

The analysis in the following section suggests a  $\text{C}_4$ -bearing species is the band carrier, and thus DFT calculations have been done on linear and fanlike ( $C_{2v}$ )  $\text{CrC}_4$  and linear  $\text{CrC}_4\text{Cr}$  (see Fig 7.1). All calculations used the GAUSSIAN 03 program suite<sup>45</sup> with the B3LYP<sup>47</sup> functional and the 6-311+G(3df) basis set. Multiple spin states were calculated for all molecules considered. The DFT calculations on  $\text{CrC}_4\text{Cr}$  are apparently the first, but calculations done on  $\text{CrC}_4$  are in good agreement with those published previously<sup>25</sup> and predict the three lowest energy isomers are the  $^5B_2$  and  $^3B_1$  fanlike and the  $^5\Pi$  linear isomers. Vibrational frequencies and ( $\text{cm}^{-1}$ ) and IR intensities ( $\text{km/mol}$ ) are listed in Table 7.1 for all three  $\text{CrC}_4$  isomers.

### 7.1.3 Results and Discussion

Potential  $\text{Cr}_n\text{C}_m$  absorptions were identified by comparing the spectrum recorded after ablation of a sintered  $\text{Cr}/^{12}\text{C}$  rod [Fig. 7.2(a)] with the spectrum produced by ablation of a  $^{12}\text{C}$  rod alone [Fig. 7.2(b)]. Many previously identified  $\text{C}_n$  absorptions<sup>49</sup> are also apparent in the  $\text{Cr}/^{12}\text{C}$  spectrum. Although trace amounts of CO and  $\text{H}_2\text{O}$  absorptions appear in the spectra, no

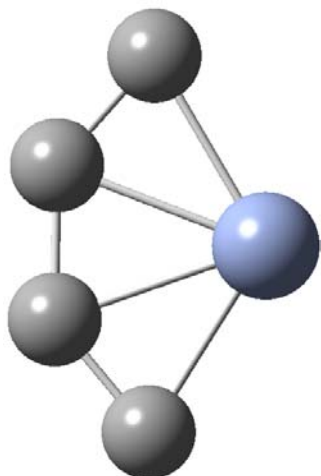
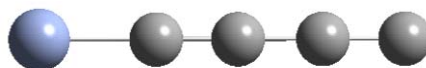
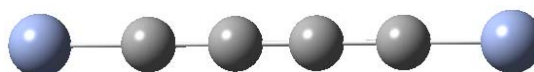
**(a) Fanlike ( $C_{2v}$ )  $CrC_4$** **(b) Linear  $CrC_4$** **(c) Linear  $CrC_4Cr$** 

Figure 7.1 Structures of (a) fanlike and (b) linear isomers of  $CrC_4$  and (c) linear  $CrC_4Cr$ , which were investigated as possible candidates for the  $1554.3\text{ cm}^{-1}$  band.

Table 7.1: DFT B3LYP/6-311+G(3*df*) predicted vibrational frequencies ( $\text{cm}^{-1}$ ) and band intensities ( $\text{km/mol}$ ) for the  ${}^5B_2$  and  ${}^3B_1$  states of fanlike  $\text{CrC}_4$  and for ( ${}^5\Pi$ ) linear  $\text{CrC}_4$ .

$\text{CrC}_4$ Isomer	Vibrational Mode	Frequency ( $\text{cm}^{-1}$ )	IR intensity ( $\text{km/mol}$ )
${}^5B_2$ Fanlike ( $C_{2v}$ )	$\nu_1(a_1)$	1968	2
	$\nu_2(a_1)$	1046	2
	$\nu_3(a_1)$	423	39
	$\nu_4(a_1)$	392	23
	$\nu_5(a_2)$	431	$\sim 0$
	$\nu_6(b_1)$	228	26
	$\nu_7(b_2)$	1835	$\sim 0$
	$\nu_8(b_2)$	603	19
	$\nu_9(b_2)$	342	30
${}^3B_1$ Fanlike ( $C_{2v}$ )	$\nu_1(a_1)$	1675	37
	$\nu_2(a_1)$	1089	6
	$\nu_3(a_1)$	620	13
	$\nu_4(a_1)$	459	31
	$\nu_5(a_2)$	539	$\sim 0$
	$\nu_6(b_1)$	268	38
	$\nu_7(b_2)$	1516	2
	$\nu_8(b_2)$	622	1
	$\nu_9(b_2)$	368	24
${}^5\Pi$ Linear	$\nu_1(\sigma)$	2093	377
	$\nu_2(\sigma)$	1815	166
	$\nu_3(\sigma)$	1012	11
	$\nu_4(\sigma)$	338	9
	$\nu_5(\pi)^a$	525/510	1/2
	$\nu_6(\pi)^a$	247/223	18/44
	$\nu_7(\pi)^a$	87/86	$\sim 0/4$

<sup>a</sup>Both Renner-Teller components are reported.

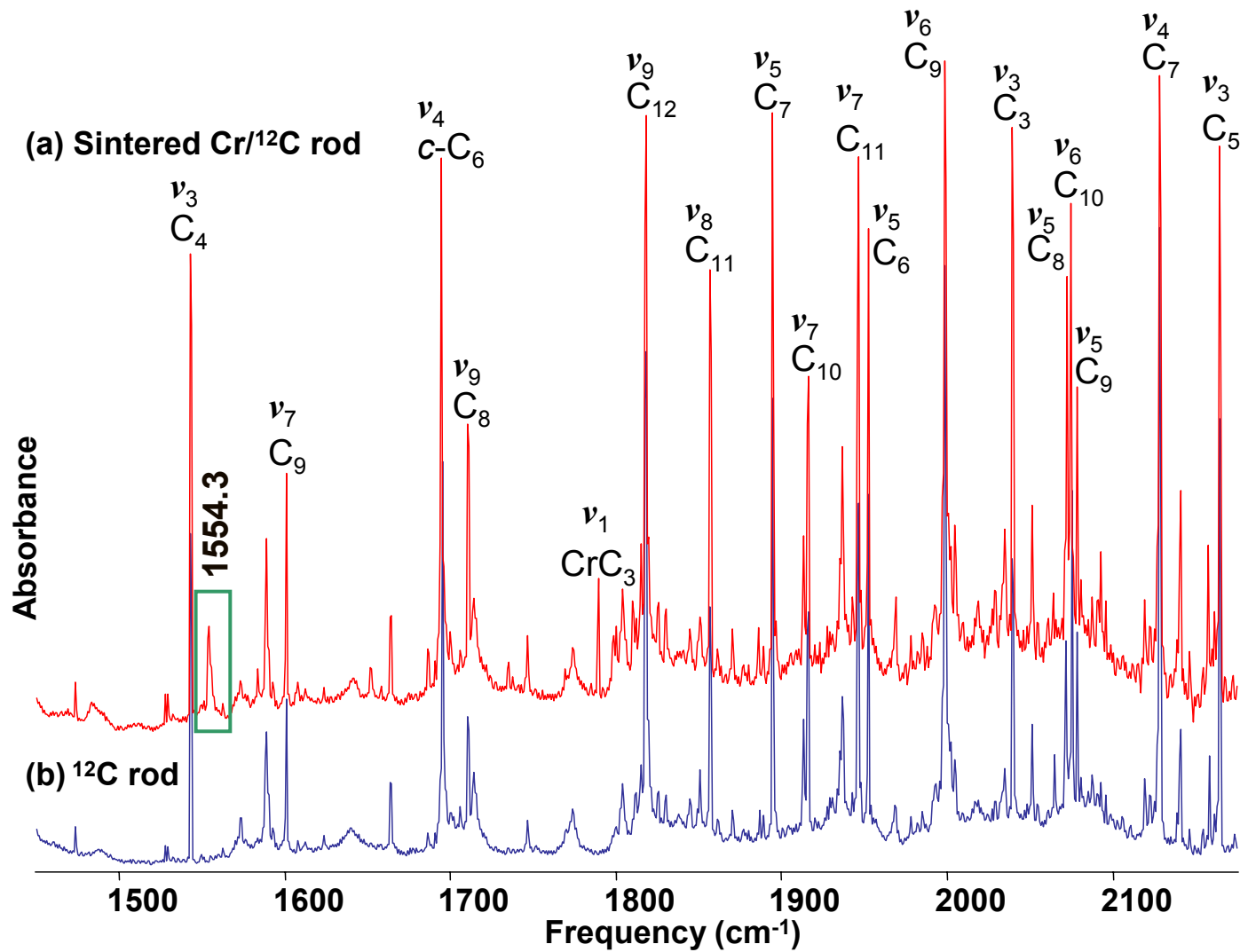


Figure 7.2 FTIR spectra obtained from ablation of (a) a sintered  $\text{Cr}/^{12}\text{C}$  rod for comparison with (b) ablation of a  $^{12}\text{C}$  rod only. Note the  $\nu_1(\sigma)=1789.5 \text{ cm}^{-1}$  mode of linear  $\text{CrC}_3$  and the  $1554.3 \text{ cm}^{-1}$  band in (a) that does not appear in (b).

evidence of Cr-contaminant species, such as CrOCO or OCrCO,<sup>50</sup> CrCO,<sup>51</sup> HCrOH,<sup>52</sup> or CrH<sub>2</sub> (Ref. 53) is observed. Hence, any absorptions appearing in the sintered Cr/C spectrum that are absent from the <sup>12</sup>C spectrum, such as the 1554.3 cm<sup>-1</sup> band, are candidates for Cr<sub>n</sub>C<sub>m</sub> species. The observation of the  $\nu_1(\sigma) = 1789.5$  cm<sup>-1</sup> mode of linear CrC<sub>3</sub>, which was identified in Chapter III, in the sintered Cr/<sup>12</sup>C rod spectrum [Fig. 7.2(a)] proves that Cr<sub>n</sub>C<sub>m</sub> species are being created.

<sup>13</sup>C isotopic shifts are essential to identify the molecule responsible for the 1554.3 cm<sup>-1</sup> band and determine its geometry, so a spectrum obtained from the ablation of a sintered Cr/C rod with 15% <sup>13</sup>C enrichment is shown in Fig. 7.3(a). Note that an intense vibration, corresponding to the  $\nu_4(\sigma_u) = 1543.4$  cm<sup>-1</sup> mode of C<sub>4</sub>,<sup>108</sup> is observed, as are its singly-, doubly-, and triply-substituted <sup>13</sup>C isotopomers [Fig. 7.3(a), green dots]. To the low frequency side of the 1554.3 cm<sup>-1</sup> band, absorptions at 1548.2 and 1531.6 cm<sup>-1</sup> appear to be good candidates for single <sup>13</sup>C isotopic shifts, which should be prominent in the spectrum at low <sup>13</sup>C enrichment. All three absorptions have similar broad line shapes, further suggesting that the latter two features are <sup>13</sup>C shifts of the main 1554.3 cm<sup>-1</sup> band.

In the spectrum of the  $\nu_3(\sigma_u)$  mode of C<sub>4</sub> [see Fig. 7.3(a)], the singly-substituted <sup>13</sup>C isotopomer frequencies at 1528.8 and 1527.5 cm<sup>-1</sup> correspond to <sup>13</sup>C substitutions at each of the two pairs of equivalent sites in the C<sub>4</sub> molecule and have intensities of ~13% of the main C<sub>4</sub> band at 1543.4 cm<sup>-1</sup>; therefore, the effective <sup>13</sup>C enrichment is ~6-7%. The intensity ratio of the 1548.2 and 1531.6 cm<sup>-1</sup> bands with respect to the main 1554.3 cm<sup>-1</sup> band is ~11%, which suggests that these bands correspond to single <sup>13</sup>C substitutions at two pairs of equivalent C atoms, similar to the pattern observed in the C<sub>4</sub> spectrum.

Assuming the molecule contains two pairs of equivalent C atoms, a C<sub>2</sub>- or C<sub>3</sub>-bearing species is eliminated as the band carrier, as is linear CrC<sub>4</sub>, which should have four single <sup>13</sup>C shifts. Because of the large discrepancies ( $\pm 5$ -11 cm<sup>-1</sup>) between the predicted and observed <sup>13</sup>C

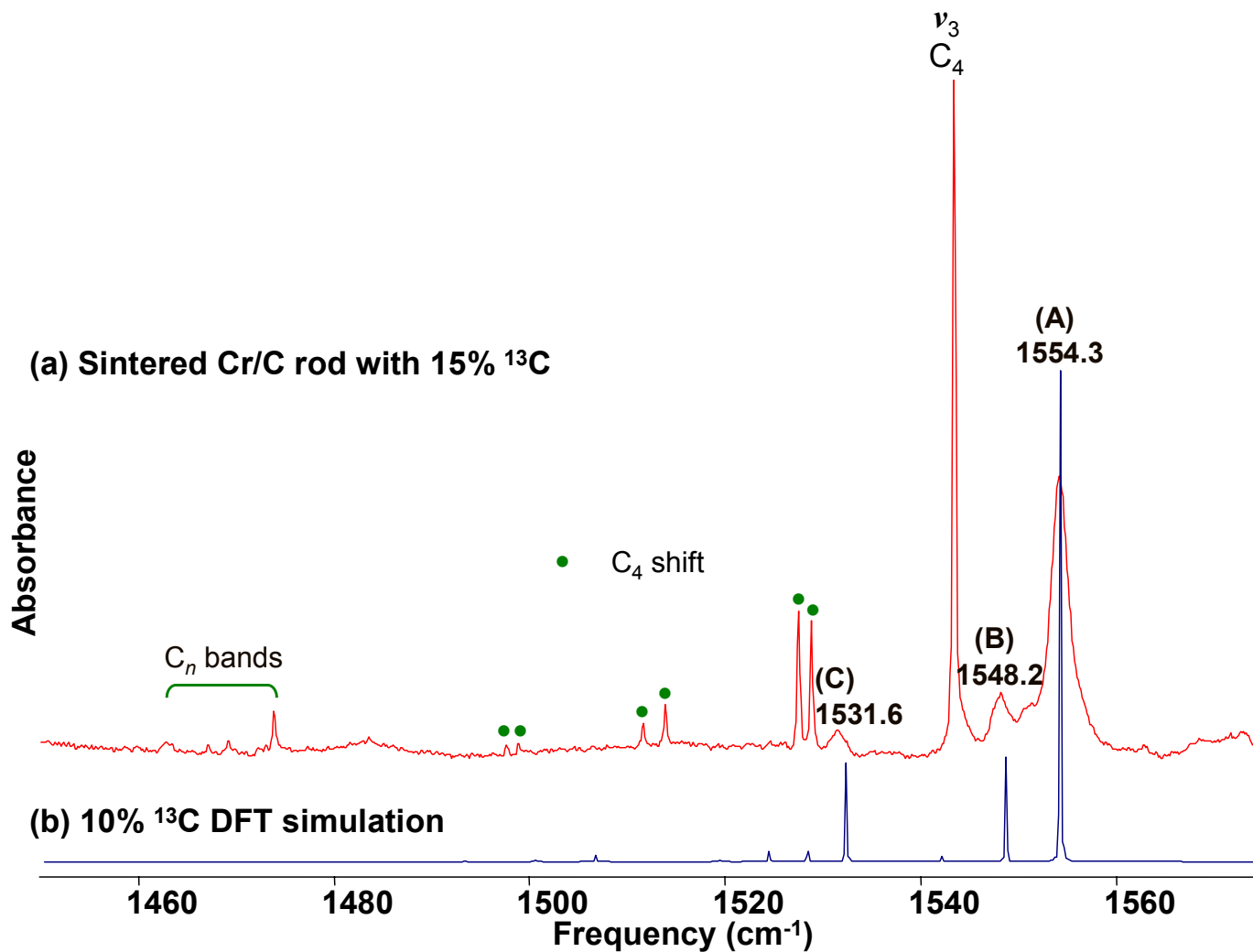


Figure 7.3 (a) FTIR spectrum obtained from the ablation of a sintered 15% Cr/85% C rod with a 15% nominal  $^{13}\text{C}$  enrichment for comparison with a (b) DFT simulation of the spectrum of the  $\nu_1(a_1)$  mode of ( $^3B_1$ ) fanlike  $\text{CrC}_4$  with a 10%  $^{13}\text{C}$  enrichment, scaled to  $1554.3 \text{ cm}^{-1}$ .



shifts for all spin multiplicities considered, linear  $\text{CrC}_4\text{Cr}$  is also readily eliminated as the carrier. Neither can ( ${}^5B_2$ ) fanlike  $\text{CrC}_4$ , which is predicted to be the ground state, be the molecular carrier because its  $\nu_7(b_2) \sim 1835 \text{ cm}^{-1}$  mode, predicted to be the closest in frequency to  $1554.3 \text{ cm}^{-1}$ , has negligible IR intensity (see Table 7.1).

DFT calculations predict that the  ${}^3B_1$  and  ${}^5B_2$  electronic states are nearly isoenergetic, and that the  $\nu_1(a_1)$  fundamental of the  ${}^3B_1$  state is at  $\sim 1675 \text{ cm}^{-1}$  (Table 7.1). Although its predicted IR intensity is low,  $\sim 37 \text{ km/mol}$ , it has sufficient intensity for detection as evidenced by the identification of three modes of ( ${}^1A_1$ ) fanlike  $\text{TiC}_3$  that have similar intensity predictions,  $\nu_5(b_2)$  with  $\sim 39 \text{ km/mol}$ ,  $\nu_3(a_1)$  with  $\sim 64 \text{ km/mol}$ , and  $\nu_4(b_1)$  with  $\sim 12 \text{ km/mol}$ .<sup>55</sup> Comparing DFT predicted isotopic shifts with FTIR measured frequencies (Table 7.2) shows very good agreement,  $\pm 0.8 \text{ cm}^{-1}$ , and tentatively supports the assignment of the  $\nu_1(a_1)$  mode of  ${}^3B_1$  fanlike  $\text{CrC}_4$  to  $1554.3 \text{ cm}^{-1}$ . A DFT simulation having 10%  ${}^{13}\text{C}$  enrichment has been scaled to  $1554.3 \text{ cm}^{-1}$  and is compared with FTIR spectra in Fig. 7.3. The geometric parameters for  ${}^3B_1$  fanlike  $\text{CrC}_4$  and the predicted principal nuclear displacements for its  $\nu_1(a_1)$  mode are shown in Fig. 7.4.

#### 7.1.4 Conclusions

Based on the good agreement between the predicted and observed single  ${}^{13}\text{C}$  shifts, the  $\nu_1(a_1)$  mode of ( ${}^3B_1$ ) fanlike  $\text{CrC}_4$  is tentatively assigned to  $1554.3 \text{ cm}^{-1}$ . Experiments with higher  ${}^{13}\text{C}$  enrichment have not produced the doubly-, triply-, and fully-substituted  ${}^{13}\text{C}$  isotopomers, which would unambiguously confirm the assignment. If substantiated, this would be the first observation of a vibrational mode of fanlike  $\text{CrC}_4$ .

## 7.2 Linear $\text{AlC}_4\text{Al}$

A thorough discussion of studies on  $\text{Al}_n\text{C}_m$  molecules was presented in Chapter V, but a few points should be noted. Prior studies combining theoretical and experimental investigations

Table 7.2: Comparison of observed vibrational fundamental and single  $^{13}\text{C}$  isotopomer frequencies ( $\text{cm}^{-1}$ ) of the  $\nu_1(a_1)$  mode of ( $^3B_1$ ) fanlike  $\text{CrC}_4$  with the predictions of B3LYP/6-311+G(3df) calculations.

Isotopomer		Observed	DFT	Scaled	Difference
Cr-C $_{\alpha}$ -C $_{\beta}$ -C $_{\beta}$ -C $_{\alpha}$		$\nu$	$\nu$	$\nu$	$\Delta\nu$
52-12-12-12-12	(A)	1554.3	1674.9	... <sup>a</sup>	...
52- <b>13</b> -12-12-12	(B)	1548.2	1668.8	1548.6	-0.4
52-12- <b>13</b> -12-12	(C)	1531.6	1651.3	1532.1	-0.8
52- <b>13</b> - <b>13</b> -12-12	(D)		1647.0	1528.4	
52- <b>13</b> -12- <b>13</b> -12	(E)		1642.6	1524.3	
52- <b>13</b> -12-12- <b>13</b>	(F)		1661.7	1542.1	
52-12- <b>13</b> - <b>13</b> -12	(G)		1623.4	1506.5	
52- <b>13</b> - <b>13</b> - <b>13</b> - <b>13</b>	(A')		1616.9	1500.5	
52-12- <b>13</b> - <b>13</b> - <b>13</b>	(B')		1637.3	1519.4	
52- <b>13</b> -12- <b>13</b> - <b>13</b>	(C')		1609.0	1493.1	

<sup>a</sup>Results of the calculation scaled by a factor of  $1554.3/1674.9=0.92800$ .

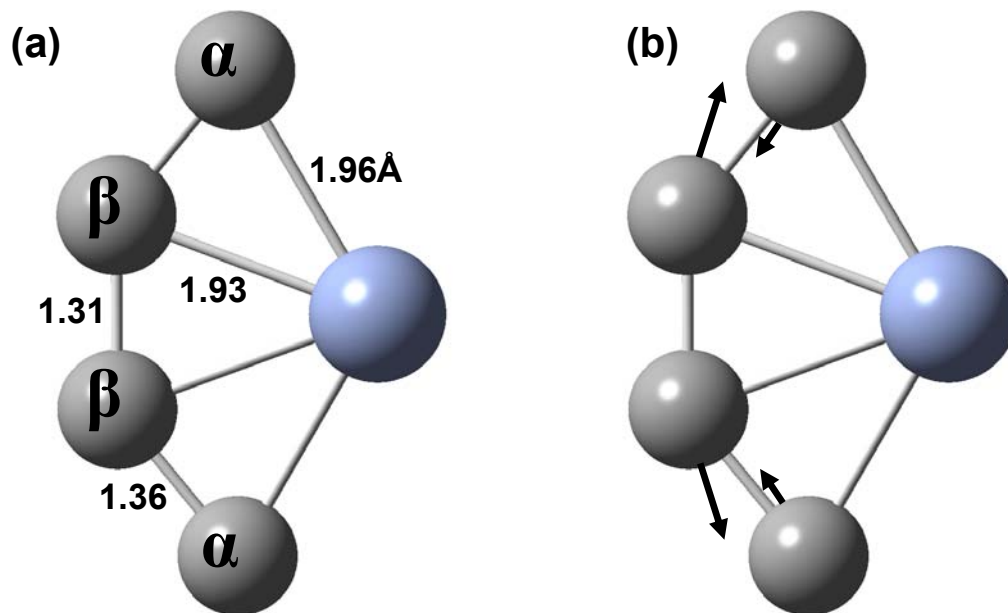


Figure 7.4 (a) DFT B3LYP/6-311+G(3df) predictions of bond lengths ( $\text{\AA}$ ) for  $(^3B_1)$  fanlike  $\text{CrC}_4$ . The  $\alpha$  and  $\beta$  denote pairs of equivalent C atoms. The predicted principal nuclear displacements of its  $\nu_1(a_1)$  mode are shown in (b).

of  $\text{Al}_n\text{C}_m$  ( $n=1,2; m=2,3$ )<sup>35,74,112</sup> clusters have reported vibrational frequency predictions and assignments for many of the IR-active modes. ( ${}^2A_1$ )  $\text{AlC}_2$  is reported to be ( $C_{2v}$ ) T-shaped<sup>74</sup> and its most intense vibrational mode,  $\nu_3(b_1)$ , is predicted at  $\sim 442 \text{ cm}^{-1}$ .<sup>35</sup> The  $\nu_3(\sigma_u)=605.1 \text{ cm}^{-1}$  mode of linear  $\text{AlC}_2\text{Al}$ , predicted to be the highest frequency IR-active mode, has been identified.<sup>35</sup> Identifications of the only two modes of  $\text{AlC}_3\text{Al}$  that have significant IR intensities,  $\nu_3(\sigma_u)=1624.0$  and  $\nu_4(\sigma_u)=528.3 \text{ cm}^{-1}$ , and of the most intense mode of  $\text{AlC}_3$ ,  $\nu_2(\sigma)=1210.9 \text{ cm}^{-1}$ , were also presented in Chapter V.<sup>112</sup>

There have been no prior investigations on either  $\text{AlC}_4$  or  $\text{Al}_2\text{C}_4$ ; hence, the calculations presented in the following sections are the first for these species. Although the identification of  $\text{AlC}_4\text{Al}$  is very tentative, if verified, it would be the first observation of this molecule.

### 7.2.1 Theoretical Calculations

Analysis of the FTIR spectra, presented in the following section, indicates an  $\text{Al}_n\text{C}_4$  species is being observed; therefore, DFT/ B3LYP<sup>47</sup> calculations with the 6-311+G(3df) basis set have been done on both  $\text{AlC}_4$  and  $\text{AlC}_4\text{Al}$  using the GAUSSIAN 03 program suite.<sup>45</sup> Predictions of the vibrational fundamentals and IR intensities of linear ( ${}^2\Sigma$ )  $\text{AlC}_4$  and linear ( ${}^1\Sigma_g^+$ )  $\text{AlC}_4\text{Al}$  are listed in Table 7.3.

### 7.2.2 Results and Discussion

In addition to the bands identified in Chapter V as the  $\nu_2(\sigma)$  mode of linear  $\text{AlC}_3$ , the  $\nu_3(\sigma_u)$  and  $\nu_4(\sigma_u)$  modes of linear  $\text{AlC}_3\text{Al}$ ,<sup>112</sup> and the  $\nu_3(\sigma_u)$  mode of  $\text{AlC}_2\text{Al}$ ,<sup>35</sup> a strong absorption at  $1987.3 \text{ cm}^{-1}$  is seen in spectra obtained from the dual ablation of Al and  ${}^{12}\text{C}$  rods that is not present during the ablation of a  ${}^{12}\text{C}$  rod alone (Fig. 7.5). Since  ${}^{13}\text{C}$  isotopic shifts are crucial to species identification and structure determination, a dual ablation Al/C experiment was performed in which a C rod was prepared with 15%  ${}^{13}\text{C}$  enrichment [Figs. 7.6(a) and (b)],

Table 7.3: DFT B3LYP/6-311+G(3df) predicted vibrational frequencies ( $\text{cm}^{-1}$ ) and band intensities ( $\text{km/mol}$ ) for ( ${}^1\Sigma_g^+$ ) linear  $\text{AlC}_4\text{Al}$  and ( ${}^2\Sigma$ ) linear  $\text{AlC}_4$ .

$({}^1\Sigma_g^+)$ Linear $\text{AlC}_4\text{Al}$			$({}^2\Sigma)$ Linear $\text{AlC}_4$		
Vibrational mode	Frequency ( $\text{cm}^{-1}$ )	Infrared intensity ( $\text{km/mol}$ )	Vibrational mode	Frequency ( $\text{cm}^{-1}$ )	Infrared intensity ( $\text{km/mol}$ )
$\nu_1(\sigma_g)$	2214	0	$\nu_1(\sigma)$	2141	2030
$\nu_2(\sigma_g)$	1056	0	$\nu_2(\sigma)$	1921	2
$\nu_3(\sigma_g)$	316	0	$\nu_3(\sigma)$	1131	30
$\nu_4(\sigma_u)$	2070	677	$\nu_4(\sigma)$	549	34
$\nu_5(\sigma_u)$	492	712	$\nu_5(\pi)$	709	87
$\nu_6(\pi_g)$	585	0	$\nu_6(\pi)$	280	33
$\nu_7(\pi_g)$	92	0	$\nu_7(\pi)$	118	2
$\nu_8(\pi_u)$	281	$\sim 0$			
$\nu_9(\pi_u)$	41	$\sim 0$			

(a) Al rod +  $^{12}\text{C}$  rod

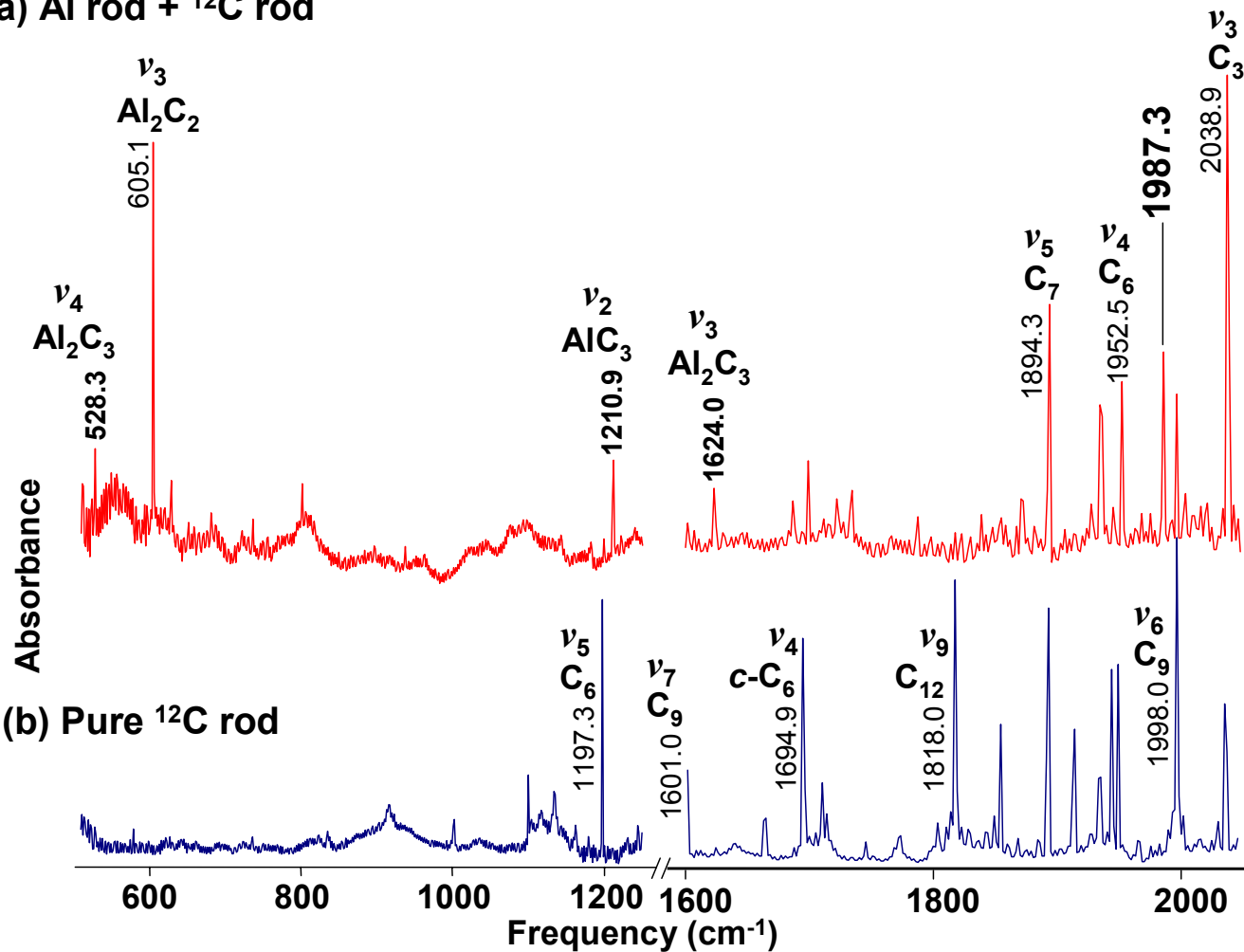


Figure 7.5 FTIR spectra obtained after (a) dual ablation of Al and  $^{12}\text{C}$  rods and (b) ablation of a  $^{12}\text{C}$  rod only, for comparison. Note the  $1987.3\text{ cm}^{-1}$  band in the Al-C spectrum that is not in the pure  $^{12}\text{C}$  spectrum. Note also the identifications of  $\text{AlC}_2\text{Al}$ ,  $\text{AlC}_3$ , and  $\text{AlC}_3\text{Al}$  in the dual ablation spectrum.

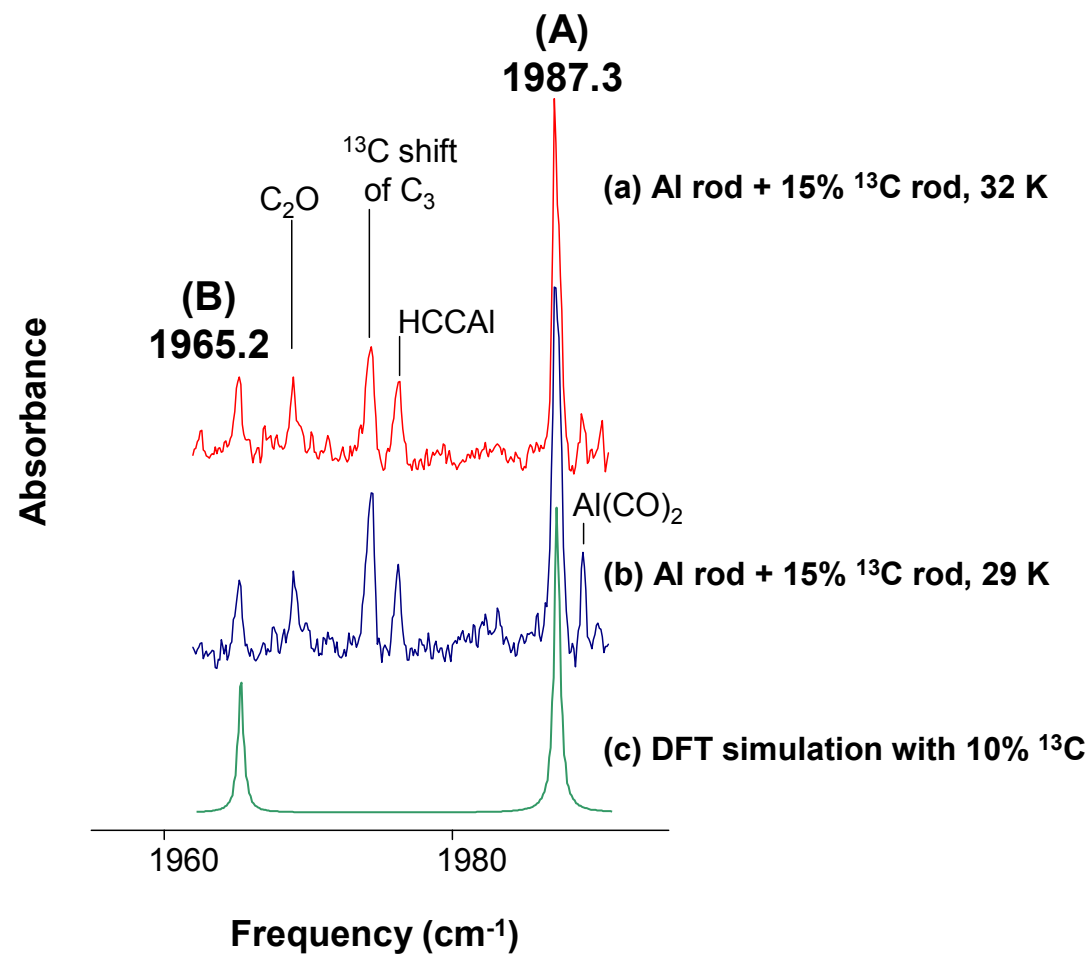


Figure 7.6 FTIR spectra obtained after dual ablation of an Al and a C rod with 15% nominal  $^{13}\text{C}$  enrichment annealed at (a) 32 K and (b) 29 K compared with a (c) DFT simulation of the spectrum of the  $\nu_4(\sigma_u)$  mode of linear  $\text{AlC}_4\text{Al}$  with a 10%  $^{13}\text{C}$  enrichment, scaled to 1987.3  $\text{cm}^{-1}$ .

however, when the intensities of the single  $^{13}\text{C}$  shifts in  $\text{C}_n$  species such as  $\text{C}_4$  and  $\text{C}_5$  are compared with the intensities of their main  $^{12}\text{C}_n$  bands, the effective enrichment is  $\sim 10\%$ .

Analysis of the  $1987.3\text{ cm}^{-1}$  band is complicated because it overlaps with the frequency of the single  $^{13}\text{C}$  substitution in the central atom of the  $\nu_3(\sigma_u)=2038.9\text{ cm}^{-1}$  mode of  $\text{C}_3$ . Possible  $^{13}\text{C}$  shifts for the  $1987.3\text{ cm}^{-1}$  band were identified in the Fig. 7.6(a) and (b) spectra by first eliminating bands belonging to known species such as  $1969.0$ ,  $1976.3$  and  $1988.7\text{ cm}^{-1}$  features, which are weak absorptions of  $\text{C}_2\text{O}$ ,  $^{121}\text{HCCAl}$ ,<sup>35,99</sup> and  $\text{Al}(\text{CO})_2$ ,<sup>96,98</sup> respectively, and the  $1974.5\text{ cm}^{-1}$  frequency is a doubly-substituted  $^{13}\text{C}$  isotopomer of  $\text{C}_3$ .

The  $1965.2\text{ cm}^{-1}$  band appears to be a  $^{13}\text{C}$  shift, but before its intensity can be compared to the main absorption at  $1987.3\text{ cm}^{-1}$ , the contribution from the 12-13-12 isotopomer of  $\text{C}_3$ , which can be estimated by dividing the band intensity of the  $^{13}\text{C}$  substitution on the equivalent C sites (at  $2026.4\text{ cm}^{-1}$ ) by two, must be subtracted from the band envelope. The intensity ratio of the  $1965.2\text{ cm}^{-1}$  feature to the corrected  $1987.3\text{ cm}^{-1}$  band intensity is  $\sim 44\%$ , indicating that the carrier could have four equivalent C atoms as the observed  $^{13}\text{C}$  enrichment is  $\sim 10\%$ .

The high frequency of the absorption suggests a C–C stretch in a linear species, but four equivalent C atoms are impossible in a linear chain. Although it is possible for two or more  $^{13}\text{C}$  shifts to overlap if a  $^{13}\text{C}$  substitution at more than one unique C site of a molecule does not appreciably change the vibrational frequency, it is very unlikely that a molecule with four inequivalent C atoms, such a linear  $\text{AlC}_4$ , would have all four  $^{13}\text{C}$  shifts predicted to overlap at the same frequency. Comparing the observed frequency with DFT predictions for linear  $\text{AlC}_4$  and  $\text{AlC}_4\text{Al}$  (see Table 7.3) shows that the  $\nu_1(\sigma)\sim 2141\text{ cm}^{-1}$  mode of linear  $\text{AlC}_4$  and the  $\nu_4(\sigma_u)\sim 2070\text{ cm}^{-1}$  mode of linear  $\text{AlC}_4\text{Al}$  are closest to the  $1987.3\text{ cm}^{-1}$  band. As expected, isotopic shift calculations for the  $\nu_1(\sigma)$  mode of linear  $\text{AlC}_4$  predict that it has four single  $^{13}\text{C}$  shifts of approximately equal intensity, which is not consistent with the isotopic shift pattern



shown in Figs. 7.6(a) and (b). Although the molecular symmetry of  $\text{AlC}_4\text{Al}$  indicates that there are two pairs of equivalent C atoms and thus two single  $^{13}\text{C}$  isotopic shifts should be observed, DFT calculations for its  $\nu_4(\sigma_u)$  mode predict that both of these frequencies will overlap. A DFT simulation of this mode with 10%  $^{13}\text{C}$  enrichment has been scaled to  $1987.3\text{ cm}^{-1}$  and compared with FTIR spectra in Fig. 7.6. Table 7.4 compares the measured and predicted single  $^{13}\text{C}$  shifts, and the results suggest that the  $1987.3\text{ cm}^{-1}$  absorption may belong to the  $\nu_4(\sigma_u)$  mode of linear  $\text{AlC}_4\text{Al}$ . Geometric parameters for  $\text{AlC}_4\text{Al}$  and the predicted principal nuclear displacements for its  $\nu_4(\sigma_u)$  mode are shown Fig 7.7.

It should be noted that since the FTIR spectra in Fig. 7.6 behave as if there were only 10%  $^{13}\text{C}$  enrichment, the doubly-, triply-, and fully-substituted  $^{13}\text{C}$  isotopomers would not have sufficient intensities for observation. Subsequent experiments with higher  $^{13}\text{C}$  enrichment have not produced spectra with sufficient signal-to-noise ratios for these isotopomers to be observable. If, however, experiments with high  $^{13}\text{C}$  enrichment ( $\sim 90\%$ ) could produce the mirror spectrum, *i.e.* the full  $^{13}\text{C}$  species and single  $^{12}\text{C}$  shifts, then an unambiguous identification might be possible. Interestingly, DFT predictions for the single  $^{12}\text{C}$  shifts from the fully-substituted  $^{13}\text{C}$  isotopomer absorption do not show an overlap, but two distinct shifts that should be observable (see Table 7.4). Additionally, observation of the  $\nu_5(\sigma_u)$  mode, which is the only other IR-active mode of this molecule that has sufficient IR intensity for observation and is predicted at  $\sim 492\text{ cm}^{-1}$  (Table 7.3), may also aid in assigning the  $\nu_4(\sigma_u)$  mode to  $1987.3\text{ cm}^{-1}$ .

### 7.2.3 Conclusions

The  $1987.3\text{ cm}^{-1}$  band appears to be a candidate for the  $\nu_4(\sigma_u)$  mode of ( $^1\Sigma_g^+$ ) linear  $\text{AlC}_4\text{Al}$  based on the good agreement between DFT predictions and FTIR spectra. DFT calculations, which are the first for  $\text{AlC}_4\text{Al}$ , show that single  $^{13}\text{C}$  substitutions on the two pairs of equivalent C atoms in its  $\nu_4(\sigma_u)$  mode overlap to produce one shift, which has been substantiated

Table 7.4: Comparison of observed vibrational fundamental and single  $^{13}\text{C}$  shift frequencies ( $\text{cm}^{-1}$ ) of the  $\nu_4(\sigma_u)$  mode of ( $^1\Sigma_g^+$ ) linear  $\text{AlC}_4\text{Al}$  with the predictions of B3LYP/6-311+G(3df) calculations.

Isotopomer		Observed	DFT	Scaled	Difference
Al-C-C-C-C-Al		$\nu$	$\nu$	$\nu$	$\Delta\nu$
27-12-12-12-12-27	(A)	1987.3	2070.1	... <sup>a</sup>	...
27- <b>13</b> -12-12-12-27	(B)	1965.2	2047.1	1965.1	0.1
27-12- <b>13</b> -12-12-27	(C)	Overlapped <sup>b</sup>	2047.1	1965.1	0.1
27- <b>13-13</b> -12-12-27	(D)		2018.3	1937.5	
27- <b>13</b> -12- <b>13</b> -12-27	(E)		2030.0	1948.7	
27- <b>13</b> -12-12- <b>13</b> -27	(F)		2027.3	1946.1	
27-12- <b>13-13</b> -12-27	(G)		2032.3	1950.9	
27- <b>13-13-13-13</b> -27	(A')		1988.7	1909.1	
27-12- <b>13-13-13</b> -27	(B')		2008.4	1928.0	
27- <b>13</b> -12- <b>13-13</b> -27	(C')		2004.2	1923.9	

<sup>a</sup>Results of the calculation scaled by a factor of  $1987.3/2070.1=0.95995$ .

<sup>b</sup>Overlapped with  $1965.2 \text{ cm}^{-1}$ .

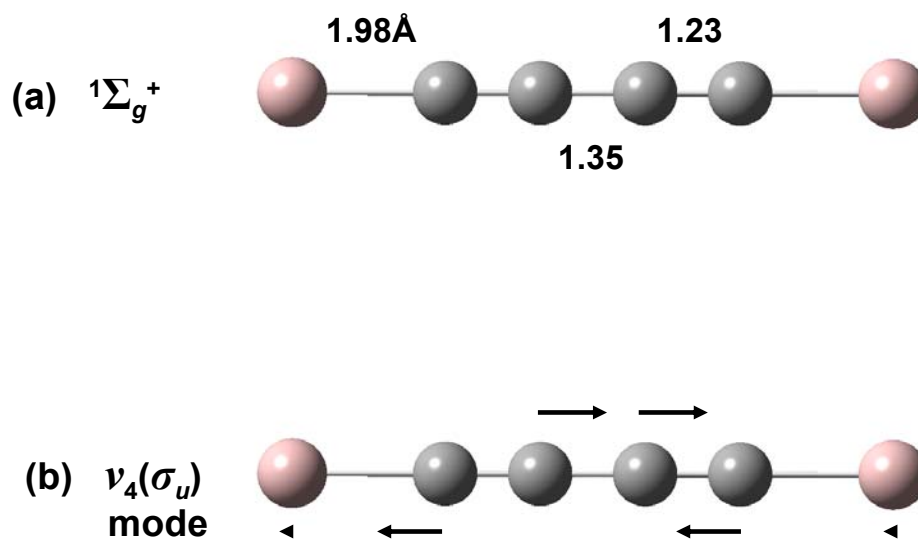


Figure 7.7 (a) DFT B3LYP/6-311+G(3*df*) predictions for the bond lengths of linear ( ${}^1\Sigma_g^+$ )  $\text{AlC}_4\text{Al}$  are given in Angstroms ( $\text{\AA}$ ). The predicted principal nuclear displacements of the atoms for its  $\nu_4(\sigma_u)$  mode are shown in (b).

by FTIR spectra. Frequency measurements of other  $^{13}\text{C}$  isotopomers are necessary to confirm this assignment. This would be the first optical detection of this species if the assignment is verified.

### 7.3 Unidentified $\text{V}_n\text{C}_m$ Candidates

Mass spectrometric data exists on some  $\text{V}_n\text{C}_m$  metcars, *e.g.*  $\text{V}_8\text{C}_{12}$  (Refs. 4, 122) and  $\text{V}_4\text{C}_9$ ,<sup>123</sup> but smaller species,  $\text{VC}_n$  ( $n=2,3$ )<sup>20,22</sup> and  $\text{V}_2\text{C}_n$  ( $n=2-4$ ),<sup>3</sup> have been studied using PES or DFT. PE spectra of  $\text{MC}_2^-$  clusters ( $\text{M} = \text{Sc}, \text{V-Co}$ )<sup>22</sup> have shown that  $\text{VC}_2$  is ( $C_{2v}$ ) cyclic with a V–C stretch at  $550\pm 40\text{ cm}^{-1}$ , which has been confirmed by subsequent investigations on  $\text{VC}_2$ ,  $\text{VC}_2^-$ , and  $\text{VC}_2^+$ ,<sup>124</sup> and on  $\text{V}_2\text{C}_n$  ( $n=2-4$ ) clusters.<sup>3</sup>  $\text{VC}_3$  is also reportedly ( $C_{2v}$ ) fanlike, based on a combined PES and DFT investigation of  $\text{MC}_3^-$  ( $\text{M} = \text{Sc}, \text{V-Ni}$ ) clusters.<sup>20</sup>

The most recent investigation<sup>125</sup> on  $\text{VC}_n$  ( $n=1-8$ ) clusters reported DFT B3LYP/6-311+G(*d*) calculations on linear, cyclic ( $C_{2v}$ ), and fanlike ( $C_{2v}$ ) isomers with spin multiplicities 2, 4, and 6. Fanlike structures have been predicted to be lower in energy than the linear or cyclic isomers for  $n\leq 6$ , but cyclic isomers were preferred for  $n>6$ . Except for VC, which has been predicted to have a doublet ground state, quartet states have been predicted to be the lowest in energy for linear and cyclic isomers. Fanlike isomers were also predicted to have quartet ground states, well-separated energetically from other electronic states, for all  $n$  except 3 and 5, for which doublet ground electronic states were predicted. Previously published vibrational frequencies<sup>126</sup> for linear ( $n=1-8$ ), fanlike ( $n=2-8$ ), and cyclic ( $n=6-8$ )  $\text{VC}_n$  species are given in Tables 7.5, 7.6, and 7.7, respectively.

Potential  $\text{V}_n\text{C}_m$  candidates presented in this work were created by the ablation of either a single rod composed of 20% V and 80%  $^{12}\text{C}$  powders at a laser power of  $\sim 2.0\text{ W}$  or the dual evaporation of a V rod ( $\sim 2.7\text{ W}$ ) and a  $^{12}\text{C}$  rod ( $\sim 0.7$  or  $\sim 1.5\text{ W}$ ). New absorptions have been observed in three different frequency regions, 2000-2050, 1450-1500, and 900-950  $\text{cm}^{-1}$ .

Table 7.5: B3LYP/6-311+G(*d*) calculations of vibrational frequencies (cm<sup>-1</sup>) for linear VC<sub>*n*</sub> (*n*=1-8) clusters (from Ref. 126).

Isomer	State	Vibrational Frequencies (cm <sup>-1</sup> )
VC	<sup>2</sup> Δ	946
	<sup>4</sup> Δ	894
	<sup>6</sup> Σ	690
VC2	<sup>2</sup> Δ	221i(2)/590/1803
	<sup>4</sup> Σ	73i(2)/570/1832
	<sup>4</sup> Φ	25/140/531/1802
	<sup>6</sup> Δ	142(2)/443/1945
VC3	<sup>2</sup> Δ	139(2)/413(2)/473/1293/1887
	<sup>4</sup> Φ	130/137/362/377/427/1264/1849
	<sup>6</sup> Σ	126(2)/373(2)/450/1294/1969
VC4	<sup>2</sup> Δ	75(2)/232(2)/393/568(2)/1067/1784/2123
	<sup>4</sup> Σ	71(2)/232(2)/411/554(2)/1072/1835/2127
	<sup>4</sup> Φ	89/92/237/258/344/528/535/1022/1795/2090
	<sup>6</sup> Φ	84/88/197/259/330/432/517/982/1830/2093
VC5	<sup>2</sup> Δ	79(2)/217(2)/380/392(2)/569(2)/896/1476/1938/2038
	<sup>4</sup> Φ	72/73/191/200/308/358/386/506/651/848/1486/1890/1980
	<sup>6</sup> Σ	70(2)/192(2)/361/365(2)/578(2)/882/1518/1967/2079
VC6	<sup>2</sup> Δ	53(2)/145(2)/270(2)/321/521(2)/769/775(2)/1295/1820/2063/2165
	<sup>4</sup> Σ	50(2)/139(2)/264(2)/338/515(2)/742(2)/783/1304/1853/2077/2174
	<sup>4</sup> Φ	56/56/151/151/271/275/287/487/495/710/732/736/1264/1857/1999/2144
	<sup>6</sup> Φ	55/55/143/154/259/278/285/429/488/685/698/716/1250/1882/2062/2137
VC7	<sup>2</sup> Δ	48(2)/136(2)/246(2)/324/388(2)/547(2)/695/831(2)/1144/1591/1863/2045/2116
	<sup>4</sup> Φ	46/46/124/127/226/233/269/364/382/496/587/646/800/881/1123/1610/1778/2011/2086
	<sup>6</sup> Σ	45(2)/121(2)/227(2)/311/371(2)/540(2)/681/828(2)/1151/1619/1919/2069/2125
VC8	<sup>2</sup> Δ	37(2)/97(2)/187(2)/279/290(2)/486(2)/606/627(2)/1025/1094(2)/1436/1832/1992/2124/2188
	<sup>4</sup> Σ	35(2)/92(2)/181(2)/281(2)/293/484(2)/613(2)/623/1031(2)/1033/1437/1867/1999/2137/2197
	<sup>4</sup> Φ	37/38/102/102/188/195/255/291/293/456/471/580/597/606/994/1000/1015/1406/1856/1963/2085/2171
	<sup>6</sup> Φ	37/37/100/101/181/195/255/288/292/418/467/568/584/586/968/974/990/1386/1898/2041/2087/2175

Table 7.6: B3LYP/6-311+G(d) calculations of vibrational frequencies (cm<sup>-1</sup>) for fanlike VC<sub>n</sub> (n=2-8) clusters (from Ref. 126).

Isomer	State	Vibrational Frequencies (cm <sup>-1</sup> )
VC <sub>2</sub>	<sup>2</sup> A''	264/659/1424
	<sup>4</sup> B <sub>1</sub>	378/578/1688
	<sup>6</sup> A <sub>1</sub>	275/397/1789
VC <sub>3</sub>	<sup>2</sup> A <sub>1</sub>	438/572/592/832/1304/1538/
	<sup>4</sup> B <sub>2</sub>	341/346/515/760/1289/1591
	<sup>6</sup> A <sub>1</sub>	323/400/443/578/1249/1570
VC <sub>4</sub>	<sup>2</sup> B <sub>1</sub>	253/414/448/515/599/622/1088/1624/1761
	<sup>4</sup> B <sub>1</sub>	272/372/402/487/515/590/1055/1738/1869
	<sup>6</sup> B <sub>1</sub>	98/175/221/375/410/537/995/1656/1990
VC <sub>5</sub>	<sup>2</sup> A'	151/365/383/389/422/524/598/686/1005/1358/1679/1703
	<sup>4</sup> A'	142/248/371/421/449/471/588/642/999/1382/1633/1709
	<sup>6</sup> B <sub>2</sub>	246/321/356/358/373/430/460/571/964/1395/1593/1714
VC <sub>6</sub>	<sup>2</sup> A'	115/220/259/339/415/416/459/538/589/609/987/1204/1645/1704/1820
	<sup>4</sup> A <sub>2</sub>	59/241/257/281/403/414/449/456/555/608/901/1191/1801/1880/2018
	<sup>6</sup> B <sub>1</sub>	95/130/135/216/332/368/380/392/481/510/896/1222/1632/1786/1902
VC <sub>7</sub>	<sup>2</sup> A	53/75/248/303/325/345/379/380/422/542/577/624/913/1158/1517/1663/1801/1861
	<sup>4</sup> B <sub>2</sub>	60/159/263/304/323/348/363/365/434/539/565/621/913/1132/1533/1673/1801/1829
	<sup>6</sup> A'	113/193/205/265/321/346/365/414/484/496/548/632/861/1089/1337/1715/1820/1892
VC <sub>8</sub>	<sup>2</sup> A''	114/133/177/265/334/345/402/406/417/433/466/475/591/641/865/1035/1266/1674/1835/1839/1971
	<sup>4</sup> B	100/100/203/216/242/248/260/325/352/402/403/456/542/545/820/1049/1334/1873/1927/2021/2064
	<sup>6</sup> B <sub>1</sub>	107/121/127/128/236/258/299/405/433/435/458/506/574/632/835/1025/1241/1598/1830/1843/2012

Table 7.7: B3LYP/6-311+G(*d*) calculations of vibrational frequencies (cm<sup>-1</sup>) for cyclic VC<sub>*n*</sub> (*n*=6-8) clusters (from Ref. 126).

Isomer	State	Vibrational Frequencies (cm <sup>-1</sup> )
VC <sub>6</sub>	<sup>2</sup> A <sub>2</sub>	50/159/228/285/307/425/432/437/505/1008/1029/1207/1931/1977/2037
	<sup>4</sup> A''	129/148/251/301/349/390/416/455/473/590/1016/1219/1799/1888/1948
	<sup>6</sup> A <sub>1</sub>	154/167/217/229/424/441/503/520/551/642/925/1083/1600/1833/1842
VC <sub>7</sub>	<sup>2</sup> B <sub>1</sub>	141/213/225/234/434/441/483/489/508/510/593/629/1021/1183/1458/1584/1865/1882
	<sup>2</sup> A <sub>1</sub>	129/209/223/236/421/452/469/492/503/522/586/610/1020/1180/1467/1580/1864/1883
	<sup>4</sup> B <sub>2</sub>	148/164/188/227/354/408/428/481/508/521/595/611/991/1147/1440/1658/1883/1899
	<sup>6</sup> A <sub>1</sub>	112/142/145/194/316/363/368/435/489/495/553/544/900/1075/1516/1547/1851/1881
VC <sub>8</sub>	<sup>2</sup> B <sub>1</sub>	68/136/142/161/198/228/296/377/379/437/476/507/571/577/843/997/1316/1912/1914/2007/2106
	<sup>4</sup> A''	39/101/120/147/230/255/288/379/380/450/461/498/546/551/835/1003/1316/1930/1975/2041/2122
	<sup>6</sup> A <sub>2</sub>	34/102/112/148/222/238/245/425/451/476/487/505/585/596/847/1004/1286/1536/1837/1849/2023

Evaporation of a single V/<sup>12</sup>C rod has produced different potential V<sub>n</sub>C<sub>m</sub> candidates than the dual evaporation of V and <sup>12</sup>C rods, as will be discussed in the following sections.

In V/C experiments, the matrix samples were often annealed, *i.e.* warmed to a specific temperature in the range of 20-30 K for several minutes and then cooled to ~10 K, after which spectra were recorded. Annealing facilitates diffusion of smaller molecules through the Ar matrix, allowing them to combine to form larger molecules. Additionally, absorptions resulting from secondary trapping sites collapse into the band corresponding to the minimum-energy trapping site, which sharpens spectra (*e.g.* TiC<sub>3</sub> in Ref. 55).

### 7.3.1 The 2000-2050 cm<sup>-1</sup> Region

Three bands at 2032.9, 2029.6, and 2019.2 cm<sup>-1</sup> were produced by the ablation of a single rod composed of 20% V and 80% <sup>12</sup>C ablated at a laser power of ~2.0 W (Fig. 7.8). Only weak absorptions of contaminant species such as H<sub>2</sub>V<sup>127</sup> and H<sub>2</sub>OV,<sup>128</sup> respectively, at 1508.3 and 1710.6 cm<sup>-1</sup> are observed in V/C spectra. No other absorptions that could be attributed to O or H atoms bonding to V<sub>n</sub> or V<sub>n</sub>C<sub>m</sub> clusters have been found including O<sub>2</sub>V, O<sub>2</sub>V<sub>2</sub>, O<sub>3</sub>V<sub>2</sub>, and O<sub>4</sub>V,<sup>129</sup> COV, CO<sub>2</sub>V, and C<sub>2</sub>O<sub>2</sub>V,<sup>130</sup> suggesting that any unidentified bands in the spectra likely result from pure V<sub>n</sub>C<sub>m</sub> species.

Experiments done with a V/C rod in which the C had 15% <sup>13</sup>C enrichment have not produced <sup>13</sup>C shifts, making molecular identifications and geometry determinations impossible, but several conclusions can be drawn from the spectra. First, the high frequencies are indicative of C–C stretching modes in linear chains so linear VC<sub>n</sub> or VC<sub>n</sub>V chains are the most probable carriers. Second, the 2032.9 cm<sup>-1</sup> band grows in during annealing and thus cannot result from the same molecule or molecules that produce the bands at 2029.6 and 2019.2 cm<sup>-1</sup>, which are present throughout the experiment. Moreover, this band likely results from a longer C<sub>n</sub>-bearing chain, such as C<sub>6</sub>, C<sub>7</sub>, or C<sub>9</sub>, that is created as smaller molecules diffuse through the Ar matrix



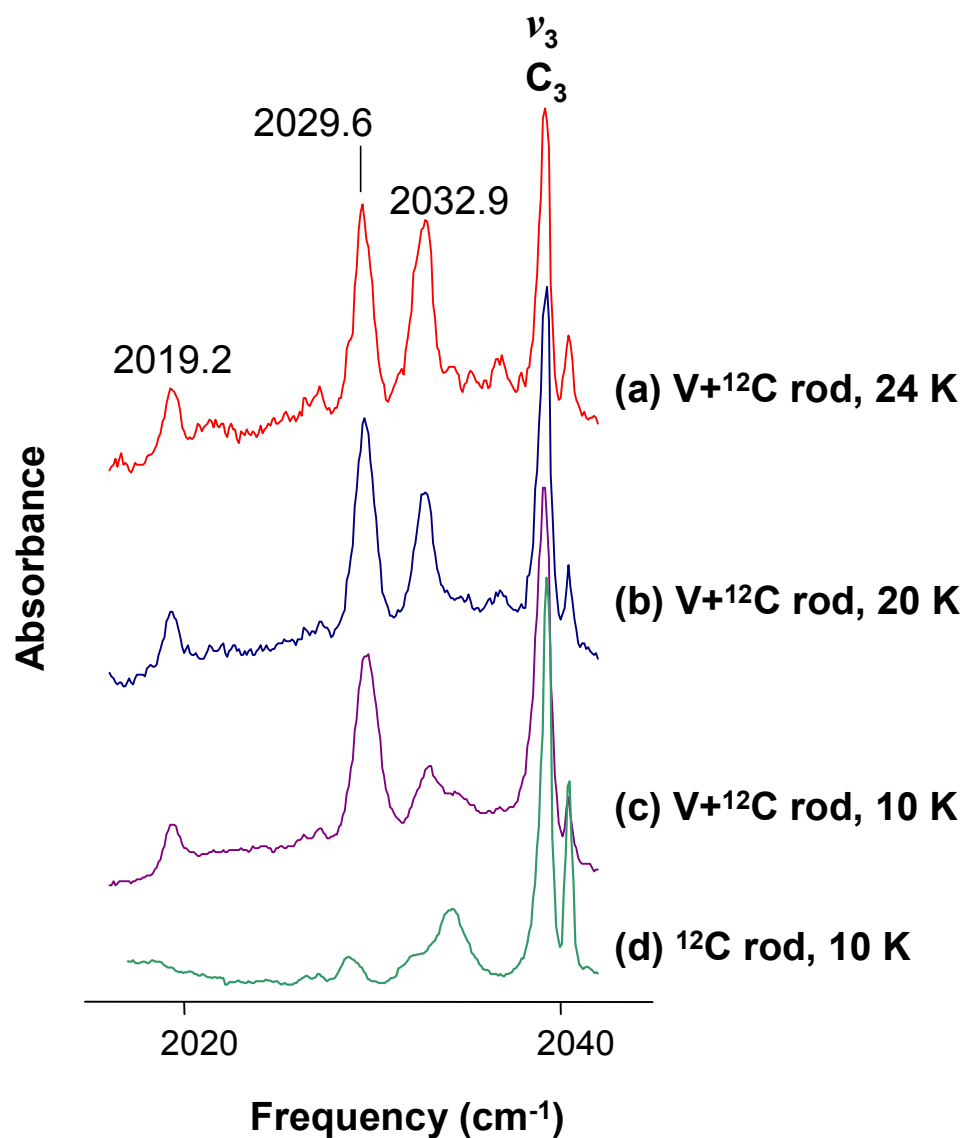


Figure 7.8 FTIR spectra of the 2000-2050 cm<sup>-1</sup> region recorded after laser ablation of a single rod pressed from 20% V and 80% <sup>12</sup>C powders annealed at (a) 24 K, (b) 20 K, and (c) prior to annealing at 10 K for comparison with (d) an FTIR spectrum obtained from ablation of a <sup>12</sup>C rod.

and combine into larger species. Finally, since the bands at 2029.6 and 2019.2  $\text{cm}^{-1}$  sharpen slightly but do not notably grow during annealing, they are probably smaller  $C_n$ -bearing species, such as  $C_3$ , or  $C_4$ , for which the band intensities do not significantly increase during annealing.

If these high frequency bands are C–C stretches of linear  $VC_n$  species, then based solely on the DFT predictions in Table 7.5, the highest frequency modes for the  $^4\Sigma$  and  $^4\Phi$  states of linear  $VC_n$  ( $n=4,6,8$ ), the  $^6\Sigma$  state of linear  $VC_5$ , and the  $^4\Phi$  and  $^6\Sigma$  states of linear  $VC_7$  are all possible candidates for these band identities, which clearly illustrates the necessity of  $^{13}\text{C}$  isotopic shifts in this work.

### 7.3.2 The 1450-1500 $\text{cm}^{-1}$ Region

Bands at 1475.4, 1478.5, and 1479.5  $\text{cm}^{-1}$  were created by dual laser ablation of V ( $\sim 2.5$ - $2.7$  W) and  $^{12}\text{C}$  ( $\sim 0.7$  W) rods (Fig. 7.9), and therefore can not be related to the three bands seen in the 2000-2100  $\text{cm}^{-1}$  region because they were produced using different techniques and are observed independently of the higher frequency bands. The bands at 1475.4 and 1479.5  $\text{cm}^{-1}$  only appear after annealing [Fig. 7.9(a)], but the 1478.5  $\text{cm}^{-1}$  is present during the ablation of V and C rods, prior to annealing [Fig. 7.9(b)]. Because these three bands were produced using the low laser power technique,<sup>37</sup> which predominantly creates  $C_3$ , they are likely small  $V_nC_m$  clusters. It is interesting to note that these three bands are in the same frequency region where the  $\nu_5(b_2)$  modes of fanlike ( $C_{2v}$ )  $\text{TiC}_3$  (Ref. 55) and  $\text{ScC}_3$  (Ref. 71) have been identified. A vibrational mode of fanlike  $VC_3$  is therefore a possible assignment for one of these bands. The  $^2A_1$  and  $^4B_2$  states of fanlike  $VC_3$  are predicted to have similar vibrational frequencies<sup>125</sup> (Table 7.6), and the  $^2A_1$  state is predicted to be the ground state by only  $\sim 5$  kcal/mol. Without  $^{13}\text{C}$  isotopic shifts, it is impossible to determine if fanlike  $VC_3$  is a carrier of one of these bands, and if so, which electronic state is the ground state. Thus far, experiments with 15%  $^{13}\text{C}$  enrichment have been unsuccessful in producing  $^{13}\text{C}$  shifts.

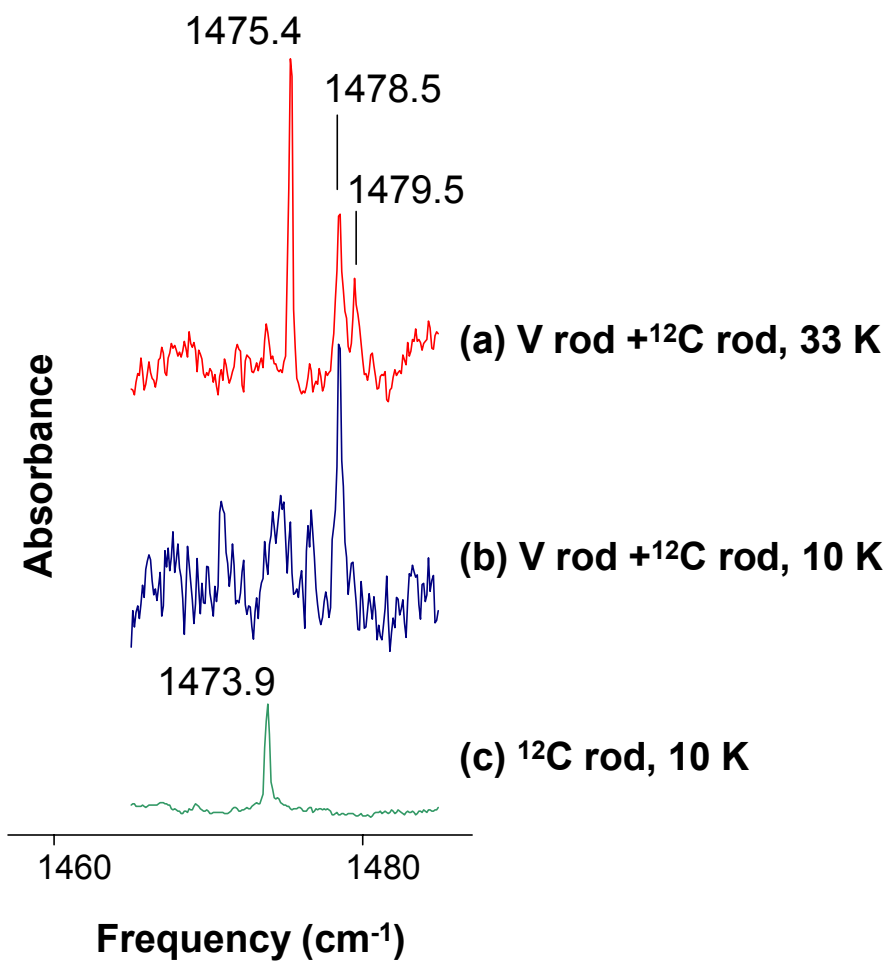


Figure 7.9 FTIR spectra of the 1450-1500 cm<sup>-1</sup> region recorded after dual laser ablation of a V rod and a <sup>12</sup>C rod (a) annealed at 33 K and (b) prior to annealing at 10 K for comparison with (c) a spectrum obtained from ablation of a <sup>12</sup>C rod.

### 7.3.3 *The 900-950 cm<sup>-1</sup> Region*

The three bands that are observed in the 900-950 cm<sup>-1</sup> region at 923.2, 919.5, and 917.3 cm<sup>-1</sup> (Fig. 7.10) were produced in experiments using a single rod composed of 20% V and 80% <sup>12</sup>C that was ablated at ~2.0 W, and also in experiments using the dual ablation and low laser power techniques.<sup>37</sup> Since the bands in the 900-950 cm<sup>-1</sup> region of the spectrum did not behave similarly to the bands in either the 1450-1500 or 2000-2100 cm<sup>-1</sup> regions of the spectrum, the molecular carriers cannot be the same as those for the bands observed at higher frequencies.

Again, no <sup>13</sup>C shifts have been observed, but several conclusions can still be drawn from knowing the experimental conditions used to create these bands and from observing their behavior during annealing. Since the three bands are produced by dual ablation of V and <sup>12</sup>C rods using the low laser power technique<sup>37</sup> and the frequencies are ~900 cm<sup>-1</sup>, the molecular carriers are likely small V<sub>n</sub>C<sub>m</sub> species with non-linear geometries. These bands are probably not modes of fanlike VC<sub>3</sub>, which does not have a vibrational fundamental predicted near 900-1000 cm<sup>-1</sup> (see Table 7.6). Finally, the 917.3 cm<sup>-1</sup> band slowly anneals out of the spectrum (see Fig. 7.10) and is therefore likely a satellite band of either the 919.5 or 923.2 cm<sup>-1</sup> features.

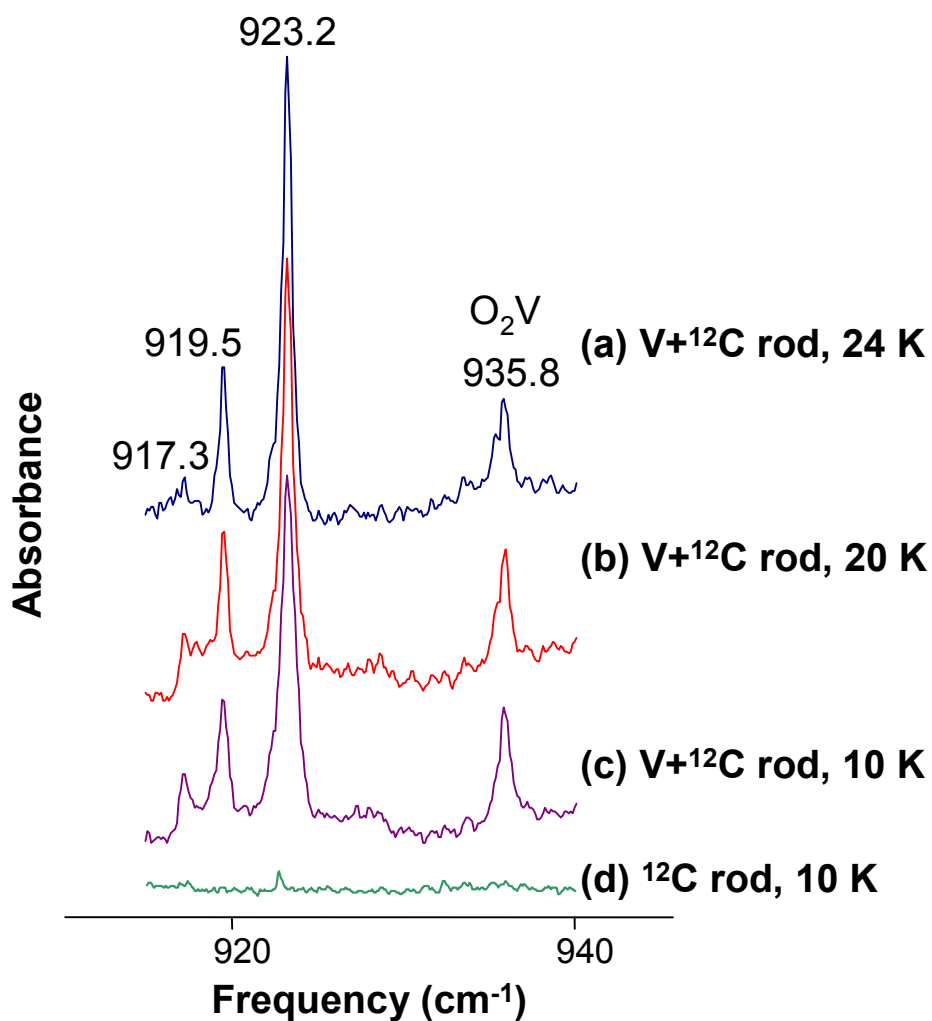


Figure 7.10 FTIR spectra of the 900-950 cm<sup>-1</sup> region recorded after laser ablation of a single rod pressed from 20% V and 80% <sup>12</sup>C powders annealed at (a) 24 K, (b) 20 K, and (c) prior to annealing at 10 K for comparison with (d) an FTIR spectrum obtained from ablation of a <sup>12</sup>C rod.

## CHAPTER VIII

### CONCLUSIONS AND FUTURE WORK

#### 8.1 Conclusions

The first FTIR investigations of transition metal–carbon clusters have been reported in Chapters III-VII this dissertation.  $M_nC_3$  ( $M = \text{Cr, Co, Al, Cu}$ )<sup>46,91,112,120</sup> clusters have been created by condensing the ablated products of the dual evaporation of metal and carbon clusters in solid Ar on a gold mirror kept at  $\sim 10$  K. Vibrational frequencies and  $^{13}\text{C}$  isotopic shifts measured in FTIR spectra are in good agreement with the predictions of DFT B3LYP/6-311+G(3*df*) calculations, which has enabled the identification of five novel molecules, unambiguously established their geometries, and permitted assignments of at least one vibrational fundamental for each species.

##### 8.1.1 *Linear CrC<sub>3</sub>*

This investigation on  $\text{CrC}_3$ , which was produced by trapping the products from the dual evaporation of Cr and C rods in Ar at  $\sim 10$  K, has resulted in the first assignment of a vibrational fundamental for the linear isomer. A prior PES study<sup>25</sup> had reported evidence of both linear and ( $C_{2v}$ ) fanlike isomers, and the first measurement of a vibrational mode for the  $C_{2v}$  structure. No evidence of the fanlike isomer was observed in the present study. The excellent agreement between  $^{13}\text{C}$  isotopic shift measurements coupled with DFT predictions has established that the ground state structure of  $\text{CrC}_3$  is linear with a  $^5\Pi$  electronic state, and its  $\nu_1(\sigma)$  carbon stretching fundamental has been identified at  $1789.5\text{ cm}^{-1}$ .

These results have been published: S. A. Bates, C. M. L. Rittby, and W. R. M. Graham *Fourier transform infrared isotopic study of linear CrC<sub>3</sub>: Identification of the  $\nu_1(\sigma)$  mode*, J. Chem. Phys. **125**, 074506 (2006).<sup>46</sup>

### 8.1.2 Linear CoC<sub>3</sub>

The first detection of the vibrational spectrum of the CoC<sub>3</sub> cluster has been reported here accompanied by the first DFT investigation of its two lowest-lying isomers. Earlier PE spectra<sup>20</sup> had broad, unresolved vibrational structure that made it impossible to determine the geometry of CoC<sub>3</sub>. In the present matrix study of the evaporated products of the dual laser ablation of Co and C rods a band at 1918.2 cm<sup>-1</sup> and the signature isotopic shift pattern for a non-centrosymmetric linear molecule with three C atoms has been observed. The excellent agreement between the FTIR measured <sup>13</sup>C shifts and the results of DFT BPW91/ and B3LYP/6-311+G(3df) calculations confirms the assignment of the 1918.2 cm<sup>-1</sup> absorption to the  $\nu_1(\sigma)$  vibrational fundamental of linear CoC<sub>3</sub>.

These results indicate that the <sup>2</sup> $\Delta$  state of the linear isomer is the universal ground state (as predicted by DFT/B3LYP calculations), rather than the <sup>2</sup> $B_1$  state of the fanlike isomer (as predicted by DFT/BPW91 calculations), lying only ~4 kcal/mol lower in energy. The linear structure found for CoC<sub>3</sub> in the present investigation contrasts with the recent report of the observation of (<sup>1</sup> $A_1$ ) fanlike TiC<sub>3</sub> which is, however, well separated energetically from competing linear and kite-shaped structures.<sup>55</sup> The current findings are similar to those presented in Chapter III for the <sup>5</sup> $\Pi$  linear CrC<sub>3</sub> species for which close-lying fanlike and linear structures are also predicted.<sup>46</sup> This study on CoC<sub>3</sub> is both the first theoretical investigation on this molecule, and the first optical detection of the linear isomer and measurement of a vibrational fundamental.

These results have been published as: S. A. Bates, J. A. Rhodes, C. M. L. Rittby, and W. R. M. Graham, *Fourier transform infrared observation of the  $\nu_1(\sigma)$  mode of linear  $\text{CoC}_3$  trapped in solid Ar*, J. Chem. Phys. **127**, 064506 (2007).<sup>91</sup>

### 8.1.3 Linear $\text{AlC}_3$ and $\text{AlC}_3\text{Al}$

This is the first experimental or theoretical characterization of the infrared vibrational spectrum of the  $\text{AlC}_3\text{Al}$  molecule. Condensing the products from dual evaporation of Al and C rods in a  $\sim 10$  K Ar matrix has produced the 1624.0 and 528.3  $\text{cm}^{-1}$  bands, which have been identified as the  $\nu_3(\sigma_u)$  C–C and  $\nu_4(\sigma_u)$  Al–C stretching fundamentals, respectively, of linear  $\text{AlC}_3\text{Al}$  in its  $^3\Sigma_g^+$  ground state, based on the good agreement between DFT predictions and the observed  $^{13}\text{C}$  isotopic shift patterns. These two vibrational fundamentals are predicted to be the only IR-active modes of this species that have significant intensity.

Although theoretical investigations<sup>26,87–89</sup> on  $\text{AlC}_3$  have indicated that the  $^2\Pi$  linear,  $^2A_1$  kite, and  $^2B_2$  fanlike isomers are close in energy,<sup>26</sup> there had been no prior experimental observation of this species. In the present work,  $^2\Pi$  linear  $\text{AlC}_3$  has been observed for the first time, establishing this isomer as the ground state, and its  $\nu_2(\sigma)=1210.9$   $\text{cm}^{-1}$  mode has been identified based on the good agreement between DFT calculations and the observed  $^{13}\text{C}$  isotopic spectrum. No evidence of either the fanlike or kite isomers has been observed. The results reported here are parallel to investigations on ( $^5\Pi$ )  $\text{CrC}_3$  (Ref. 46) and ( $^2\Delta$ )  $\text{CoC}_3$  (Ref. 91), presented in Chapters III and IV of this work, respectively, for which close-lying fanlike and linear structures have been predicted but only the linear isomers detected.

These results are in preparation for submission to J. Chem. Phys. as: S. A. Bates, C. M. L. Rittby, and W. R. M. Graham, *FTIR observation and DFT study of the  $\text{AlC}_3$  and  $\text{AlC}_3\text{Al}$  linear chains trapped in solid Ar*, J. Chem. Phys., *in preparation* (2008).<sup>112</sup>



#### 8.1.4 Linear $\text{CuC}_3$

There are no prior theoretical investigations on  $\text{CuC}_3$  or experimental investigations on any  $\text{Cu}_n\text{C}_m$  cluster; therefore, this work is the first experimental and theoretical study of  $\text{CuC}_3$ , resulting not only in the first assignment of a vibrational fundamental for  $\text{CuC}_3$ , but also for any  $\text{Cu}_n\text{C}_m$  cluster. The  $\text{CuC}_3$  molecule was created by the dual laser ablation of Cu and C rods and trapping the evaporated products in solid Ar at  $\sim 10$  K, which produced the band at  $1830.0\text{ cm}^{-1}$  and the signature  $^{13}\text{C}$  isotopic shift pattern of a non-centrosymmetric linear molecule with three inequivalent carbon atoms.

DFT calculations have predicted that a ( $^2A'$ ) *trans*-bent geometry is the universal ground state,  $\sim 0.7$  kcal/mol lower in energy than the  $^2\Pi$  linear isomer; however, the predicted  $^{13}\text{C}$  isotopic shift pattern is not in agreement with the observed spectra. The predicted  $^{13}\text{C}$  shifts for the ( $^2\Pi$ ) linear isomer of  $\text{CuC}_3$  is in very good agreement with FTIR spectra; however, this isomer is predicted to have one imaginary frequency at  $\sim 168i\text{ cm}^{-1}$ , suggesting that the linear geometry is a transition state and not the true ground state at the DFT B3LYP/6-311+G(3df) level of theory. A similar situation occurred for  $\text{NiC}_3\text{Ni}$ , as reported by Kinzer *et al.*,<sup>92</sup> where the molecular geometry has been found to be slightly floppy. It should be noted that the vibrational spectrum of  $\text{CuC}_3$  behaves as if the molecule were linear; thus the molecule can be considered as such and its  $\nu_1(\sigma)$  mode is assigned to  $1830.0\text{ cm}^{-1}$ . This is the first assignment of a vibrational fundamental for any  $\text{Cu}_n\text{C}_m$  molecule.

These results are in preparation for submission to J. Chem. Phys. as: S. A. Bates, C. M. L. Rittby, and W. R. M. Graham, *The Vibrational Spectrum of  $\text{CuC}_3$ : An FTIR and DFT Investigation*, J. Chem. Phys., *in preparation* (2008).<sup>120</sup>

### 8.1.5 *Fanlike (C<sub>2v</sub>) CrC<sub>4</sub>*

An absorption at 1554.3 cm<sup>-1</sup> has been produced by trapping the evaporated products of the laser ablation of a sintered Cr/C rod in Ar at ~10 K, and is tentatively identified as the  $\nu_1(a_1)$  vibrational mode of fanlike CrC<sub>4</sub> in its <sup>3</sup>B<sub>1</sub> electronic state, which if substantiated, would be the first observation and assignment of a vibrational fundamental for this molecule.

A prior PE investigation<sup>25</sup> that included DFT BPW91/6-311+G\* calculations predicted that the <sup>3</sup>B<sub>1</sub> and <sup>5</sup>B<sub>2</sub> electronic states of fanlike CrC<sub>4</sub> were nearly isoenergetic, with the <sup>5</sup>B<sub>2</sub> state being slightly more stable. The isotopic shift pattern observed in FTIR spectra in the present study indicates that a molecular carrier with two pairs of equivalent carbon atoms is responsible, such as fanlike CrC<sub>4</sub>. DFT calculations on the <sup>5</sup>B<sub>2</sub> state, however, predict that its  $\nu_7(b_2)$ ~1835 cm<sup>-1</sup> mode, predicted to be the closest in frequency to 1554.3 cm<sup>-1</sup>, has negligible IR intensity. The predictions of DFT calculations for the single <sup>13</sup>C shifts of the  $\nu_1(a_1)$  mode of the <sup>3</sup>B<sub>1</sub> state are in good agreement with the observed spectrum; therefore, this vibrational fundamental is tentatively assigned to 1554.3 cm<sup>-1</sup>. Experiments with higher <sup>13</sup>C enrichment have not produced the doubly-, triply-, and fully-substituted <sup>13</sup>C isotopomers, which would unambiguously confirm the assignment; therefore, the identification must be considered tentative.

### 8.1.6 *Linear AlC<sub>4</sub>Al*

The 1987.3 cm<sup>-1</sup> band appears to be a candidate for the  $\nu_4(\sigma_u)$  mode of (<sup>1</sup>Σ<sub>g</sub><sup>+</sup>) linear AlC<sub>4</sub>Al based on the good agreement between DFT predictions and FTIR spectra. This is the first theoretical investigation on the AlC<sub>4</sub>Al molecule and this would also be the first detection of its vibrational spectrum if the very tentative assignment is verified. The 1987.3 cm<sup>-1</sup> absorption was created by the dual ablation of Al and C rods and condensing the evaporated products in an ~10 K Ar matrix. DFT calculations show that single <sup>13</sup>C substitutions on the two pairs of

equivalent C atoms in its  $\nu_4(\sigma_u)$  mode overlap to produce one shift, which has been substantiated by FTIR spectra. Frequency measurements of other  $^{13}\text{C}$  isotopomers are necessary to confirm this assignment.

### 8.1.7 $V_nC_m$ Candidates

None of the  $V_nC_m$  candidate bands in the 2000-2100, 1450-1500, or 900-950  $\text{cm}^{-1}$  regions of the spectrum appear to be correlated with any of the other observed bands and therefore will not have the same molecular carrier. The bands at high frequencies, 2032.9, 2029.6, and 2019.2  $\text{cm}^{-1}$ , were created by the ablation of a single V/C rod and are likely C–C stretching modes of linear  $VC_n$  or  $VC_nV$  species. The 1475.4, 1478.5, and 1479.5  $\text{cm}^{-1}$  bands were created using the dual ablation and low laser power<sup>37</sup> techniques, similar to the conditions in which the  $\nu_5(b_2)$  modes of fanlike ( $C_{2v}$ )  $\text{TiC}_3$  (Ref. 55) and  $\text{ScC}_3$ ,<sup>71</sup> respectively, have been identified at 1478.2 and 1478.0  $\text{cm}^{-1}$ ; therefore, the analogous vibration of fanlike  $VC_3$  appears to be a good candidate for the identity of one of these absorptions. The low-frequency absorptions at 923.2, 919.5, and 917.3  $\text{cm}^{-1}$  were created in experiments in which V and C rods were simultaneously ablated and during evaporation of a single V/C rod. The bands at 923.2 and 919.5  $\text{cm}^{-1}$  probably also result from small, non-linear  $V_nC_m$  species, while the band at 917.3  $\text{cm}^{-1}$  is likely a satellite band of one of the other features.

## 8.2 Future Work

The primary focus of future studies is to create other novel  $M_nC_m$  clusters, which can include continuing the unfinished work on the absorptions and tentative identifications presented Chapter VII, performing experiments using different metals, or creating larger  $C_n$  species to which metal atoms can attach. Additionally, observation of low frequency, low intensity M–C stretches and bending modes is desired and a technique that may aid in that endeavor is presented

in Section 8.2.2. Finally, an improvement to the current rod fabrication technique is discussed so that rods with >50%  $^{13}\text{C}$  enrichment can be produced.

### 8.2.1 *Continuing Work on CrC<sub>4</sub>, AlC<sub>4</sub>Al, and V<sub>n</sub>C<sub>m</sub> Species*

Tentative identifications for the  $\nu_1(a_1)=1554.3\text{ cm}^{-1}$  mode of  ${}^3B_1$  fanlike CrC<sub>4</sub> and for the  $\nu_4(\sigma_u)=1987.3\text{ cm}^{-1}$  mode of  ${}^1\Sigma_g^+$  linear AlC<sub>4</sub>Al have been presented in Chapter VII, Sections 7.1 and 7.2, respectively (see also Chapter VIII, Sections 8.1.5 and 8.1.6, respectively). These assignments are tentative because only singly-substituted  $^{13}\text{C}$  isotopomer frequencies have been measured. Experiments with ~50%  $^{13}\text{C}$  enrichment could be done to observe all of the isotopomers or ~90%  $^{13}\text{C}$  enrichment may enable the observation of the mirror spectrum, *i.e.* the fully-substituted  $^{13}\text{C}$  isotopomer band and its single  $^{12}\text{C}$ -substituted shifts. Additionally, a number of absorptions appear in vanadium-carbon spectra, which have not been identified, because  $^{13}\text{C}$  shifts have not been observed (see Chapter VII, Section 7.3 and Chapter VIII, Section 8.1.7). Since the chromium-carbon absorption at  $1554.3\text{ cm}^{-1}$  and several of the potential V<sub>n</sub>C<sub>m</sub> bands were created by laser ablation of a single metal/carbon rod, future experiments may benefit from the proposed sintering process in Section 8.2.3.

### 8.2.2 *Metal–Carbon Clusters*

As mentioned in Chapter I of this dissertation, relatively few M<sub>n</sub>C<sub>m</sub> cluster studies have been done and more investigations, specifically on molecules larger than diatomics, are needed. Although a variety of metals are currently being studied in the TCU Molecular Physics Lab, the present investigations have primarily focused on first-row transition metals and Al. Moreover, concrete molecular identifications have so far been restricted to M<sub>n</sub>C<sub>3</sub> species. The next logical steps are to initiate investigations on second- and third-row transition metal–carbon clusters and also to try to create larger M<sub>n</sub>C<sub>m</sub> clusters.

When experiments on second- and third-row transition–metal carbon clusters are done, it seems likely that the dual ablation, low laser power, and soft rod techniques used in the creation of  $M_nC_3$  species, where  $M = \text{Ti},^{55} \text{Sc},^{71} \text{Ni},^{92} \text{Cr},^{46} \text{Co},^{91} \text{Al},^{112}$  and  $\text{Cu},^{120}$  could also be used to create other small  $M_nC_3$  molecules.

Creation of larger  $M_nC_m$  clusters, specifically longer  $C_n$  chains with a metal atom attached to one or both ends could be achieved by modifying the experimental conditions, detailed in Chapter II, that were shown to affect the size of the clusters produced. In experiments done as part of this work, a low laser power ( $<1.0$  W) and a loose beam focus ( $\sim 3.0$  mm diameter) was used on the C rods, which has produced the  $\nu_3$  mode of  $C_3$  as the dominant absorption in FTIR spectra. In future studies, a tighter beam focus,  $\leq 2.0$  mm diameter, or a laser power of  $1.0$ – $1.5$  W could be used on the C rod, which would likely produce longer  $C_n$  chains like  $C_5$ ,  $C_6$ ,  $C_7$ , and  $C_9$ .

The spectrum in Fig. 8.1 was obtained by using a laser power of  $\sim 1.0$  W and a medium beam focus ( $\sim 2.0$  mm diameter) in which the absorptions of linear  $C_n$  species such as  $C_5$  at  $2164.3$ ,  $C_6$  at  $1952.5$ ,  $C_7$  at  $1894.3$  and  $2127.8$ ,  $C_9$  at  $1601.0$ ,  $1998.1$ , and  $2078.1$ ,  $C_{11}$  at  $1946.1$  and  $1856.7$ , and  $C_{12}$  at  $1818.0$   $\text{cm}^{-1}$  are prominent features. Intense absorptions of the cyclic  $C_n$  clusters,  $c\text{-}C_6$  at  $1694.9$  and  $c\text{-}C_8$  at  $1844.2$   $\text{cm}^{-1}$  are also observed. Note that the  $\nu_6(\sigma_u)=1998.1$   $\text{cm}^{-1}$  mode of  $C_9$  is the most intense absorption. If the laser power and laser focus on the carbon rod could be modified to limit  $C_3$  production so that predominantly longer  $C_n$  chains like  $C_6$  or  $C_9$  are observed in the spectrum, then it seem likely that a dual ablation experiment with metal and carbon rods would produce  $MC_n$  or  $MC_nM$  ( $n>3$ ) species in an analogous way to the  $MC_3$  and  $MC_3M$  species production.

### 8.2.3 Sintering Metal–Carbon Rods

One technique that has been successful in production of  $Ge_nC_m$  bands is sintering both Ge

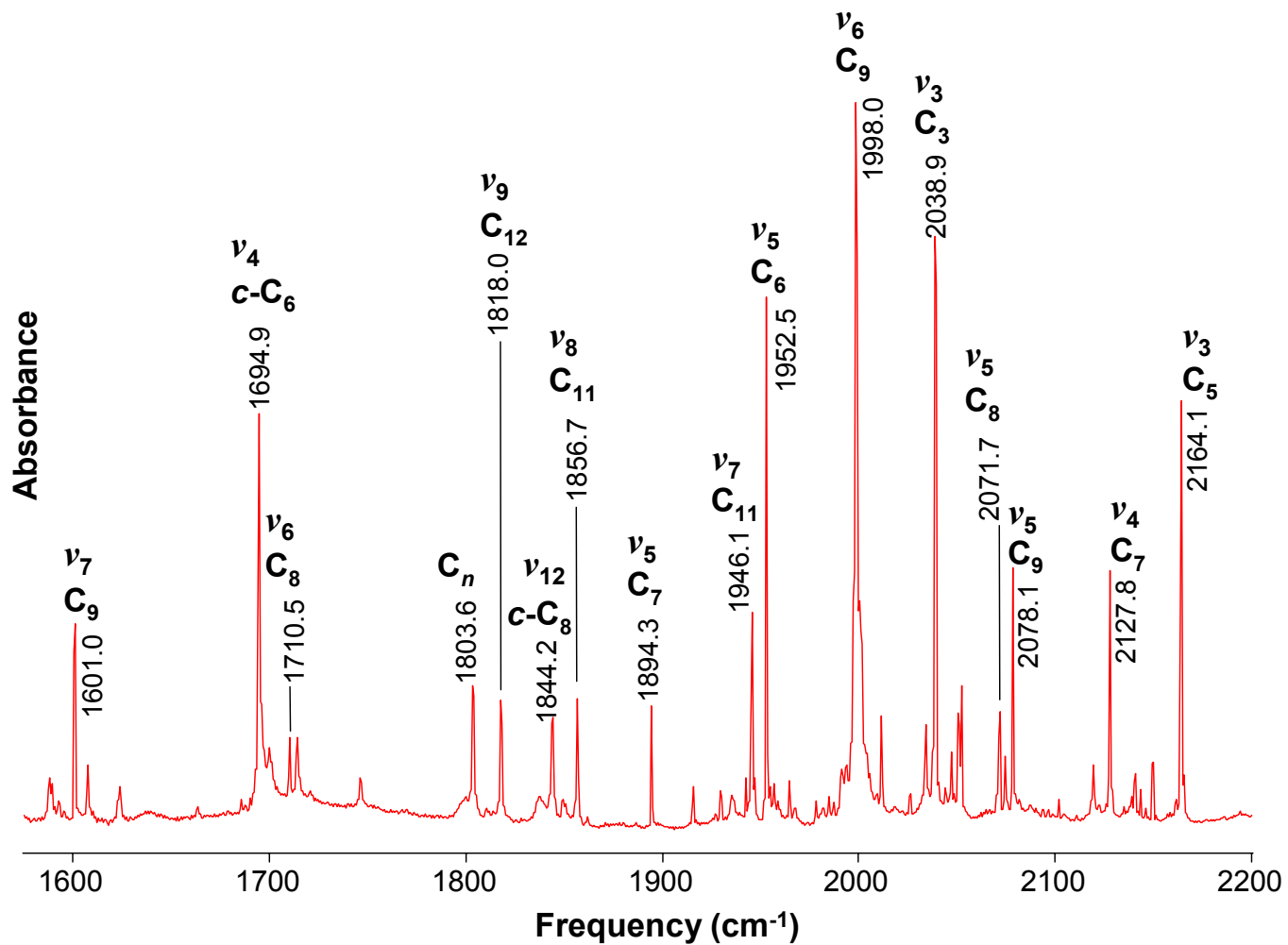


Figure 8.1 Spectrum obtained from <sup>12</sup>C ablation using a higher laser power, ~1.0 W, and tighter laser beam focus, ~2.0 mm, which produces intense absorptions for a number of of larger C<sub>n</sub> molecules.

and C into a single rod.<sup>131</sup> In this technique, Ge and C powders are pressed into a rod and heated in a furnace for 2-3 days at a temperature that is approximately equal to the melting point of Ge. This technique has been especially useful in the observation of several low frequency Ge–C stretching and bending fundamentals that also have weak intensities, presumably because  $Ge_nC_m$  clusters are created during the sintering process and thus result in the formation of a sufficiently large number of a specific  $Ge_nC_m$  molecule so that even weak vibrational fundamentals can be observed. Using a similar process in which metal–carbon rods are heated at a temperature approximately equal to the melting point of the specific metal used in the rod, sintered rods could be fabricated for experiments and may aid in the observation and identification of low intensity metal–carbon stretching and bending fundamentals.

#### **8.2.4 Rod Fabrication with Higher $^{13}C$ Enrichments**

The biggest obstacle in carbon rod fabrication has been to create rods with high (>50%)  $^{13}C$  enrichments. Although a  $^{12}C/^{13}C$  sintering process that can create rods with high  $^{13}C$  enrichments ( $\leq 95\%$ ) has been detailed,<sup>34</sup> it requires baking the C rods for ~20-30 days, which is not always feasible. A new technique, in which the  $^{12}C/^{13}C$  powder mixture is pressed into a “soft” rod and not baked, was presented in Chapter II. Its major drawback has been that C rods with >50%  $^{13}C$  enrichment cannot be created, which is probably caused by the use of a solid die when the rods are pressed. The higher the  $^{13}C$  enrichment, the more delicate the rod; consequently, the rod breaks as it is pushed out of the solid die. A possible solution to this problem is to create a split die that can be opened, allowing the delicate, high  $^{13}C$  enrichment rod to be removed without the use of excessive pressure and stress. This type of die has been successfully used in conjunction with a press housed on the top floor of the TCU Machine Shop, however, the weight and size of the die make it unwieldy. A schematic for the split die has been drawn (Fig. 8.2) and this die is currently under construction in the TCU Machine Shop.

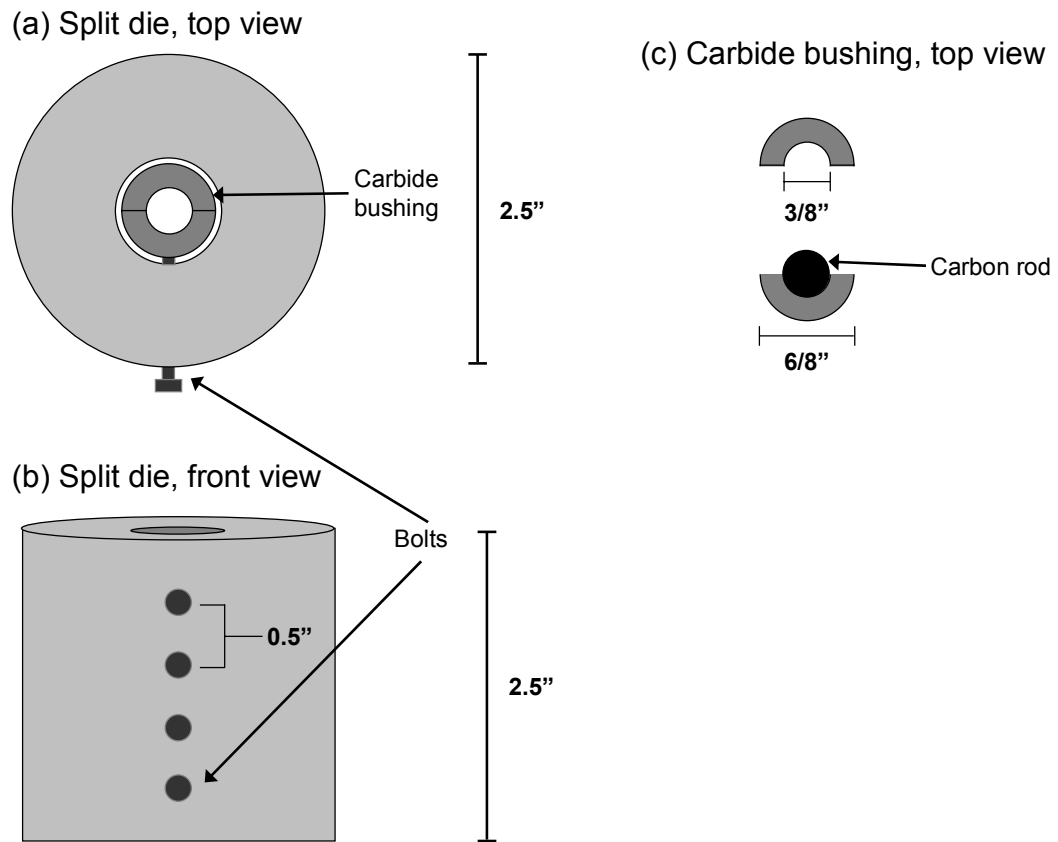


Figure 8.2 Proposed schematic for the (a) top and (b) front views of the split die. Note the bolts on the front are used to squeeze the carbide bushing together. Because of the small gap between the carbide bushing and the die casing, the bushing will easily slide out from the casing when the bolts are unscrewed. (c) An illustration of how the carbide bushing would be opened to remove a C rod fabricated with high  $^{13}\text{C}$  enrichment without putting excessive stress on the rod.



## REFERENCES

- <sup>1</sup> J. Cernicharo, J. Goicoechea, and Y. Benilan, *Astrophys. J.* **580**, L157 (2002).
- <sup>2</sup> S. Wei, B. C. Guo, J. Purnell, S. Buzza, and A. W. Castleman, Jr., *J. Phys. Chem.* **96**, 4166 (1992).
- <sup>3</sup> K. Tono, A. Terasaki, T. Ohta, and T. Kondow, *J. Chem. Phys.* **117**, 7010 (2002).
- <sup>4</sup> B. C. Guo and A. W. Castleman, Jr., in Advances in Metal and Semiconductor Clusters, ed. M. A. Duncan (Jai Press, London, 1994), Vol. 2, 137.
- <sup>5</sup> Cologne Database for Molecular Spectroscopy (<http://www.ph1.uni-koeln.de/vorhersagen/>). Last updated 07/2007; Wootten's Database, NRAO (<http://www.cv.nrao.edu/~awootten/allmols.html>). Last updated 11/2005.
- <sup>6</sup> M. J. Travers, M. C. McCarthy, P. Kalmus, C. A. Gottlieb, and P. Thaddeus, *Astrophys. J.* **469**, L65 (1996); M. B. Bell, P. A. Feldman, M. J. Travers, M. C. McCarthy, C. A. Gottlieb, and P. Thaddeus, *Astrophys. J.* **483**, L61 (1997).
- <sup>7</sup> Y. Kasai, Y. Sumiyoshi, Y. Endo, and K. Kawaguchi, *Astrophys. J.* **477**, L65 (1997); M. Grutter, M. Wyss, and J. P. Maier, *J. Chem. Phys.* **110**, 1492 (1999).
- <sup>8</sup> P. F. Bernath, K. H. Hinkle, and J. J. Keady, *Science* **244**, 562 (1989).
- <sup>9</sup> L. M. Ziurys, *Proc. Nat. Acad. Sci.* **103**, 12274 (2006).
- <sup>10</sup> E. Yamazaki, T. Okabayashi, and M. Tanimoto, *Astrophys. J. Lett.* **551**, L199 (2001).
- <sup>11</sup> M. Guélin, S. Mullen, J. Cernicharo, A. J. Apponi, M. C. McCarthy, C. A. Gottlieb, and P. Thaddeus, *Astron. & Astrophys.* **363**, L9 (2000), and references therein.
- <sup>12</sup> K. H. Hinkle, J. J. Keady, and P. F. Bernath, *Science* **241**, 1319 (1988).
- <sup>13</sup> *About Spitzer*. Retrieved April 25, 2005 from the Spitzer Science Center website, part of NASA's IR Processing and Analysis Center: <http://www.spitzer.caltech.edu/about/index.shtml>
- <sup>14</sup> B. C. Guo, K. P. Kerns, and A. W. Castleman, Jr., *Science* **255**, 1411 (1992), and references therein.
- <sup>15</sup> B. C. Guo, K. P. Kerns, and A. W. Castleman, Jr., *Science* **256**, 515 (1992), and references therein.
- <sup>16</sup> I. J. Dance, *J. Am. Chem. Soc.* **118**, 6309 (1996); I. J. Dance, *ibid.* **118**, 2699 (1996).
- <sup>17</sup> M. M. Rohmer, M. Benard, and J. M. Poblet, *Chem. Rev.* **100**, 495 (2000); H. Hou, J. T. Muckerman, P. Liu, and J. A. Rodriguez, *J. Phys. Chem. A* **107**, 9344 (2003).

- <sup>18</sup> M. E. Jacox, *J. Phys. Chem. Ref. Data* **32**, (2003).
- <sup>19</sup> X. -B. Wang, C. -F. Ding, and L. -S Wang, *J. Phys. Chem. A* **101**, 7699 (1997).
- <sup>20</sup> L. -S. Wang and X. Li, *J. Chem. Phys.* **112**, 3602 (2000).
- <sup>21</sup> H. -J. Zhai, S. -R. Liu, X. Li, and L. -S. Wang, *J. Chem. Phys.* **115**, 5170 (2001).
- <sup>22</sup> X. Li and L. -S. Wang, *J. Chem. Phys.* **111**, 8389 (1999).
- <sup>23</sup> *Matrix Isolation Infrared Spectroscopy*. from the NIST Physics Laboratory Optical Division website: <http://physics.nist.gov/Divisions/Div844/facilities/matrix/matrix.html>; M. E. Jacox, *Chem. Soc. Rev.* **31**, 108 (2002).
- <sup>24</sup> P. A. Withey, L. N. Shen, and W. R. M. Graham, *J. Chem. Phys.* **95**, 820 (1991).
- <sup>25</sup> H.-J. Zhai, L.-S. Wang, P. Jena, G. L. Gustev, and C. W. Bauschlicher, Jr., *J. Chem. Phys.* **120**, 8996 (2004).
- <sup>26</sup> C. Barrientos, P. Redondo, and A. Largo, *Chem. Phys. Lett.* **320**, 481 (2000).
- <sup>27</sup> J. D. Presilla-Márquez, C. M. L. Rittby, and W. R. M. Graham, *J. Chem. Phys.* **104**, 2818 (1996).
- <sup>28</sup> J. D. Presilla-Márquez, C. M. L. Rittby, and W. R. M. Graham, *J. Chem. Phys.* **106**, 8367 (1997).
- <sup>29</sup> X. D. Ding, S. L. Wang, C. M. L. Rittby, and W. R. M. Graham, *J. Chem. Phys.* **110**, 11214 (1999).
- <sup>30</sup> X. D. Ding, S. L. Wang, C. M. L. Rittby, and W. R. M. Graham, *J. Phys. Chem.* **104**, 3712 (2000).
- <sup>31</sup> D. L. Robbins, C. M. L. Rittby, and W. R. M. Graham, *J. Chem. Phys.* **114**, 3570 (2001).
- <sup>32</sup> D. L. Robbins, C. M. L. Rittby, and W. R. M. Graham, *J. Chem. Phys.* **120**, 4664 (2004).
- <sup>33</sup> D. L. Robbins, C. M. L. Rittby, and W. R. M. Graham, *J. Chem. Phys.* **117**, 3811 (2002).
- <sup>34</sup> R. Cárdenas, *Dissertation*, (2007).
- <sup>35</sup> G. V. Chertihin, L. Andrews, and P. R. Taylor, *J. Am. Chem. Soc.* **116**, 3513 (1994).
- <sup>36</sup> J. Drowart, R. P. Burns, G. DeMaria, and M. G. Inghram, *J. Chem. Phys.* **31**, 1131 (1959).
- <sup>37</sup> R. E. Kinzer, Jr., *Predissertation* (2005).
- <sup>38</sup> L. N. Shen, T. J. Doyle and W. R. M. Graham, *J. Phys. Chem.* **93**, 1597 (1990).
- <sup>39</sup> A. D. Becke, *Phys. Rev. A* **38**, 3098 (1988); J. P. Perdew and Y. Wang, *Phys. Rev. B* **45**, 13244 (1992).

- <sup>40</sup> J. D. Presilla-Márquez, W. R. M. Graham, and R. A. Shepherd, *J. Chem. Phys.* **93**, 5424 (1990).
- <sup>41</sup> P. A. Withey and W. R. M. Graham, *J. Chem. Phys.* **96**, 4068 (1992); J. D. Presilla-Márquez and W.R.M. Graham, *J. Chem. Phys.* **95** 5612 (1991); C. M. L. Rittby, *ibid.* **95**, 5609 (1991); J. D. Presilla-Márquez, S. C. Gay, C. M. L. Rittby, and W. R. M. Graham, *J. Chem. Phys.* **102**, 6354 (1995).
- <sup>42</sup> J. D. Presilla-Márquez and W. R. M. Graham, *J. Chem. Phys.* **96**, 6509 (1992); C. M. L. Rittby, *ibid.* **96**, 6768 (1992).
- <sup>43</sup> J. D. Presilla-Márquez and W. R. M. Graham, *J. Chem. Phys.* **100**, 181 (1994); C. M. L. Rittby, *ibid.* **100**, 175 (1994).
- <sup>44</sup> X. D. Ding, S. L. Wang, C. M. L. Rittby, and W. R. M. Graham, *J. Chem. Phys.* **112**, 5113, (2000), and references therein.
- <sup>45</sup> Gaussian 03, Revision B.01, M. J. Frisch, G. W. Trucks, H. B. Schlegel, G. E. Scuseria, M. A. Robb, J. R. Cheeseman, J. A. Montgomery, Jr., T. Vreven, K. N. Kudin, J. C. Burant, J. M. Millam, S. S. Iyengar, J. Tomasi, V. Barone, B. Mennucci, M. Cossi, G. Scalmani, N. Rega, G. A. Petersson, H. Nakatsuji, M. Hada, M. Ehara, K. Toyota, R. Fukuda, J. Hasegawa, M. Ishida, T. Nakajima, Y. Honda, O. Kitao, H. Nakai, M. Klene, X. Li, J. E. Knox, H. P. Hratchian, J. B. Cross, C. Adamo, J. Jaramillo, R. Gomperts, R. E. Stratmann, O. Yazyev, A. J. Austin, R. Cammi, C. Pomelli, J. W. Ochterski, P. Y. Ayala, K. Morokuma, G. A. Voth, P. Salvador, J. J. Dannenberg, V. G. Zakrzewski, S. Dapprich, A. D. Daniels, M. C. Strain, O. Farkas, D. K. Malick, A. D. Rabuck, K. Raghavachari, J. B. Foresman, J. V. Ortiz, Q. Cui, A. G. Baboul, S. Clifford, J. Cioslowski, B. B. Stefanov, G. Liu, A. Liashenko, P. Piskorz, I. Komaromi, R. L. Martin, D. J. Fox, T. Keith, M. A. Al-Laham, C. Y. Peng, A. Nanayakkara, M. Challacombe, P. M. W. Gill, B. Johnson, W. Chen, M. W. Wong, C. Gonzalez, and J. A. Pople, Gaussian, Inc., Pittsburgh PA, 2003.
- <sup>46</sup> S. A. Bates, C. M. L. Rittby, and W. R. M. Graham, *J. Chem. Phys.* **125**, 074506 (2006).
- <sup>47</sup> J. B. Foresman and A. Frisch, *Exploring Chemistry with Electronic Structure Methods*, (Gaussian, Inc., Pittsburgh 1993); A. Szabo and N. S. Ostlund, *Modern Quantum Chemistry*, (McGraw-Hill, New York, 1982).
- <sup>48</sup> J. Szczepanski, S. Ekern, C. Chapo, M. Vala, *Chem. Phys.* **211**, 359 (1996).

- <sup>49</sup> M. E. Jacox, NIST Vibrational and Electronic Energy Levels Database (<http://webbook.nist.gov/chemistry>).
- <sup>50</sup> P. F. Souter and L. Andrews, *J. Am. Chem. Soc.* **119**, 7350 (1997).
- <sup>51</sup> S. B. H. Bach, C. A. Taylor, R. J. Van Zee, M. T. Vala, and W. Weltner Jr., *J. Am. Chem. Soc.* **108**, 7104 (1986); L. Andrews, M. Zhou, G. L. Gustev, and X. Wang, *J. Phys. Chem. A* **107**, 561 (2003).
- <sup>52</sup> J. W. Kauffman, R. H. Hauge, and J. L. Margrave, *J. Phys. Chem.* **89**, 3541 (1985).
- <sup>53</sup> Z. L. Xiao, R. H. Hauge, and J. L. Margrave, *J. Phys. Chem.* **96**, 636 (1992); X. Wang and L. Andrews, *J. Phys. Chem. A* **107**, 570 (2003).
- <sup>54</sup> J. Szczepanski, C. Wehlburg, M. Vala, *J. Phys. Chem. A* **101**, 7039 (1997).
- <sup>55</sup> R. E. Kinzer, Jr., C. M. L. Rittby, and W. R. M. Graham, *J. Chem. Phys.* **125**, 074513 (2006).
- <sup>56</sup> A. V. Arbuznikov and M. Hendrickx, *Chem. Phys. Lett.* **320**, 575 (2000).
- <sup>57</sup> Y. -B. Yuan, K. -M. Deng, Y. -Z. Liu, and C. -M. Tang, *Chin. Phys. Lett.* **23**, 1761 (2006).
- <sup>58</sup> E. Gonzalez, C. M. L. Rittby, and W. R. M. Graham, *J. Chem. Phys.* **125**, 044504 (2006) and references therein.
- <sup>59</sup> C. M. L. Rittby, *unpublished work* (2007).
- <sup>60</sup> J. Szczepanski, S. Eckern, M. Vala, *J. Phys. Chem. A* **101**, 1841 (1997).
- <sup>61</sup> B. Tremblay, M. E. Alikhani, L. Manceron, *J. Phys. Chem. A* **105**, 11388 (2001).
- <sup>62</sup> L. A. Hanlan, H. Huber, E. P. Kundig, B. R. McGarvey, G. A. Ozin, *J. Am. Chem. Soc.* **97**, 7054 (1975).
- <sup>63</sup> B. Tremblay, L. Manceron, G. L. Gustev, L. Andrews, H. Partridge, III, *J. Chem. Phys.* **117**, 8479 (2002); M. Zhou, L. Andrews, *J. Phys. Chem. A* **102**, 10025 (1998).
- <sup>64</sup> W. E. Billups, S. -C. Chang, R. H. Hauge, J. L. Margrave, *J. Am. Chem. Soc.* **117**, 1387 (1995), and references therein.
- <sup>65</sup> M. Zhou, B. Liang, and L. Andrews, *J. Phys. Chem. A* **103**, 3013 (1999).
- <sup>66</sup> G. V. Chertihin, A. Citra, L. Andrews, C. W. Baushlicher, Jr., *J. Phys. Chem. A* **101**, 8793 (1997).
- <sup>67</sup> G. Maier, H. P. Reisenauer, U. Schafer, H. Balli, *Angew. Chem.* **100**, 590 (1988).
- <sup>68</sup> D. E. Milligan and M. E. Jacox, *J. Chem. Phys.* **51**, 277 (1969).
- <sup>69</sup> S. A. Bates, *unpublished work* (2007).
- <sup>70</sup> R. H. Kranze, C. M. L. Rittby, and W. R. M. Graham, *J. Chem. Phys.* **105**, 5313 (1996).

- <sup>71</sup> R.E. Kinzer, Jr., C.M.L. Rittby, and W.R.M. Graham, *J. Chem. Phys.*, *in preparation*.
- <sup>72</sup> N. A. Cannon, A. I. Boldyrev, X. Li, and L. -S. Wang, *J. Chem. Phys.* **113**, 2671 (2000), and references therein.
- <sup>73</sup> C. W. Bauschlicher, Jr., S. R. Langhoff, and L. G. M. Pettersson, *J. Chem. Phys.* **89**, 5747 (1988); G. L. Gustev, P. Jena, and R. J. Bartlett, *J. Chem. Phys.* **110**, 2928 (1999).
- <sup>74</sup> L. B. Knight, Jr., S. T. Cobranchi, J. O. Herlong, and C. A. Arrington, *J. Chem Phys.* **92**, 5856 (1990).
- <sup>75</sup> C. R. Brazier, *J. Chem. Phys.* **98**, 2790 (1993); A. Thoma, N. Caspary, B. E. Wurfel, and V. E. Bondybey, *J. Chem. Phys.* **98**, 8458 (1993).
- <sup>76</sup> D. Tzeli and A. Mavridis, *J. Phys. Chem. A* **105**, 1175 (2001), and references therein; D. Tzeli and A. Mavridis, *ibid.* **105**, 7672 (2001).
- <sup>77</sup> X. Zheng, Z. Wang, and A. Tang, *J. Phys. Chem. A* **103**, 9275 (1999).
- <sup>78</sup> A. Largo, P. Redondo, and C. Barrientos, *J. Am. Chem. Soc.* **126**, 14611 (2004).
- <sup>79</sup> A. I. Boldyrev, J. Simons, X. Li, and L. -S. Wang, *J. Am. Chem. Soc.* **121**, 10193 (1999).
- <sup>80</sup> X. Li, L. -S. Wang, N. A. Cannon, and A. I. Boldyrev, *J. Chem. Phys.* **116**, 1330 (2002).
- <sup>81</sup> A. I. Boldyrev, J. Simons, X. Li, W. Chen, and L. -S. Wang, *J. Chem. Phys.* **110**, 8980 (1999).
- <sup>82</sup> X. Li, L. -S. Wang, A. I. Boldyrev, and J. Simons, *J. Am. Chem. Soc.* **121**, 6033 (1999).
- <sup>83</sup> A. I. Boldyrev, J. Simons, X. Li, and L. -S. Wang, *J. Chem. Phys.* **111**, 4993 (1999).
- <sup>84</sup> Q. Sun, Q. Wang, X. G. Gong, V. Kumar, and Y. Kawazoe, *Eur. Phys. J. D* **18**, 77 (2002), and references therein.
- <sup>85</sup> X. Li and L. -S. Wang, *Phys. Rev. B* **65**, 153404 (2002), and references therein.
- <sup>86</sup> D. E. Bergeron, A. W. Castleman, Jr., T. Morisato, and S. N. Khanna, *Science* **304**, 84 (2004), and references therein.
- <sup>87</sup> A. Largo, P. Redondo, and C. Barrientos, *J. Phys. Chem. A* **106**, 4217 (2002).
- <sup>88</sup> G. Li and Z. Tang, *J. Phys. Chem. A* **107**, 5317 (2003).
- <sup>89</sup> P. Redondo, C. Barrientos, and A. Largo, *Int. J. Qm. Chem.* **96**, 615 (2004).
- <sup>90</sup> P. Redondo, A. Largo, F. García, and C. Barrientos, *Int. J. Qm. Chem.* **84**, 660 (2001).
- <sup>91</sup> S. A. Bates, J. A. Rhodes, C. M. L. Rittby, and W. R. M. Graham, *J. Chem. Phys.* **127**, 064506 (2007).
- <sup>92</sup> R. E. Kinzer, Jr., C. M. L. Rittby, and W. R. M. Graham, *J. Chem. Phys.* **128**, 164312 (2008).

- <sup>93</sup> L. Andrews, T. R. Burkholder, and J. T. Yustein, *J. Phys. Chem.* **96**, 10182 (1972), and references therein; D. A. Lynch, Jr., M. J. Zehe, and K.D. Carlson, *J. Phys. Chem.* **78**, 2361 (1976).
- <sup>94</sup> G. V. Chertihin and L. Andrews, *J. Phys. Chem.* **97**, 10295 (1993).
- <sup>95</sup> P. Pullumbi, Y. Bouteiller, L. Manceron, and C. Mijoule, *Chem. Phys.* **185**, 25 (1994).
- <sup>96</sup> C. Xu, L. Manceron, and J. P. Perchard, *J. Chem. Soc. Faraday Trans.* **89**, 1291 (1993); A. Feltrin, M. Guido, and S. Nunziante Cesaro, *Vib. Spectrosc.* **8**, 175 (1995).
- <sup>97</sup> G. V. Chertihin, I. L. Rozhanskii, L. V. Serebrennikov, and V. F. Shevel'kov, *Zh. Fiz. Khim.* **62**, 2256 (1988).
- <sup>98</sup> L. Zhang, J. Dong, M. Zhou, and Q. Qin, *J. Chem. Phys.* **113**, 10169 (2000).
- <sup>99</sup> T. R. Burkholder and L. Andrews, *Inorg. Chem.* **32**, 2491 (1993).
- <sup>100</sup> R. H. Hauge, J. W. Kauffman, and J. L. Margrave, *J. Am. Chem. Soc.* **102**, 6005 (1980).
- <sup>101</sup> Q. Kong, M. Chen, J. Dong, Z. Li, K. Fan, and M. Zhou, *J. Phys. Chem. A* **106**, 11709 (2002).
- <sup>102</sup> J. C. Stephens, E. E. Bolton, H. F. Shaefer, III, and L. Andrews, *J. Chem. Phys.* **107**, 119 (1997).
- <sup>103</sup> I. L. Rozhanskii, G. V. Chertihin, L. V. Serebrennikov, and V. F. Shevel'kov, *Sh. Fiz. Khim.* **62**, 2351 (1988).
- <sup>104</sup> I. L. Rozhanskii, L. V. Serebrennikov, and V. F. Shevel'kov, *Vestn. Mosk. Univ. Khim.* **43**, 560 (1988).
- <sup>105</sup> L. V. Serebrennikov, S. B. Osin, and A. A. Mal'tsev, *J. Mol. Struct.* **81**, 25 (1982).
- <sup>106</sup> J. Szczepanski, R. Hodyss, and M. Vala, *J. Phys. Chem. A* **102**, 8300 (1998).
- <sup>107</sup> R. H. Kranze, P. A. Withey, C. M. L. Rittby, and W. R. M. Graham, *J. Chem. Phys.* **103**, 6841 (1995).
- <sup>108</sup> L. N. Shen and W. R. M. Graham, *J. Chem. Phys.* **91**, 5115 (1989).
- <sup>109</sup> V. M. Rayón, P. Redondo, C. Barrientos, and A. Largo, *Chem. Eur. J.* **12**, 6963 (2006), and references therein.
- <sup>110</sup> H. J. Hwang, O.-K. Kwon, and J. W. Kang, *Solid State Comm.* **129**, 687 (2004); W. Y. Choi, J. W. Kang, and H. J. Hwang, *Phys. Rev. B* **68**, 193405 (2003).
- <sup>111</sup> V. M. Rayón, P. Redondo, C. Barrientos, and A. Largo, *J. Phys. Chem. A* **111**, 6345 (2007).
- <sup>112</sup> S. A. Bates, C. M. L. Rittby, and W. R. M. Graham, *J. Chem. Phys.*, *to be submitted* (2008).

- <sup>113</sup> S. L. Wang, C. M. L. Rittby, and W. R. M. Graham, *J. Chem. Phys.* **107**, 6032 (1997).
- <sup>114</sup> R. H. Hauge, Z. H. Kafafi, and J. L. Margrave, *Physics and Chemistry of Small Clusters*, edited by P. Jena, B. K. Rao, and S. N. Khanna, (Plenum 1987), 787; X. Wang, L. Andrews, L. Manceron, and C. Marsden, *J. Phys. Chem. A* **107**, 8492 (2003); L. Andrews and X. Wang, *J. Am. Chem. Soc.* **125**, 11751 (2003).
- <sup>115</sup> S. -C. Chang, Z. H. Kafafi, R. H. Hauge, W. E. Billups, and J. L. Margrave, *J. Am. Chem. Soc.* **109**, 4508 (1987).
- <sup>116</sup> X. Wang and L. Andrews, *Inorg. Chem.* **44**, 9076 (2005).
- <sup>117</sup> G. V. Chertihin, L. Andrews, and C. W. Bauschlicher, Jr., *J. Phys. Chem. A* **101**, 4026 (1997), and references therein; L. -S. Wang, H. Wu, S. R. Desai, and L. Lou, *Phys. Rev. B* **53**, 8028 (1996); H. Wu, S. R. Desai, and L. -S. Wang, *J. Phys. Chem. A* **101**, 2103 (1997).
- <sup>118</sup> M. Zhou and L. Andrews, *J. Chem. Phys.* **111**, 4548 (1999), and references therein.
- <sup>119</sup> D. Moran, A. C. Simonetti, F. E. Leach, III, W. D. Allen, P. v. R. Schleyer, and H. F. Schaeffer, III, *J. Am. Chem. Soc.* **128**, 9342 (2006).
- <sup>120</sup> S. A. Bates, C. M. L. Rittby, and W. R. M. Graham, *J. Chem. Phys.*, *in preparation* (2008).
- <sup>121</sup> M. E. Jacox, D. E. Milligan, N. G. Moll, and W. E. Thompson, *J. Chem. Phys.* **43**, 3754 (1965); R. L. DeKock and W. Weltner, Jr., *J. Am. Chem. Soc.* **93**, 7106 (1971).
- <sup>122</sup> S. E. Kooi, B. D. Leskiw, and A. W. Castleman, Jr., *Nano Letters*, **1**, 113 (2001).
- <sup>123</sup> R. Selvan, L. Gowrishankar, and T. Pradeep, *Proc. Indian Acad. Sci. (Chem. Sci.)*, **113**, 681, (2001).
- <sup>124</sup> D. Majumdar, S. Roszak, and K. Balasubramanian, *J. Chem. Phys.*, **118**, 130 (2003).
- <sup>125</sup> P. Redondo, C. Barrientos, and A. Largo, *J. Chem. Theor. Comp.* **2**, 885 (2006).
- <sup>126</sup> Supporting information for Ref. 125, which can be obtained at <http://pubs.acs.org>.
- <sup>127</sup> Z. L. Xiao, R. H. Hauge, and J. L. Margrave, *J. Phys. Chem.* **95**, 2696 (1991).
- <sup>128</sup> L. Zhang, J. Dong, and M. Zhou, *Chem. Phys. Lett.* **335**, 334 (2001).
- <sup>129</sup> G. V. Chertihin, W. D. Bare, and L. Andrews, *J. Phys. Chem. A* **101**, 5090 (1997).
- <sup>130</sup> M. Zhou and L. Andrews, *J. Phys. Chem. A* **103**, 2066 (1999).
- <sup>131</sup> E. Gonzalez, C. M. L. Rittby, and W. R. M. Graham, *J. Chem. Phys.*, *submitted*.

## VITA

Personal	Sarah Anne Bates
Background	Born on 30 June 1981, York, PA Eldest daughter of William A. and M. Ann Bates
Education	Diploma ( <i>summa cum laude</i> ), Red Lion Area Sr. High, Red Lion, PA, 1999. B.S. ( <i>cum laude</i> ), Physics & Astronomy; B.A. ( <i>cum laude</i> ), Philosophy; Japanese and mathematics minors, Texas Christian University, Ft. Worth, TX, 2003. Ph.D., Physics, Texas Christian University, Ft. Worth, TX, 2008.
Experience	Research Assistant, Baylor University, Research Experience for Undergraduates (REU), June 2001-August 2001 Physics Tutor, Texas Christian University, January 2004- December 2005 Teaching Assistant, Texas Christian University, January 2001-present Research Assistant, TCU Molecular Physics Laboratory, Texas Christian University, June 2003-present
Memberships	American Physical Society
Awards	Texas Space Grant Consortium Fellowship recipient (2003-2006) Barnett Scholar (2003-2004) American Physical Society Graduate Student Presentation Award (2006) Student Research Symposium Graduate Presentation Award (2007) Research Stipend from the Welch Foundation (2003-2008)
Publications	1. S. A. Bates, C. M. L. Rittby, and W. R. M. Graham <i>Fourier transform infrared isotopic study of linear CrC<sub>3</sub>: Identification of the <math>\nu_1(\sigma)</math> mode</i> , J. Chem. Phys. <b>125</b> , 074506 (2006). 2. S. A. Bates, J. A. Rhodes, C. M. L. Rittby, and W. R. M. Graham, <i>Fourier transform infrared observation of the <math>\nu_1(\sigma)</math> mode of linear CoC<sub>3</sub> trapped in solid Ar</i> , J. Chem. Phys. <b>127</b> , 064506 (2007). 3. S. A. Bates, C. M. L. Rittby, and W. R. M. Graham, <i>FTIR observation and DFT study of the AlC<sub>3</sub> and AlC<sub>3</sub>Al linear chains trapped in solid Ar</i> , J. Chem. Phys., <i>in preparation</i> (2008). 4. S. A. Bates, C. M. L. Rittby, and W. R. M. Graham, <i>The Vibrational Spectrum of CuC<sub>3</sub>: An FTIR and DFT Investigation</i> , J. Chem. Phys., <i>in preparation</i> (2008).



## ABSTRACT

### FOURIER TRANSFORM INFRARED ISOTOPIC STUDIES ON NOVEL METAL–CARBON CLUSTERS TRAPPED IN Ar MATRIX ENVIRONMENTS

by Sarah Anne Bates, Ph.D. 2008  
Department of Physics and Astronomy  
Texas Christian University

Dissertation Advisor:

Dr. W. R. M. Graham, Professor of Physics and Astronomy, Director of the Graduate Program

The characterization of the vibrational spectra and structures of small metal–carbon ( $M_nC_m$ ) clusters is important to the detection of astrophysical species and may elucidate the bonding and growth mechanisms of metallocarbohedrenes, or metcars. Additionally, transition metal–carbon clusters have applications in modern materials science as catalysts for nanomaterial formation.

A new experimental apparatus for the preparation of  $M_nC_m$  clusters has been designed and constructed, incorporating a new closed cycle refrigeration system, a chamber for the deposition of samples, associated vacuum system, and a fully automated mechanism to simultaneously translate and rotate carbon and metal rods during laser ablation. A new technique for fabricating carbon rods has been developed to expedite carbon rod production and to facilitate the formation of the  $M_nC_m$  clusters studied.

Fourier transform infrared (FTIR) investigations have been done for the first time on transition metal–carbon clusters. The molecular clusters were formed by trapping the products from dual laser ablation of metal and carbon rods in solid Ar at ~10 K. Comparing FTIR measurements of vibrational fundamentals and  $^{13}\text{C}$  isotopic shifts with the predictions of density functional theory (DFT) calculations has enabled the identification of five novel metal–carbon molecules, establishing their ground state geometries and permitting the assignment of

vibrational fundamentals, including the  $\nu_1(\sigma)$  modes of ( $^5\Pi$ ) linear CrC<sub>3</sub>, ( $^2\Delta$ ) linear CoC<sub>3</sub>, and ( $^2\Pi$ ) linear CuC<sub>3</sub> at 1789.5, 1918.2, and 1830.0 cm<sup>-1</sup>, respectively, the  $\nu_3(\sigma_u)$ =1624.0 and  $\nu_4(\sigma_u)$ =528.3 cm<sup>-1</sup> modes of ( $^1\Sigma_g^+$ ) linear AlC<sub>3</sub>Al, and the  $\nu_2(\sigma)$ =1210.9 cm<sup>-1</sup> mode of linear AlC<sub>3</sub>. Evidence for the tentative identification of the  $\nu_1(a_1)$ =1554.3 cm<sup>-1</sup> mode of ( $^3B_1$ ) fanlike CrC<sub>4</sub> and the  $\nu_4(\sigma_u)$ =1987.3 cm<sup>-1</sup> mode of ( $^1\Sigma_g^+$ ) linear AlC<sub>4</sub>Al is also presented. All FTIR measurements of vibrational frequencies and <sup>13</sup>C shifts are in very good agreement with DFT predictions, resulting in the first identification of vibrational fundamentals and the characterization of molecular geometries for these species specifically and for transition metal-carbon clusters in general. A catalog of potential V<sub>n</sub>C<sub>m</sub> absorptions has also been developed to aid in future vanadium-carbon studies.